WCAP10337

BASH: AN INTEGRATED CORE AND RCS REFLOOD CODE FOR ANALYSIS OF PWR LOSS-OF-COOLANT ACCIDENTS

J. N. Kabadi
S. R. Rod
M. El Shanawany
J. M. Willis
M. Y. Young

Approved: F. F. Cadek, Manager
Safeguards Engineering and Development

6133B:1/051983

8307080325 830620
PDR TOPRP EMVWEST
C PDR

TABLE OF CONTENTS

		Page
1	INTRODUCTION	1-1
2	THE BART CODE	
	2.1 Introduction	2-1
	2.2 Major Model Descriptions	2-1
3	THE NOTRUMP CODE	
	3.1 Introduction	3-1
	3.2 Major Model Descriptions	3-2
4	THE BART/NOTRUMP INTERFACE	
	4.1 Core Pressure Drop	4-1
	4.2 BART-NOTRUMP Information Transfer	4-5
5	BART MODIFICATIONS FOR BASH	
	5.1 Models	5-1
	5.2 Reverse Flow Model	5-2
	5.3 Flow Blockage Models	5-16
	5.4 Grid Heat Transfer Enhancement Effects	5-20
6	NOTRUMP MODIFICATIONS FOR BASH	
	6.1 Two-Volume Nonequilibrium Model	6-1
	6.2 Metal Heat Release Model	6-23
7	BASH VERIFICATION	
	7.1 FLECHT-SET System Description	7-1
	7.2 FLECHT Experiment Used for BASH Verification	7-4
	7.3 BASH Modeling of FLECHT-SET	
	7.4 BASH Comparison to FLECHT-SET 3105B	
	7.5 FLECHT-SEASET	

TABLE OF CONTENTS

		Page
8	PROPOSED ECCS EVALUATION MODEL Using BART/BASH	
	8.1 Descriptions of the Codes in the Model	
	8.2 Proposed ECCS Evaluation Model Code Integration	
9	CONCLUSION	9-1
10	REFERENCES	10-1

LIST OF ILLUSTRATIONS

Figure	Title	Page
1-1.	PWR Core Flooding Rate as Calculated by WREFLOOD and BASH	1-3
2-1.	Typical Conditions in Rod Bundle During Reflood	2-5
2-2.	The BART Quench Front Heat Release Model	2-8
4-1.	Core Pressure Drop Model	4-2
4-2.	BART - NOTRUMP Data Transfer	4-6
5-1.	Visualization of the Two-Channel Flow Redistribution Model	5-18
6-1.	Possible Connections from Volume Set i, j to Other Fluid Nodes	6-2
6-2.	Typical Link Connection Between Volume Sets and Fluid Nodes	6-5
6-3.	Mandhane Flow Regime Map for Horizontal Flow	6-11
6-4.	Heat and Mass Transfer Within Volume Set	6-17
6-5.	Piping System (per FLECHT-SET) for Comparison of Nonequilibrium Model and H.T.F.S. Correlation	6-24
6-6a.	Nonequilibrium Model and H.T.F.S. Correlation Comparison: Pressure Drop in Horizontal Pipe Flow; Dispersed, Annular and Slug Regime	6-26

LIST OF ILLUSTRATIONS (Cont)

Figure	Title	Page
6-6b.	Nonequilibrium Model and H.T.F.S. Correlation Comparison: Pressure Drop in Horizontal Pipe Flow; Bubbly, Stratified, and Rough Stratified Regimes	6-27
7-1.	FLECHT-SET Phase B Facility Schematic	7-3
7-2.	Test Vessel and Rod Bundle Details	7-5
7-3.	Cross Section of 10 x 10 Bundle Showing Instrument Locations and Radial Power Profiles	7-6
7-4.	BART Core Noding for FLECHT-SET B	7-8
7-5.	NOTRUMP Noding for FLECHT-SET B	7-10
7-6.	BASH/FLECHT 3105B Comparison: 6-Foot Elevation Cladding Temperatures	7-12
7-7.	BASH/FLECHT 3105B Comparison: 8-Foot Elevation Cladding Temperatures	7-13
7-8.	BASH/FLECHT 3105B Comparison: Quench Front Showing Maximum and Minimum Times for Each Elevation	7-14
7-9.	BASH/FLECHT 3105B Comparison: Core Flooding Rate (Raw Data)	7-16
7-10.	BASH/FLECHT 3105B Comparison: Core Flooding Rate (Smoothed)	7-17

LIST OF ILLUSTRATIONS (Cont)

Figure	Title	Page
7-11.	BASH/FLECHT 3105B Comparison: Integral of Mass Entering the Core	7-18
7-12.	BASH/FLECHT 3105B Comparison: Downcomer Head	7-19
7-13.	BASH/FLECHT 3105B Comparison: Test Section (Core) Mass	7-20
7-14.	BASH/FLECHT 3105B Comparison: Exit Flow Mass Out Integral	7-21
7-15.	BASH Noding for FLECHT-SEASET Gravity Reflood Test	7-23
7-16.	Comparison of Flooding Rates from BASH and Test Data (Calculated From Mass Balances)	7-25
7-17.	Collapsed Liquid Level in Core (Indicates Mass Stored in Test Vessel)	7-26
7-18.	Quench Front Elevation	7-27
7-19.	Rod Temperature at Approximately 4 Feet	7-28
7-20.	Rod Temperatures at Six Feet Six Inches	7-29
7-21.	Rod Temperatures at Approximately 9 Feet	7-30
8-1.	Current ECCS Evaluation Model	8-9
8-2.	Proposed ECCS Evaluation Model	8-10

LIST OF TABLES

		Page
6-1	Nonequilibrium Model Verification (10-Foot Length of 5-Inch ID Pipe, per FLECHT)	6-25

NOMENCLATURE

A	Cross-section area (ft^2)
C	Frictional energy loss per unit mass
C_d	Friction loss coefficient
C_p	Heat capacity (Btu/lbm)
D_d	Droplet diameter (ft)
D_m	Hydraulic diameter of volume m (ft)
D_p	Pipe diameter (ft)
E	Internal energy (Btu)
f	Friction factor
F_{mn}	Interfacial friction force (lbf)
F_w	Wall friction force (lbf)
G	Mixture mass flux (lbm/ft^2-sec)
g	Gravitational acceleration (ft/sec^2)
H	Total enthalpy (Btu)
h	Specific enthalpy (Btu/lbm)
J, j	Volumetric flux (ft^3/ft^2-sec = ft/sec)
k	Thermal conductivity (Btu/ft-sec)
L	Length (ft)
M	Mass (lbm)
n_d	Droplet number density (lb/ft^3)
Nu	Nusselt number
P	Pressure (psia)
P_{mn}	Interfacial surface area per unit length of pipe (ft^2/ft = ft)
P_w	Wetted perimeter (ft)
Pr	Prandtl number
Q	Total heat transfer rate (Btu/sec)
q'''	Heat generation rate (Btu/ft^3-sec)
q''_d	Heat flux at droplet surface (Btu/ft^2-sec)
q_{il}	Energy flow rate from liquid to interface (Btu/sec)
q_{iv}	Energy flow rate from vapor to interface (Btu/sec)
Re	Reynolds number
S_f	Liquid mass flow rate from vapor volume (lbm/sec)

NOMENCLATURE (cont.)

S_g	Vapor mass flow rate from liquid volume (lbm/sec)
S_l	Liquid mass flow rate from liquid volume (lbm/sec)
St	Stanton number
T	Temperature (degree F)
t	Time (sec)
U	Internal energy (Btu) [see context]
U, u	Velocity (ft/sec)
U_r	Relative velocity between phases (ft/sec)
V	Total volume (ft^3)
v	Specific volume (ft^3/lbm)
V_α	Void propagation velocity (ft/sec)
W	Mass flow rate (lbm/sec)
We	Weber number
X	Thermodynamic quality
S_v	Average void fraction (2-volume model)
Z	Elevation (ft)
Z_F	Elevation of two-phase/vapor interface in core (ft)
Z_S	Elevation of liquid/two-phase interface in core (ft)

GREEK NOMENCLATURE

α	Void fraction
Γ	Volumetric rate of vapor generation (ft^3/ft^3-sec = 1/sec) [see context]
Γ	Net evaporation rate (lbm/sec) [2-volume model]
μ	Viscosity (lbm/ft-sec)
ρ	Density (lbm/ft^3)
ρ_j	Flowing mixture density
ρ_s	Static mixture density (lbm/ft^3)
σ	Surface tension (lbf/ft)

SUBSCRIPTS

1	Node at bottom of core
b	Bubble
c	Continuous phase
d	Droplet
i	Current node number [see context]
i	Liquid volume [two-volume model]
j	Vapor volume
l	Liquid
lv	Difference between liquid and vapor states
m	Condition within node [see context]
m	Liquid flow link [two-volume model]
N	Node at top of core
n	Vapor flow link [two-volume model]
n	Current time step [see context]
p	Pipe [see context]
p	Condition at node boundary [see context]
r	Relative property
s	Mixture property
sat	Saturation condition
T	Total volume
v	Vapor

SECTION 1
INTRODUCTION

Over the past several years Westinghouse has been developing an improved reflood model for use in the evaluation of large loss-of-coolant accidents in PWRs. The motivation behind this effort was a desire to demonstrate additional safety margin to the cladding temperature limits imposed by Appendix K of 10CFR.50. Since current evaluation models[1] indicated that the peak cladding temperature occurs during the reflood phase of the accident, major emphasis was placed on developing improved models to calculate heat transfer and thermal-hydraulics in a PWR during reflood.

The first step in the reflood model development program was to improve the core heat transfer and thermal-hydraulic model. The current evaluation model employs the FLECHT correlation followed, as required by Appendix K, by a steam cooling model when blockages are predicted at flooding rates less than one inch per second. The improved core heat transfer model, intended to replace the current approach, is named BART (Best Estimate Analysis of Reflood Transients) and is described in WCAP-9561.[2] In this reference, an interim reflood evaluation model is also proposed in which BART is used in place of the FLECHT correlation and steam cooling model. However, other aspects of the evaluation model are kept essentially the same. In particular, the entrainment rate used in the WREFLOOD code to determine flooding rate is still calculated using the FLECHT entrainment correlation.[3] This correlation is based on constant low flooding rate data and the resulting flooding rate exhibits a quasi-steady behavior as shown in Figure 1-1.

A more dynamic interaction between the core thermal-hydraulics and system behavior is expected and recent experiments have borne this out. Therefore, a logical next step in the reflood model development was to use BART to calculate the entrainment rate for a given flooding rate, use a system code to determine loop flows and pressure drops in response to the calculated core exit flow, and supply BART with an updated inlet flow with which to calculate

a new entrainment rate. This system was expected to produce a more dynamic flooding transient, somewhat as shown in Figure 1-1, which reflected the close coupling between core thermal-hydraulics and loop behavior.

The system code chosen for the above applications was NOTRUMP.[4] This code with some modifications would allow additional flexibility in modeling upper plenum mass storage, steam generator heat transfer, and loop resistance.

This report covers the latest phase of reflood model development, outlined above. Using the BART and NOTRUMP reports as reference documents, the report describes changes in these codes required for their combination into the reflood system code BASH. Additional sections cover verification of BASH against available gravity reflood data. Finally, an evaluation model using BART/BASH for ECCS performance in PWRs is proposed to replace the current evaluation model.

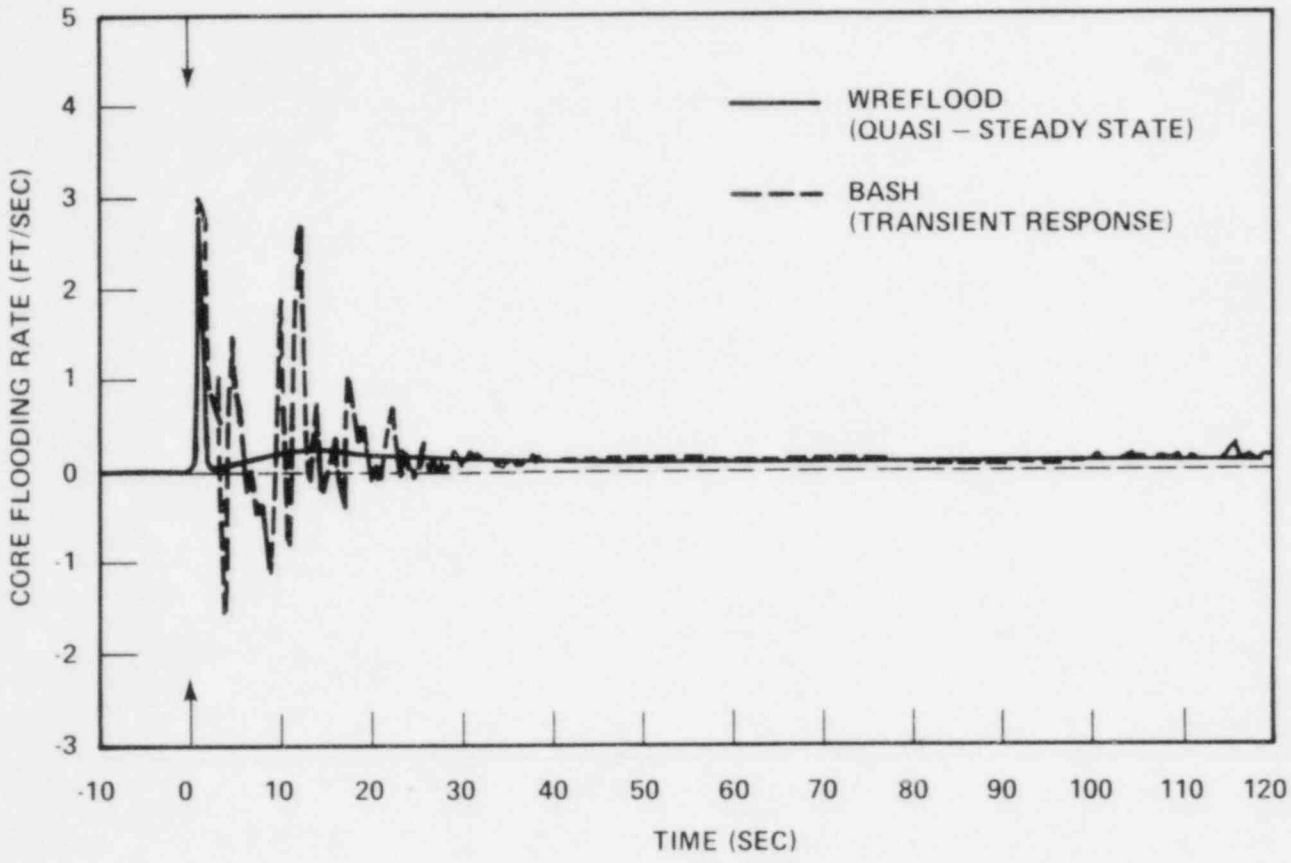

Figure 1-1. PWR Core Flooding Rate as Calculated by WREFLOOD and BASH

SECTION 2
THE BART CODE

2.1 INTRODUCTION

The BART computer code was developed primarily as a best-estimate design code for application to the reflood stage of loss-of-coolant accident analysis. The basic features of BART are described in detail in the original Westinghouse report on the code, WCAP-9561.[2] The following models comprise the basis of the original work and are the foundation for the refinements described in Section 5 of this report. Brief summaries of these basic features are given here as background to the development of BART and its integration into a comprehensive LOCA analysis model:

1. Basic conservation of mass and energy in liquid, vapor, and two-phase regions in the reactor core.

2. Radial conduction heat transfer within the fuel rod.

3. Heat transfer from rods to coolant in liquid, vapor and two-phase regions in the core.

4. Quench-front propagation and heat release.

5. Thermal nonequilibrium and heat transfer between phases.

2.2 MAJOR MODEL DESCRIPTIONS

2.2.1 Basic Conservation Equations.

Reflood heat transfer, which determines the peak cladding temperature during the reflood phase of a LOCA, is governed by local fluid conditions in the core. In BART, it is assumed that axial variations dominate so that a one-dimensional representation will suffice.

The reflood process occurs at relatively low pressure and flow. Because local pressure variation is a second-order effect, it is assumed in BART that core pressure is constant in time. Thus, only the continuity and energy equations, augmented by a volume flux equation, an equation of state, and an equation for relative velocity between liquid and vapor are considered.

From a hydraulic viewpoint, the core at any time consists of a least one of three regions; single phase liquid, two-phase mixture, and single-phase vapor. Each region is separated from the others by a fluid interface. For the purpose of illustration, only the two-phase region will be discussed here, since the single-phase equations follow directly from the two-phase system. A detailed description of the entire system can be found in the original BART report.[2]

Mixture continuity equation:

$$\frac{\partial \rho_s}{\partial t} + \frac{\partial}{\partial z}(G) = 0$$

Vapor energy equation:

$$\rho_v \left[\alpha \frac{\partial H_v}{\partial t} + j_v \frac{\partial H_v}{\partial z}\right] = q''' - q'''_{boil} \left[1 + \frac{H_v - H_{vsat}}{H_{\ell v}}\right]$$

Volume flux equation:

$$\frac{\partial j}{\partial z} + \alpha \frac{\partial}{\partial t} \ln \rho_v + j_v \frac{\partial}{\partial z} \ln \rho_v = \Gamma \left(\frac{1}{\rho_v} - \frac{1}{\rho_\ell}\right)$$

Equation of state:

$$\rho_v = \rho_v (H, P)$$

where

j = volumetric flux

j_v = vapor volumetric flux

ρ = ρ_ℓ = liquid density

ρ_v = vapor density

ρ_s = mixture density

Γ = volumetric rate of vapor generation

G = mixture mass flux

The relative velocity, U_r, is determined from drift flux correlations or, in the case of dispersed flow, is calculated from a vapor-droplet force balance.

Simplifying assumptions are:

1. One-dimensional equations

2. Fluid properties are independent of small variations in pressure

2.2.2 Radial Conduction Heat Transfer in Fuel Rod

A detailed conduction heat transfer model is used to calculate fuel rod temperature history and energy transfer to the fluid in BART. For "hot channel" calculations (these will determine the temperature of the hot rod, see Section 8) the model used is identical to the model developed for the LOCTA-IV program.[5] For "average channel" calculations (to determine core conditions for reflood calculations) a simpler model is used which does not include the mechanical deformation of the cladding. This model is described in WCAP-9561.[2]

2.2.3 Heat Transfer From Rod to Coolant

The following regions, characteristic of the reflood transient, are described below and depicted schematically in Figure 2-1.

As coolant enters the core, the first region encountered is one in which the fuel rod surface temperature is near the fluid saturation temperature. Liquid is heated or boils in this region due to decay power generated within the rod. All heat flowing from the rod is assumed to either heat the water to saturation or generate vapor. The mixture is therefore in thermal equilibrium. Heat transfer below the quench front is due to forced convection if the wall temperature is less than saturation temperature, or to a combination of nucleate boiling and forced convection if the wall temperature is greater than the saturation temperature.

The next general core heat transfer region encountered is in the vicinity of the quench front, where the fuel rod surface temperature rises from near saturation to a value on the order of 1000°F over a very short axial distance. In this region, the fluid undergoes complex changes in flow regime because the rod can no longer be wet by the liquid and because the heat transfer rates become large in both the axial and radial directions.

The final state of the fluid as it passes up the core is characterized by a highly dispersed liquid phase and a highly superheated vapor phase.

There are four possible mechanisms for heat transfer from the rod surface to the fluid in dispersed flow:

1. Forced convection to vapor
2. Radiation to fluid
3. Radiation to other rods
4. Droplet contact

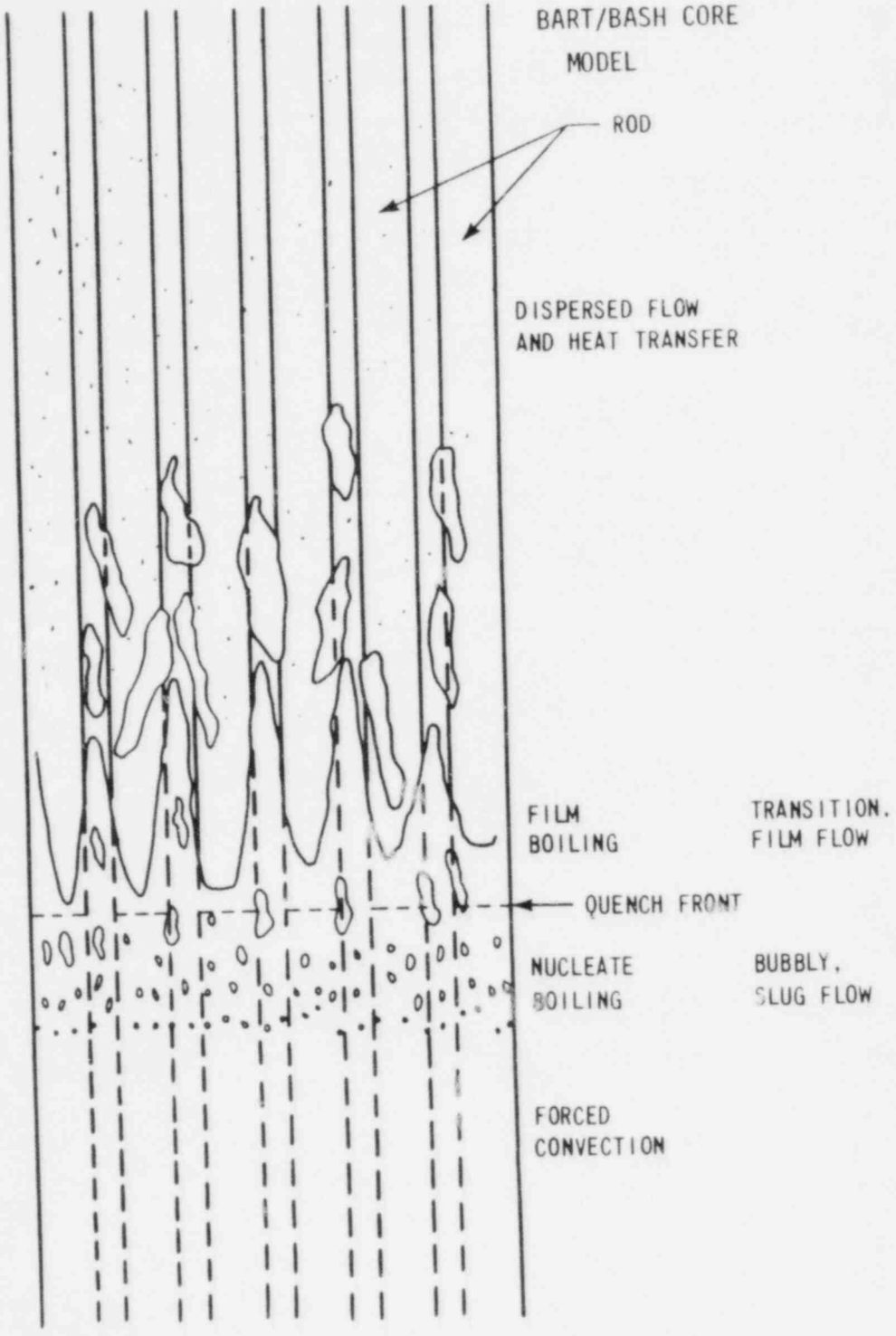

Figure 2-1. Typical Conditions in Rod Bundle During Reflood

For rod-to-vapor heat transfer, a careful analysis was made of the forced convection and radiation components of the heat transfer in the FLECHT cosine and skewed tests.[6][7] From that analysis, the following conclusions were drawn:

a. Radiation accounted for roughly 20 percent of the total heat flux from the heater rods at upper elevations. The three components of radiation were found to be of the same order of magnitude.

b. The remaining heat flux, attributed to forced convection from the rod surface to the vapor, was significantly higher than could be accounted for by standard correlations such as Dittus-Boelter.

It was concluded in the FLECHT analysis that the physical mechanism providing the most consistent explanation for the excess heat transfer was the level of turbulence within the vapor. Given the same local Reynolds number, turbulent diffusion of heat was more effective during two-phase flow in the FLECHT bundle than would be the case in single-phase flow in a tube.

In addition to forced convection, radiation from the rod to the vapor and the liquid is calculated. Rod-to-rod radiation is ignored, although it is recognized that this component may become important at upper elevations of the rod bundle.

Droplet contact with rods and subsequent drop breakup effects on heat transfer are ignored in the original version of BART.

2.2.4 Quench Front Propagation and Heat Release

The model of quench front heat release establishes an array of isotherms which migrate along the rod as the quench front propagates as shown in Figure 2-2. The isotherm model accounts for both radial temperature gradients within the rod and the severe axial gradient above the quench front. The isotherm temperatures are input values and can be chosen to provide any desired degree of detail at the quench front.

The model considers radial conduction in the rod and axial conduction along the rod, which is of the same magnitude as boiling heat transfer to the liquid. The axial conduction leads to additional preheating of the liquid before it reaches the actual quench front. A typical heat flux profile is shown in Figure 2-2.

A boiling curve based on the assumption of hydrodynamically controlled heat flux at the quench front is used to locate appropriate heat transfer regimes and the accompanying heat transfer coefficients. The regimes near the quench front include single-phase, forced convection, nucleate boiling, transition boiling and film boiling. Closely spaced isotherms allow very fine detail in locating boiling zones in the region immediately around the quench front, which is typically very narrow, while sacrificing little in computer running time.

2.2.5 Liquid-to-Vapor Heat Transfer

Liquid droplets in the dispersed regime will evaporate as they travel up the bundle. Convective heat transfer between a droplet and superheated vapor is calculated using standard correlations for convective heat transfer to spheres.

In addition to heat transfer due to conduction and convection, radiation between the vapor and liquid is accounted for.

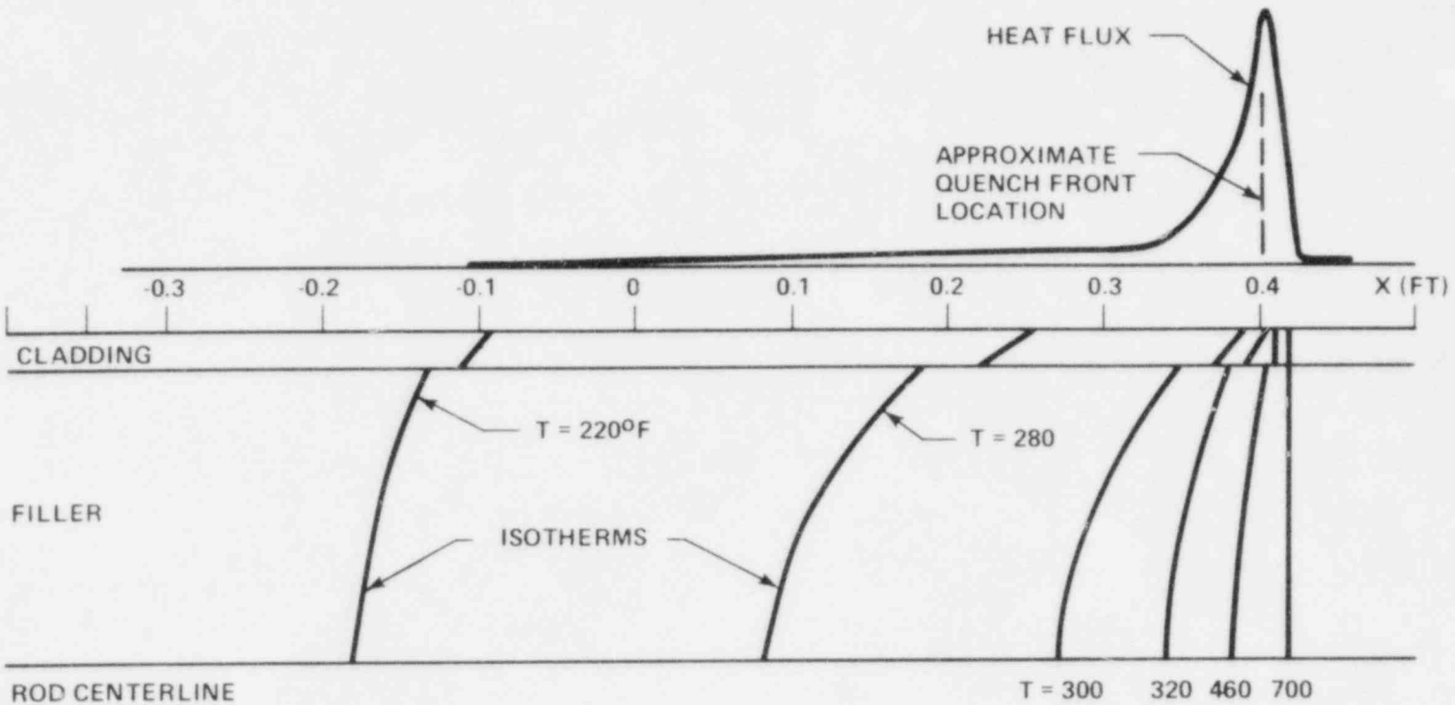

Figure 2-2. The BART Quench Front Heat Release Model

SECTION 3
THE NOTRUMP CODE

3.1 INTRODUCTION

NOTRUMP is a nodal network code designed for application to problems requiring general one-dimensional thermal-hydraulic analysis. A rigorous description of NOTRUMP and its capabilities is presented in a WCAP-9236.[4] A brief overview of NOTRUMP is provided here as background to the formulation of the more comprehensive PWR transient analysis model, BASH.

The basic components of the NOTRUMP model are fluid nodes, metal nodes, fluid flow links (called "flow links") and heat flow links ("heat links"), each of which may be of several types. The major node types are "interior" and "boundary" nodes, and the main link types are "noncritical" and "critical" links. Interior nodes and noncritical links are the general-purpose components used for most parts of the system being modeled. Boundary nodes and critical links are designed to be convenient vehicles for imposing boundary conditions in the modeling of transients.

Physical problems are modeled by assembling the components to form a network of fluid and metal nodes appropriately interconnected by flow and heat links. The nodes provide for mass and energy storage while the links provide for mass and energy transfer.

Thermal hydraulic effects are modeled in the code through various correlations. Flow correlations account for the effects of pressure drop and phase separation. Heat transfer correlations represent all regimes, such as liquid convection, nucleate boiling, stable film boiling, forced convection vaporization and steam forced convection.

Several specific component models supplement the correlations, permitting detailed analysis of equipment which is otherwise beyond the scope of the

general noding scheme. Examples of specially modeled components are steam generator swirl-vane moisture separators, chevron separators and primary coolant pumps.

NOTRUMP has mixed implicit/explicit solution capabilities. The implicit (backwards time differencing) technique follows the scheme outlined in the references. Longer time steps are usually possible with this technique than with the explicit (forward time differencing) approach. However, where explicit equations are adequate, NOTRUMP takes advantage of the reduced calculational effort associated with them. For example, metal nodes in steam generator tubes can typically be treated explicitly.

NOTRUMP has a detailed momentum balance. Gravitational terms account for elevations of fluid nodes and flow links and for the effects of phase distribution in stratified nodes. Frictional terms in the momentum balance account for the effects of flow through tubes, flow across and parallel to tube bundles, and form losses. Friction and form factors can be supplied externally or calculated internally. Momentum flux terms are also included in the momentum balance equations.

Drift flux and bubble rise models in NOTRUMP simulate vertical slip flow, including countercurrent flow. These models facilitate treating gravitational and mechanical phase separation and predicting water level behavior.

Many other models which apply to specific PWR components and calculational options used at the discretion of the programmer are described in the NOTRUMP report but are beyond the scope of this summary. In the next section, the basic constituents of a typical nodal network are briefly described.

3.2 MAJOR MODEL DESCRIPTIONS

A NOTRUMP network consists of a finite collection of flow and heat links joining together a system of fluid and metal nodes. Along with user-supplied boundary conditions and some component-specific model options, this nodal network can effectively simulate a great variety of actual thermal-hydraulic

systems. The present application is to the primary coolant loops of a PWR during the reflood phase of a LOCA transient. The different properties of the various building blocks of the NOTRUMP network are discussed below.

3.2.1 Interior Fluid Nodes

An interior fluid node is defined as a fixed control volume containing fluid at thermodynamic equilibrium and having associated with it one conservation equation for total mass and one for total internal energy. No flow (only mass and energy inventory) is associated with a fluid node. An interior fluid node may be connected with other fluid nodes via flow links and with metal nodes via heat links.

An interior fluid node has associated with it a number of important quantities. The total volume, V (ft^3), is a constant. The total internal energy, U (Btu), is the unknown in the energy conservation equation. The total mass M (lbm) is the unknown in the mass conservation equation. The pressure P (psia), temperature T (°F), thermodynamic quality, x, and various pressure and temperature derivatives are determined from the fluid equation of state given V, U, and M. Saturation properties are then found from P.

Although an interior fluid node is restricted to being in thermodynamic equilibrium, it need not be homogeneous. Stratified nodes are allowed. In these, there is a mixture of steam (bubbles) and liquid at the bottom of the node with a separated layer of steam at the top.

3.2.2 Boundary Fluid Nodes

A boundary fluid node is defined as a control volume containing fluid at a specified pressure P (psia) and enthalpy h (Btu/lbm). A boundary fluid node may be connected with other fluid nodes via flow links and with metal nodes via heat links.

The pressure and enthalpy for boundary fluid nodes are specified as arbitrary functions of time.

Other important boundary fluid node quantities are the temperature T (°F), thermodynamic quality, x, and saturation properties. They are determined from the fluid equation of state, when P and h are given.

Boundary fluid nodes provide a convenient means of imposing boundary conditions. A pressure boundary condition uses the specified pressure. If flow is out of the boundary fluid node, the donor enthalpy for the flow link is the specified enthalpy of the boundary fluid node. The temperature can also be used as a boundary condition for heat transfer.

3.2.3 Interior Metal Nodes

An interior metal node is defined as a fixed control volume containing metal at thermodynamic equilibrium and having associated with it one conservation equation for total internal energy (actually, the equation is written in terms of the metal temperature). An interior metal node may be connected with fluid nodes via heat links.

An interior metal node has associated with it a number of important quantities. The total mass M (lbm) is a constant. The metal temperature T (°F) is the unknown in the energy conservation equation. The heat capacity C_p (Btu/lbm-°F) and the thermal conductivity k (Btu/sec-°F-ft) are specified functions of temperature. The thermal conductivity is used in determining the heat transfer characteristics of heat links connected to the interior metal node.

3.2.4 Boundary Metal Nodes

A boundary metal node is defined as a control volume containing metal at a specified temperature T (°F). A boundary metal node may be connected with fluid nodes via heat links.

The metal temperature for a boundary metal node is specified as an arbitrary function of time.

The other important boundary metal node quantity is the thermal conductivity k (Btu/sec-°F-ft), which is a specified function of temperature.

Boundary metal nodes provide a convenient means of imposing boundary conditions. A temperature boundary condition uses a user-specified temperature.

3.2.5 Noncritical Flow Links

A noncritical flow link is defined as a path for fluid flow having associated with it a momentum conservation equation for the time rate of change of the total mass flow rate. No mass and energy inventories (only flow) are associated with a flow link. A noncritical flow link is always connected to two fluid nodes.

A noncritical flow link has associated with it a number of quantities. The inertial length, L/A (ft^{-1}), is a constant. The total mass flow rate, W (lbm/sec), is the unknown in the momentum equation. The liquid mass flow rate, W_f (lbm/sec), and the steam mass flow rate, W_g (lbm/sec), are determined by a slip or drift flux model.

The void fraction in a noncritical flow link, α, is determined from slip and drift flux models. The specific volume, v (ft^3/lbm), is found from the void fraction.

The continuous flow link model is used in conjunction with the stratified node models. It allows modeling of a flow link as a finite diameter circular pipe for the purpose of determining the flow composition at the intersection of the flow link with a stratified fluid node.

The momentum flux model calculates the momentum flux terms in the momentum balance equations. It also limits the flow in flow links to less than sonic flow.

These models calculate W_f, W_g, and α in a flow link. They allow for relative motion, i.e., slip, between the liquid and steam phase, and even for countercurrent flow. They are extremely useful in modeling natural or mechanical separation effects in vertical flow.

3.2.6 Critical Flow Links

A critical flow link is defined as a path for fluid flow having associated with it an equation for the total mass flow (rather than the time rate of change of the total mass flow rate). A critical flow link is always connected to two fluid nodes.

Other than the fact that a critical flow link does not have a differential equation for the total mass flow rate, it is treated as a non-critical flow link. The quantities, W_f, W_g, α, and v are found in the same way. The slip, drift flux, momentum flux, and continuous flow link models are available for use in critical flow links as well as noncritical flow links.

Critical flow links provide a convenient means of imposing flow boundary conditions or modeling choked flow at pipe breaks (e.g., steam or feed line breaks). All flow links have both upstream and downstream fluid nodes, which can be either interior or boundary nodes. Often a boundary node is used as a donor node for a critical flow link so that the enthalpy as well as the flow in the link can be specified as a function of time.

3.2.7 Noncritical Heat Links

A noncritical heat link is defined as a path for energy flow having associated with it an equation for the energy flow (heat rate). Only energy flow is associated with a heat link. A noncritical heat link is always connected to a fluid node and a metal node.

The major quantities associated with a noncritical heat link are the heat transfer rate, Q (Btu/sec) and a constant heat transfer area, A (ft^2).

3.2.8 Critical Heat Links

A critical heat link is defined as a path in which the energy flow is specified as a function of time only.

A critical heat link is always connected to a fluid node and a metal node. Critical heat links provide a convenient means of imposing heat flux boundary conditions.

SECTION 4
BART-NOTRUMP INTERFACE

The BASH Code, designed to simulate the reflood portion of a LOCA transient in a PWR, uses NOTRUMP to model the loops outside the reactor core and BART for the core thermal hydraulics.

Starting with the upper plenum, all the loop components including the downcomer and the lower plenum are modeled as NOTRUMP nodes. BART, modeling the reactor core, has two interfaces with the NOTRUMP nodes:

1. Core-upper plenum interface (at the top of the core)
2. Core-lower plenum interface (at the bottom of the core)

The data transfer between the two codes provides the necessary boundary conditions for both codes.

The conditions in the core, determined by BART, are sensitive to the flooding rate and the inlet fluid conditions. A large inlet velocity, in general, leads to an increase in the mass flow rate out of the core and eventually to an increase in the pressure in the upper plenum. An increase in this pressure, which works against the downcomer head, then forces the flooding rate to decrease.

4.1 CORE PRESSURE DROP

To evaluate pressure drop in the core, the conservation of momentum for unit flow area is written as follows (refer to Figure 4-1)

$$\frac{\partial}{\partial t}\int_{Z_1}^{Z_N} \rho u dz = \left(\begin{array}{l}\text{Rate of momentum}\\ \text{entering at } Z_1\end{array}\right) - \left(\begin{array}{l}\text{Rate of momentum}\\ \text{leaving at } Z_n\end{array}\right) \qquad (4\text{-}1)$$

$$- (P_N - P_1) - \int_{Z_1}^{Z_N} \rho_s g dz - \Delta P_{friction}$$

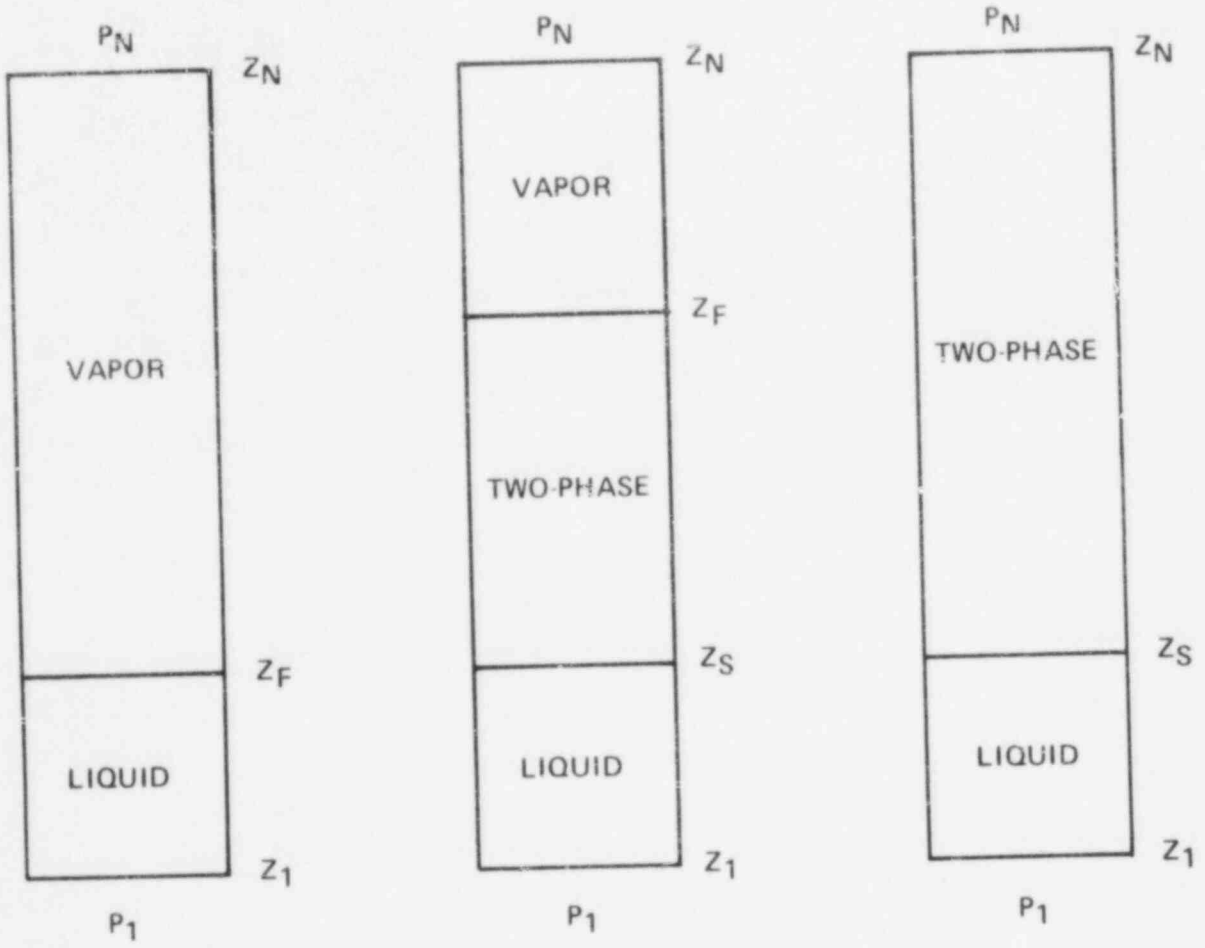

P_N = PRESSURE AT TOP OF CORE

P_1 = PRESSURE AT BOTTOM OF CORE

Z_S = LOCATION OF SUBCOOLED LIQUID, TWO-PHASE INTERFACE

Z_F = LOCATION OF TWO-PHASE VAPOR INTERFACE OR LOCATION OF SUBCOOLED LIQUID – VAPOR INTERFACE

ρ_s = STATIC DENSITY = $\alpha \rho_V + (1 - \alpha) \rho_\ell$

$\rho u dz$ = MOMENTUM OF MASS IN ELEMENT dZ

= $[\alpha \rho_V \quad U_V + (1 - \alpha) \rho_\ell U_\ell]\, dz$

Figure 4-1. Core Pressure Drop Model

The rate of momentum entering (or leaving) the core is given by $\alpha \rho_v U_v^2 + (1-\alpha) \rho_\ell U_\ell^2$ evaluated at Z_1 (or Z_n).

The first and second terms on the right-hand side of Eq. (4-1), taken together, represent the pressure drop due to acceleration of the mass through the core. The third term is the total pressure drop in the core, whereas the fourth term denotes the pressure drop due to gravitational forces.

When all three regions, namely subcooled liquid, two-phase, and vapor, exist in the core, the left hand side of Eq. (4-1) is written as

[ ]a

Using Leibniz's Theorem for the three integrals and after simplification, we obtain

[ ]a (4-2)

Z_F^+ refers to the location just upstream of Z_F, whereas Z_F^- refers to the location just downstream of Z_F. Assuming that (ρL) remains constant in the subcooled liquid region:

[ ]a (4-3)

The above equation is modified according to the type of interfaces in the core at any particular time in the transient, as shown in Figure 4-1.

The pressure drop in the core is therefore given by:

[a

(4-4)

In Eq. (4-4), $\Delta P_{gravity}$ represents the major part of the total core pressure drop.

$$\Delta P_{gravity} = \int_{Z_1}^{Z_N} \rho_s \, g dZ$$

The frictional pressure drop is calculated by using a suitable friction factor representing the total resistance of fuel assemblies and grids. The rate of momentum stored at the two-phase vapor interface is denoted by the next two terms in the equation. These terms drop out of the equation once this interface moves out of the core.

$(Z_s - Z_1) \frac{\partial}{\partial t} (\rho u)$ represents the pressure drop due to inertia of the liquid in the liquid region of the core. The last two terms in Eq. (4-4), which account for the pressure drop due to the time rate of change of momentum in the two-phase and vapor regions, contribute little to the total pressure drop and are presently ignored.

4.2 BART-NOTRUMP INFORMATION TRANSFER

In the BART-NOTRUMP combination, NOTRUMP determines the flooding rate to be used in BART, which in turn feeds back to NOTRUMP the apropriate mass flow rate into the upper plenum and the core pressure drop. The pressure drop in the core added to the upper plenum pressure provides the pressure at the lower plenum, required by NOTRUMP as a boundary condition for the flow link from the lower plenum to the core.

The sequence of calculations within BART and NOTRUMP is shown schematically in Figure 4-2. The figure also summarizes the specific information transferred between the codes. The calculational sequence is listed below:

BART

1. Select a time step Δt
2. Perform calculations to evaluate new conditions at time $t + \Delta t$
3. Calculate quantities required by NOTRUMP
4. Transfer to NOTRUMP the following data:
    a. Mass flow out of the core
    b. Enthalpy of fluid leaving the core
    c. Core pressure drop
    d. Fluid thermodynamic conditions at the bottom of the core
    e. Core liquid level
    f. Time in the transient

BART - NOTRUMP DATA TRANSFER

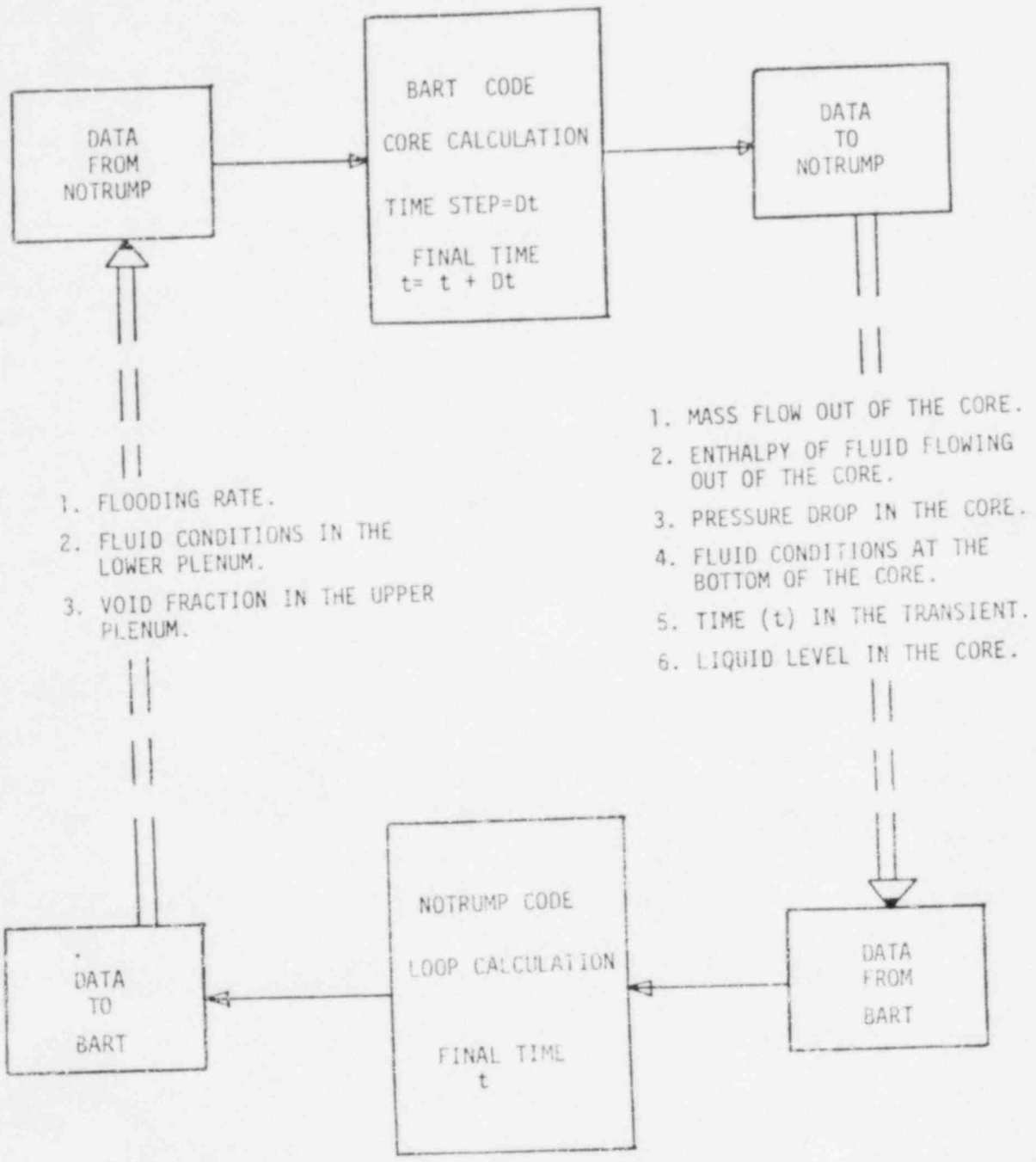

Figure 4-2. BART - NOTRUMP Data Transfer

[[a]

SECTION 5
BART MODIFICATIONS FOR BASH

The BART code described in Reference [2] is a thermodynamic model of the fuel rod bundle under conditions encountered during the reflood transient. The model has been extensively verified against FLECHT tests, as indicated in the reference. This section describes several model improvements and modifications made to the original BART code to make possible calculation of flow blockage and grid effects during the reflood portion of the accident.

A key aspect of the reflood transient is the presence of a dispersed droplet regime in highly superheated steam at upper elevations in the core. The heat transfer process may also be affected by flow oscillations induced by core-RCS loop feedback effects.

For integration into BASH, several areas were identified in which BART could be improved to yield significantly better predictions of real core response to transients:

1. Possible flow reversal in the core

2. The effects of flow blockage

3. Rod support grid effects

5.1 MODELS

In the following sections, the various models are outlined. A detailed description and verification of these models appears in Reference [8]. The BART code with these model improvements is applicable to the analysis of reflood transients in which reverse core flow and cladding ballooning and rupture occur. The calculation is mechanistic and is a best-estimate in the thermal/hydraulic area. The cladding swelling and flow blockage models remain conservative because of the manner in which flow blockage is calculated.

5.1.1 Nonequilibrium Two-Phase Fluid Model

A one-dimensional nonequilibrium two-phase fluid model is used in BASH to determine the local fluid conditions in the core as a function of time.

The basic regions of interest are:

1. Single-Phase Region -- Equations written for this region and their solutions are valid for single-phase (subcooled) liquid and single-phase (superheated) vapor.

2. Two-Phase Region -- This region covers the major portion of the core during the reflood transient. The flow regimes considered are: inverted annular, transition, and droplet. Nonequilibrium between the phases allows the vapor to be superheated while the liquid is assumed to be at saturation temperature.

The details of modeling the single-phase and two-phase regions, along with their equations, are provided in Reference [2].

5.2 REVERSE FLOW MODEL

Since oscillations in the flooding rate are expected during the reflood transient, the BART code was modified to handle both the negative and positive flows.

In the single-phase region, the calculational scheme is not much different for the two cases if the integrations of the equations are performed in the right direction. However, the procedure for void fraction calculation in the two-phase region is dependent on the direction of the void propagation.

5.2.1 Void Propagation Velocity

The mass conservation equation for the mixture, which is one of the equations

describing the dynamic behavior inside the core, is given by:

$$\frac{\partial}{\partial t}\left[\alpha\rho_v + (1-\alpha)\rho_\ell\right] + \frac{\partial}{\partial x}\left[\alpha\rho_v U_v + (1-\alpha)\,\rho_\ell U_\ell\right] = 0 \qquad (5\text{-}1)$$

In Eq. (5-1), α refers to void fraction; U_v, U_ℓ the vapor and liquid velocities; ρ_v, ρ_ℓ, the vapor and liquid densities.

The volumetric flux j is defined as

$$j = \alpha U_v + (1-\alpha)U_\ell \qquad (5\text{-}2)$$

In a manner similar to Reference [9], Eq. (5-1) can be converted into the void propagation equation.

Introducing U_r as the relative velocity between the phases, we have:

$$U_r = U_v - U_\ell$$

$$U_v = j + (1-\alpha)\,U_r \qquad (5\text{-}3)$$

and

$$U_\ell = j - \alpha U_r$$

1) Film and Transition Regimes (Drift flux model)

Equation (5-1) can be converted into the void propagation equation of the form

$$\frac{\partial\alpha}{\partial t} + V_\alpha \frac{\partial\alpha}{\partial x} = A \qquad (5\text{-}4)$$

With U_v, and U_ℓ as given by Eq. (5-3), Eq. (5-1) simplifies to

$$\frac{\partial \alpha}{\partial t} + \left[j + (1-2\alpha)\, U_r + \alpha(1-\alpha)\, \frac{\partial U_r}{\partial \alpha} \right] \frac{\partial \alpha}{\partial x} = \frac{\alpha}{(\rho_\ell - \rho_v)} \frac{d\rho_v}{dt} + \frac{\rho_s}{(\rho_\ell - \rho_v)} \frac{\partial j}{\partial x} \tag{5-5}$$

where

$$\rho_s = \alpha \rho_v + (1-\alpha)\, \rho_\ell$$

Comparing with Eq. (5-4), the void propagation velocity is given by

$$V_\alpha = j + (1-2\alpha)\, U_r + \alpha(1-\alpha)\, \frac{\partial U_r}{\partial \alpha} \tag{5-6}$$

This can also be written as

$$V_\alpha = j + (1-\alpha)\, U_r + \alpha \frac{\partial}{\partial \alpha} \left[(1-\alpha)\, U_r \right] \tag{5-6a}$$

or

$$V_\alpha = j + \frac{\partial}{\partial \alpha} \left[\alpha(1-\alpha) U_r \right] \tag{5-6b}$$

ii) Droplet regime:

a) In this regime, the droplet velocity U_ℓ is determined by the droplet acceleration equation. Equation (5-1) can thus be written as

$$\frac{\partial \alpha}{\partial t} + U_\ell \frac{\partial \alpha}{\partial x} = \frac{\alpha}{(\rho_\ell - \rho_v)} \frac{d\rho_v}{dt} + \frac{\rho_v}{(\rho_\ell - \rho_v)} \frac{\partial j}{\partial x} + (1-\alpha) \frac{\partial U_\ell}{\partial x} \tag{5-7}$$

From Eq. (5-7), one obtains the characteristic velocity as

$$V_\alpha = U_\ell \tag{5-8}$$

b) If the droplets move with terminal velocity with respect to the vapor, the relative velocity U_r becomes independent of void fraction α. Then,

$$\frac{\partial U_r}{\partial \alpha} = 0$$

From Eq. (5-6), therefore, void propagation velocity is given as

$$V_\alpha = j + (1-2\alpha)\, U_r \tag{5-9}$$

The core fluid dynamic models in BART use void propagation approach for calculating the void fractions in the nodes. Since calculations are done on a node-by-node basis, the method of calculation of void fraction α for a node depends on the directions of void propagation velocities (V_α) at the boundaries of the node.

Two void fractions α_m and α_p i.e., void fraction within a node and void fraction at the boundary, are defined for each node. The mass conservation equation for each node is then solved to obtain the void fraction α_m.

The way α_m and α_p are related to each other depends on the direction of velocity, V_α, as α_p is taken as the void fraction of the donor node. For example,

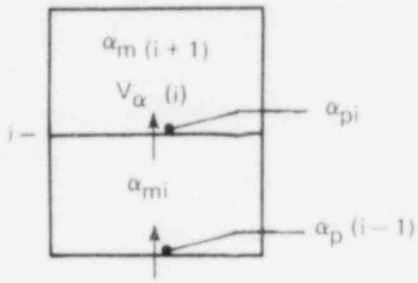

$$\alpha_{pi} = \alpha_{mi} \text{ if } V_\alpha(i) \text{ is positive}$$

and

$$\alpha_{pi} = \alpha_{m(i+1)} \text{ if } V_\alpha(i) \text{ is negative}$$

Depending on the directions of V_α at the boundaries of a node, four different cases exist. BART calculations (implicit) for α_m are performed using new time values for α_m, and as such, logic in the code is designed to handle the calculations for each of the above-mentioned four cases separately.

The four cases are:

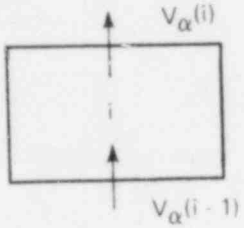

CASE 1

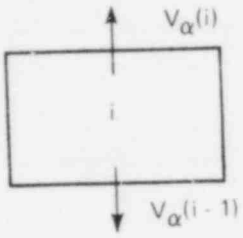

CASE 2

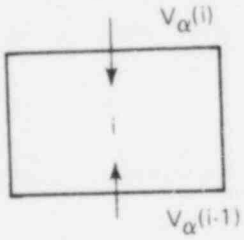

CASE 3

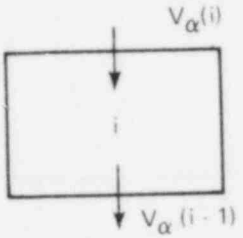

CASE 4

5.2.2 Numerical Solution

From the known local fluid and heat transfer conditions at time t, the fluid flow equations are solved numerically to obtain the conditions at time $t + \Delta t$. The numerical solution procedure explained in this section supplements the one given in Reference [2].

In determining the void fraction from the mixture mass conservation equation, since calculations are done in the direction of void propagation velocity (V_α) using implicit differencing, no time step size limitation due to numerical instability arises.

For a control volume i, the boundaries i and i-1 are as defined below.

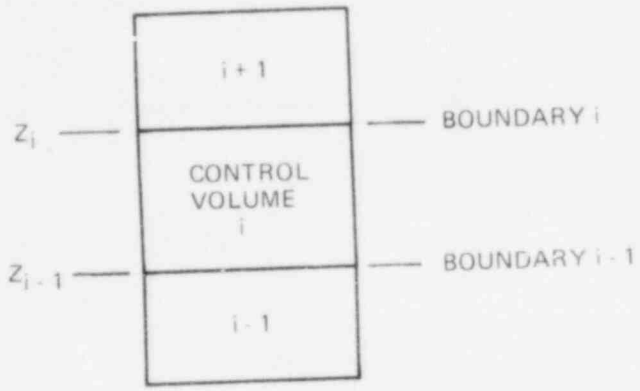

The void fraction α_{mi} refers to the void fraction in the control volume i, whereas the velocities are defined at the volume boundaries, so that U_{ℓ_i}, j_i, etc. correspond to the boundary i of control volume i.

The void fraction (α_p) required for mass flow calculation at a volume boundary is obtained from the donor node based on the direction of V_α. The mass flow rate at a boundary i is

$$\alpha_{pi} \cdot U_{v_i} \cdot \rho_{v_i} + (1-\alpha_{pi})\, U_{\ell_i} \cdot \rho_\ell$$

Since velocities are defined at the node boundaries, it is appropriate to use α_p as the void fraction in Eqs. (5-2) and (5-3).

[ ]a

and is the mass flow rate at the boundary i-1. ρ_j is called the flowing mixture density. This mass flow at the boundary i-1 is known from an earlier calculation for control volume i-1. (Superscript n+1 denotes the new time level).

Denoting $\rho^{n+1}_{j_{i-1}} J^{n+1}_{i-1}$ by XM and using Eqs. (5-3), (5-10) simplifies to

[redacted] (5-11)

The relative velocity Ur_i used in the calculation is based on the present known value of α_i. Equation (5-11) can be solved to obtain α^{n+1}_i. $U^{n+1}_{v_i}$ and $U^{n+1}_{\ell_i}$ are then calculated from Eq. (5-3).

Case 2.

When the void fraction propagates in opposite directions (outward) at the two boundaries of a control volume, void fraction in the control volume is calculated by setting

$$\alpha_{p_{i-1}} = \alpha_{p_i} = \alpha_{mi}$$

The relative velocity Ur_{i-1} becomes the same as Ur_i, as both are functions of the void fraction α_i.

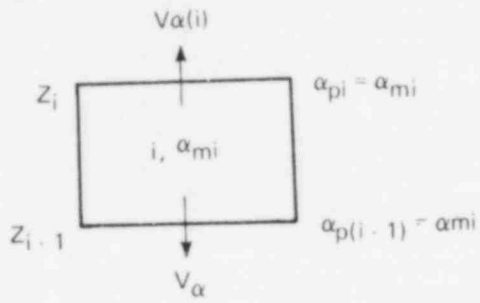

Equation (5-1) in finite difference form becomes

[a

(5-12)

(5-13)

]

Case 3.

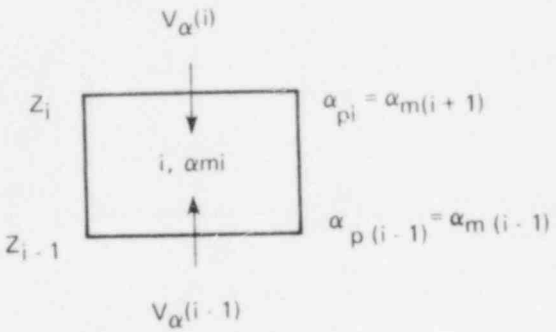

Void fractions $\alpha_{m_{i-1}}$ and $\alpha_{m_{i+1}}$ are known from the solutions for control volumes i-1 and i+1.

Mass balance for control volume i, gives

[a

(5-14)

[

Case 4.

In this configuration, V_α is negative at both the boundaries, so that

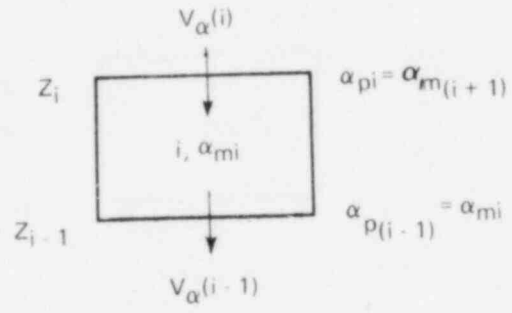

The mass conservation equation in finite difference form, after simplification, yields the following equation for void fraction α_1^{n+1}.

[a

(5-15)

(5-16)

$(\rho_{j_i}^{n+1} \; J_i^{n+1})$ is the mass flow rate at the boundary i.

$U_{r_{i-1}}$ is the relative velocity calculated from the present known value of α_i.

2. Droplet Regime

Liquid velocity U_ℓ is first calculated from the droplet acceleration equation. The mass conservation equation is then used for getting the void fraction in the node.

5.2.3 Number Density

In the droplet regime, a variation in droplet diameter is related to the total droplet heat flux q_d'' by

$$\frac{\partial D_d}{\partial t} + U_\ell \frac{\partial D_d}{\partial x} = - \frac{2q_d''}{\rho_\ell H_{\ell v}} \qquad (5\text{-}18)$$

where $H_{\ell v}$ is the latent heat of vaporization, ρ_ℓ the liquid density and D_d the droplet diameter.

Liquid mass conservation equation in this region gives

$$\frac{\partial}{\partial t} \left[(1-\alpha)\rho_\ell\right] + \frac{\partial}{\partial x} \left[(1-\alpha)\rho_\ell U_\ell\right] = - \frac{6q_d''(1-\alpha)}{D_d H_{\ell v}} \qquad (5\text{-}19)$$

Defining droplet number density n_d as

$$n_d = \frac{(1-\alpha)6}{\pi D_d^3}$$

the above two equations can be combined to obtain

$$\frac{\partial n_d}{\partial t} + \frac{\partial}{\partial x}(n_d U_\ell) = 0 \qquad (5\text{-}19)$$

Equation (5-19) is the equation for conservation of number of droplets and can be used in the droplet regime for calculating the number density of droplets. The droplet diameter is then obtain from

$$D_d = \left[\frac{6(1-\alpha)}{n_d \pi} \right]^{1/3} \qquad (5\text{-}20)$$

The above principle of conservation of number of drops, applied to a control volume, can be written as:

[Rate of change of number of drops in a volume] =

[Rate of number of drops entering the volume] - [Rate of number of drops leaving the volume].

To calculate the droplet diameter, the droplet number density equation is solved first to obtain the droplet number density in a control volume i.

The finite difference form of this equation is

$$\frac{(n_{d_i}^{n+1} - n_{d_i}^{n})}{\Delta t} + \frac{(n_d U_\ell)_i^{n+1} - (n_d U_\ell)_{i-1}^{n+1}}{\Delta Z_{i-1}} = 0 \qquad (5\text{-}21)$$

The droplet number densities and the velocities in the two terms $(n_d U_\ell)_i^{n+1}$ and $(n_d U_\ell)_{i-1}^{n+1}$ denote their values at the two boundaries i and i-1, respectively, of the control volume i. Number densities being defined within control volumes, n_d at the boundary i can be n_{d_i} or $n_{d_{i+1}}$ depending on whether U_{ℓ_i} is greater or less than zero.

Droplet diameter is then given as

$$D_{d_i}^{n+1} = \left[\frac{6(1-\alpha_i^{n+1})}{n_{d_i}^{n+1} \pi} \right]^{1/3} \qquad (5\text{-}22)$$

5.3 FLOW BLOCKAGE MODELS

5.3.1 Clading Swelling and Flow Blockage

Appendix K of 10CFR50 requires that the effects of flow blockage due to fuel rod cladding swelling and burst be taken into account in a LOCA analysis. In addition, the flow blockage to be used for the analysis is to be calculated as described in NUREG 0630.[10]

The methods used to calculate fuel rod cladding swelling, burst, and flow blockage in the Westinghouse ECCS evaluation model are described in detail in the LOCTA[5] and 1981 Evaluation Model reports.[1] As described in Section 2, the thermal and mechanical response of the fuel rod will be calculated in BASH using the LOCTA code. Thus, the models described in the above references are used in an identical manner in this report. The difference among previous models and this model arises in the calculation of flow redistribution and thermal-hydraulic conditions in and near the blockage zone and in the treatment of grid effects.

5.3.2 Flow Distribution Model

A flow redistribution model was developed to calculate the flow around strained and burst fuel rod arrays in BART. The model employs two channels in

which thermal-hydraulic conditions are calculated using the basic BART equations and between which flow is calculated using a simplified set of axial and radial momentum equations. There are two assumptions employed in the flow redistribution model:

1. The flow redistribution is by steam only. This assumption rests on the fact that droplets possess significant inertia and cannot easily be deflected from their axial path through the bundle.

2. The steam crossflow can be adequately calculated with simplified momentum equations outlined in Reference [8]. The applicability of these equations is demonstrated in the detailed description and verification of the model.[8]

5.3.2.1 Two-Channel Model -- Two BART channels are employed to calculate steam flow redistribution from a blocked channel. The two-channel model is illustrated in Figure 5-1. Calculations begin at the point where dispersed droplet flow is first calculated. At this location, axial flow is assumed uniform and the crossflow is assumed to be zero. It is assumed that the blocked assembly resides in an infinite array of unblocked assemblies. This will maximize the flow out of the hot assembly. Conditions in each channel are calculated using the models described in References [2] and [8].

One of the primary objectives of the improved BART code models is to calculate the local heat transfer effects caused by the fuel rod blockage interaction with the two-phase flow.

A review of the available flow blockage data indicates that there are perhaps four heat transfer effects which need to be examined during reflooding:

1. Flow redistribution effects due to blockage and their effect on the enthalpy rise of the steam behind the blockage. Bypass of steam flow may result in increased superheating of the remaining steam flow behind the blockage region. The higher the steam temperature, the lower the rod heat flux and resulting heat transfer behind the blockage.

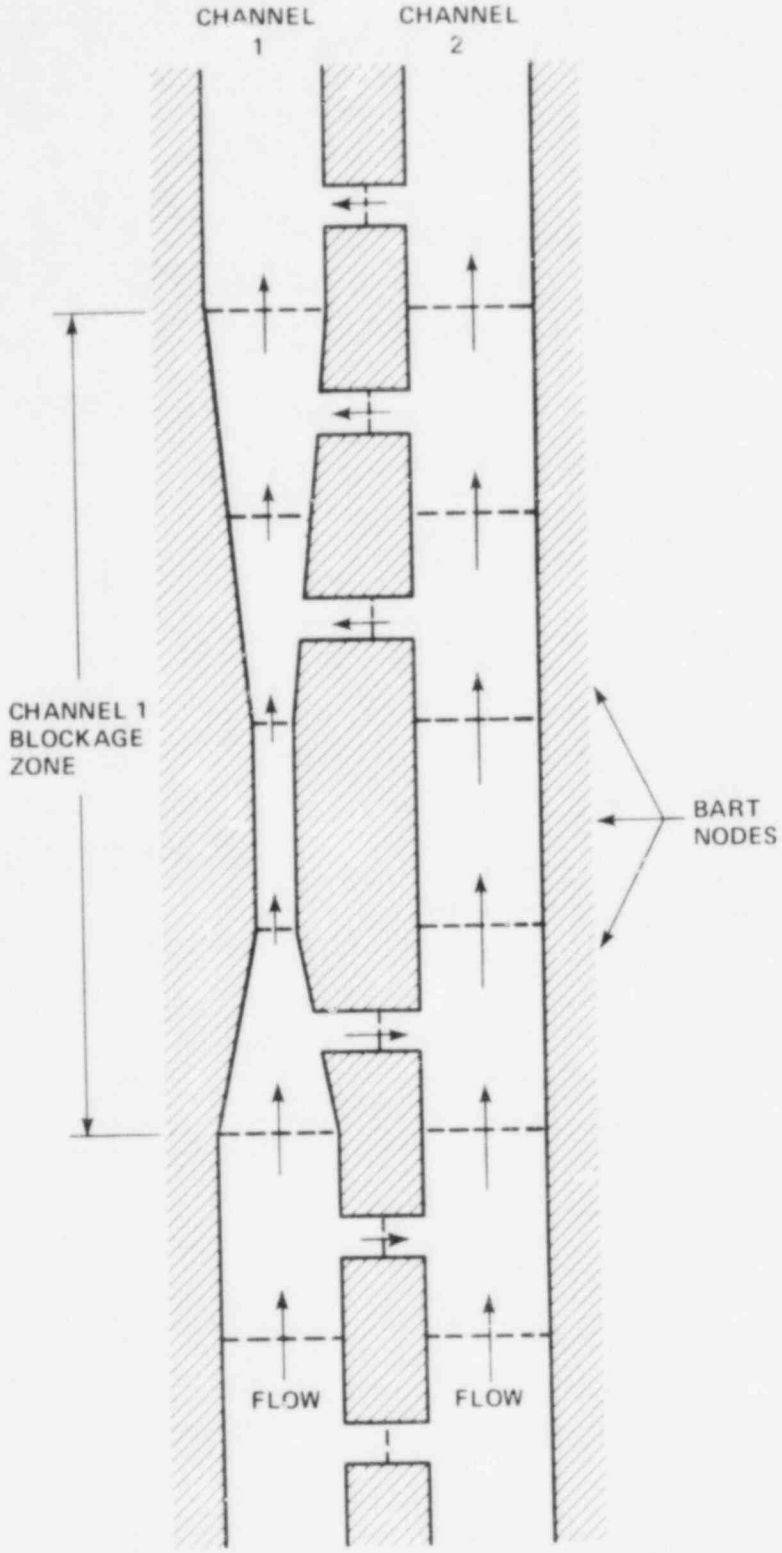

Figure 5-1. Visualization of the Two-Channel Flow Redistribution Model

2. Effect of blockage downstream of the blockage zone and the resulting mixing of the steam and droplet breakup behind the blockage. The breakup of the entrained water droplets will increase the liquid surface area so that the drops will become a more effective heat sink for the steam. The droplet breakup should desuperheat the steam; this would result in greater rod heat transfer behind the blockage zone in the wake of the blockage. The crossflow effects of the vapor can also enhance the cooling of adjacent rods.

3. The heat transfer effects in the immediate blockage zone due to drop impact, breakup, and mixing, as well as the increased steam velocity due to blockage flow area changes. The drop breakup is a localized effect primarily caused by the blockage geometry; it will influence the amount of steam cooling which can occur farther downstream of the blockage.

4. Effect of blockage on the upstream region of the blockage zone due to steam bypass, droplet velocities, and sizes.

In simpler terms, the flow blockage heat transfer effects are a combination of two key thermal-hydraulic phenomena:

1. A flow bypass effect, which reduces the mass flow in the blocked region and consequently decreases the heat transfer

2. A flow blockage effect, which can cause flow acceleration, droplet breakup, improved mixing, steam desuperheating, and establishment of new boundary layers, which consequently increases the heat transfer.

These two effects are dependent on the blockage geometry, the amount of blockage, and the flow regime (single- or two-phase). They counteract each other such that it is not evident which effect dominates over a range of flow conditions.

Since the BART code is a best-estimate, state-of-the-art model which can mechanistically account for individual heat transfer effects, it was felt that a basic heat transfer approach of modeling individual blockage heat transfer effects listed above was possible.

The blockage is modeled differently depending upon which phase interacts with the blockage. For the vapor flow, the blockage is assumed to act as a converging-diverging region and flow separation, reattachment, wake effects, and increased turbulence in the vapor phase and is accounted for downstream of a separation point.

For the liquid phase, the blockage is modeled as a droplet impacting and shattering surface which is above the wetting temperature. Droplets will bounce or shatter as they hit the blockage surface and will provide a direct wall-to-drop heat flux component as well as an additional source of saturated vapor.

With the mechanistic models currently in BART, the single-phase flow redistribution and acceleration can be calculated around and in the blockage zone. The vapor acceleration effects will increase the droplet/vapor heat transfer resulting in additional generation of saturated vapor. Therefore, the droplet interaction with the blockage and the single-phase acceleration will both provide additional saturated vapor at a given BART node which will then mix with the existing superheated vapor. The combination causes vapor desuperheating at and downstream of the blockage. Criteria on droplet impact heat transfer and droplet breakup are also established to predict these two effects. A detailed description of each model for flow blockage is given in Reference [8].

5.4 GRID HEAT TRANSFER ENHANCEMENT EFFECTS

Spacer grids are structural members in the reactor core which support the rod bundle array at the proper rod pitch. All fuel assemblies have grids at the same elevations in the core so that the core flow is accelerated through the grids at each location and no flow bypass or redistribution occurs. Since the grid is an obstruction in the flow stream, it causes an increased pressure drop due to form and skin friction losses. In addition, the grid may rewet

prematurely and cause droplets to shatter in the two-phase environment encountered during reflood. These effects will cause additional liquid evaporation and desuperheat the steam downstream of the grid, with a resulting improvement in heat transfer.

Models to calculate these effects in BART are developed and described in Reference [8].

SECTION 6
NOTRUMP MODIFICATIONS FOR BASH

6.1 TWO-VOLUME NONEQUILIBRIUM MODEL

At several times and in several parts of the RCS, phase separation occurs during a LOCA. That is, liquid falls to the bottom of a component such as a reactor vessel lower plenum, while vapor collects at the top. To model this phenomenon, a bubble rise, or "stratified" model was developed and incorporated into the NOTRUMP code.[4] The bubble rise model accounts for the flow of vapor from a lower two-phase mixture to an upper, vapor phase. The volume of the two-phase mixture is determined by calculating the rate at which vapor is accumulating in the lower phase.

The bubble rise model is a thermal equilibrium model in which the liquid and vapor are at saturation. Thus, situations in which subcooled water or superheated vapor are injected into the volume cannot be adequately analyzed. In addition, the upper phase of the bubble rise model is assumed to be vapor. Therefore, situations in which the upper phase is a dispersed droplet mixture (such as would occur in the upper plenum during reflood), cannot be modeled.

To account for these and other special situations the following two-volume nonequilibrium model has been put into the NOTRUMP code.

6.1.1 Two-Volume Model Pressure Calculation

Let two fluid volumes i and j be connected to each other and to other nodes in the system as shown in Figure 6-1. This arrangement is typical of node connections in NOTRUMP. The number and nature of flow links which connect the two volumes to other fluid nodes in the system is arbitrary; however, for physically realistic situations some restrictions apply, as will be discussed later.

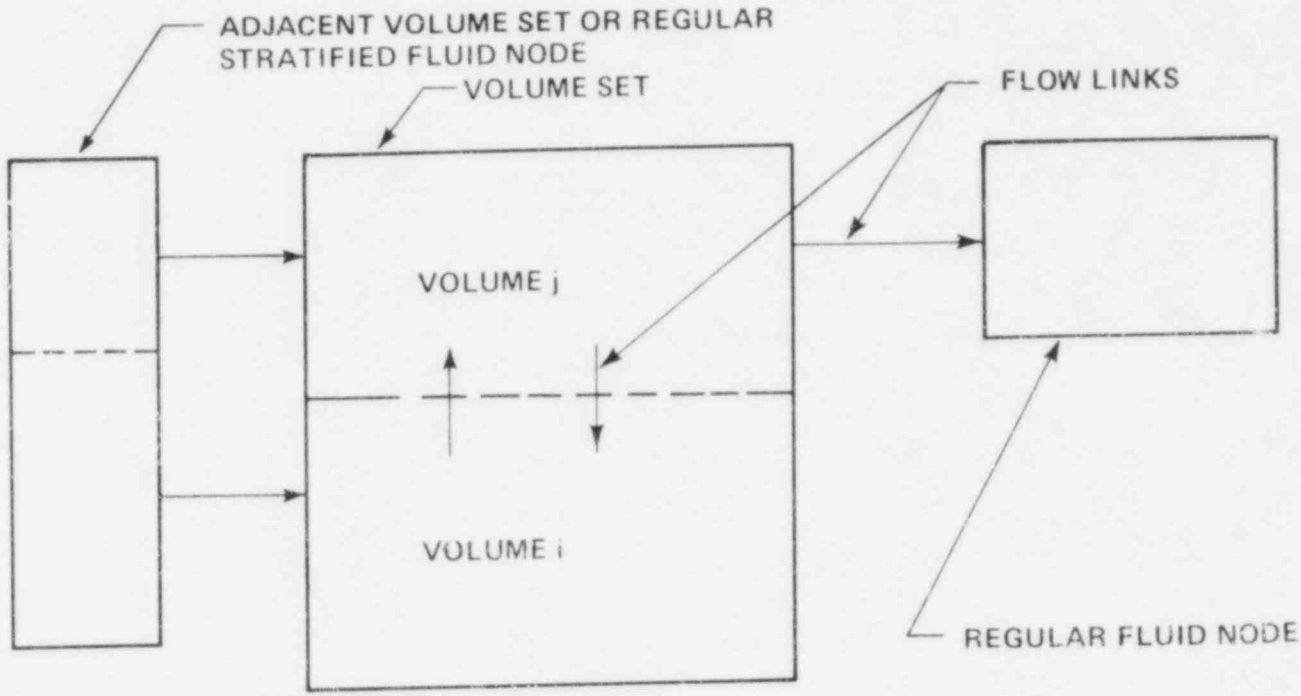

Figure 6-1. Possible Connections from Volume Set i, j to Other Fluid Nodes

At each new time step a mass and energy balance over every fluid node yields new values of total mass, M, and internal energy, E. At the end of the integration step, the pressure is obtained in each regular fluid node by iteration using an equation of state. For each pair of a volume set, however, the pressures are assumed to be equal. To satisfy this condition, the relative size of each volume in the pair is allowed to change.

The specific volume of each control volume in the set is given by:

$$V_i = X_V \, V_T / M_i \tag{6-1}$$

$$V_j = (1 - X_V) \, V_T / M_J \tag{6-2}$$

where

X_v = V_i / V_T

V_i = volume of node i

V_T = total volume of volume pair

= $V_i + V_J$

The specific volumes calculated by Eqs. (6.1) and (6.2) must be equal to the specific volumes calculated by an equation of state using P, h_i, and h_j; that is,

[a

(6-3)

(6-4)

(6-5)

(6-6)

]

M_I, M_J, E_I, and E_J are known. The unknowns p and X_v are found by iteration using the following recursion formulas:

[a]

(6-7)

(6-8)

(6-9)

(6-10)

(6-11)

(6-12)

(6-13)

After convergence, other thermodynamic properties are calculated and fluid node geometric quantities, such as node height, are adjusted.

6.1.2 Flow Links

A typical application of the two-volume model is shown in Figure 6-2. It can be seen that, to accurately represent some of the flows entering and leaving the volumes, each volume of the pair must have the capability to "share" a pipe. This is accomplished by supplying each volume with a flow link representing the pipe. If the top of the lower volume is below the pipe, all flow through the pipe is from the upper volume. If the top of the lower volume is above the pipe, all flow is from the lower volume. Finally, if the top of the lower volume is within the pipe region, as shown in Figure 6-2, then each flow link shares a fraction of the total pipe area.

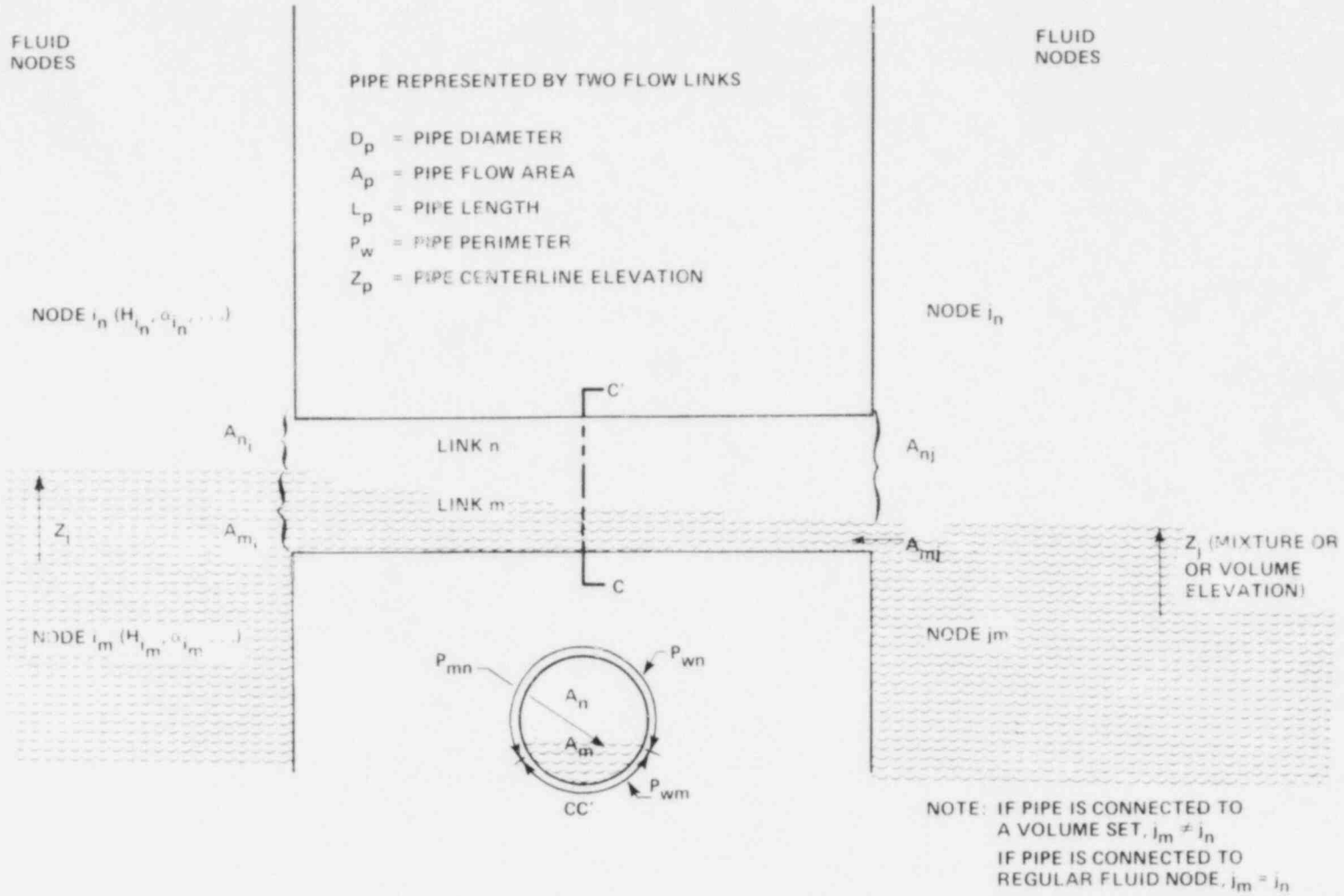

Figure 6-2. Typical Link Connection Between Volume Sets and Fluid Nodes

The momentum equation for each member of a flow link pair such as the one shown in Figure 6-2, contains an additional interfacial friction term. For example, for flow link m, the NOTRUMP momentum equation is:

$$d W_m/dt = (A_m/L_p)(\Delta p - F_{wm}/A_m - F_{mn}/A_m) \quad (6\text{-}14)$$

where

Δp = pressure difference across L due to pressure gradient, elevation change

W_m = flow rate in link m

A_M = flow area of link m

L_p = length of pipe

F_{wm} = force on link m due to friction on solid surfaces

F_{mn} = force due to friction between links m and n

In NOTRUMP, momentum exchange is given in terms of link mass flowrate for the wall force and relative velocity for the interface force:

[ ]a (6-15)

(6-16)

(6-17)

[ ] a (6-18)

where

C_d = loss coefficient (wall or interface)

f_{wm} = wall friction factor

f_{mn} = interface friction factor

P_{wm} = perimeter of pipe which is wet by link m

P_{mn} = interface area per unit length

ρ_c = continuous phase density (depends on flow regime)

A_{om} = projected area in link m of resistance C_d

Equations similar to (6-17) and (6-18) can be derived for link n

The various void fractions which will be used in the two-volume model should be defined at this point (see Figure 6-2):

Let:

α = volume occupied by link n in the pipe

= $A_n/(A_m + A_n) = A_n/A_p$

α_n = void fraction within flow link m

α_m = void fraction within flow link m

a_{i_m}, a_{i_n}, a_{j_n} = void fraction in fluid nodes i_m, i_n, j_m and j_n.

A flow link pair can be connected to two volume sets, or to one volume set and one regular fluid node. In each case, the link void fractions α_n, α_n, α, are defined as follows:

a) Flow Link between two volume sets

$$\begin{aligned}
\alpha &= A_{n_i}/A_p && , \quad \text{if } W_m > 0,\ W_n > 0 \\
\alpha &= A_{n_j}/A_p && , \quad \text{if } W_m < 0,\ W_n < 0 \\
&= 0.5\,(A_{n_j}/A_p + A_{n_i}/A_p) && , \quad \text{if } W_m \cdot W_n < 0 \\
\alpha_n &= \alpha_{in} && , \quad \text{if } W_n > 0 \\
&= a_{jn} && \quad W_n < 0 \\
\alpha_m &= \alpha_{im} && , \quad \text{if } W_m > 0 \\
&= \alpha_{jm} && \quad W_m < 0
\end{aligned} \tag{6-19}$$

The areas A_{mi}, A_{ni}, A_{nj} are defined by the volume heights. The relationship between flow link cross-section areas and volume heights is based on the geometry of a horizontal pipe of circular cross-section, as indicated in Figure 6-2:

$$A_{mi} = [\theta_{mi} - \tfrac{1}{2} \sin(2\theta_{mi})]\, D_p^{\,2}/4 \tag{6-20}$$

where

θ_{mi} = $\frac{1}{2}$ the angle subtended by the liquid/vapor interface (radians)

$$\theta_{mi} = \cos^{-1}[2(Z_i - Z_p + D_p/2)/D_p]$$

b. Flow link between a volume set and a stratified fluid node

If (i_m, i_n) represents the two-phase mixture and upper vapor phase of a stratified fluid node, α_{im} is equal to the mixture void fraction and α_{in} is equal to one. Otherwise the same relationships as in "a" are employed to calculate α, α_m, and α_n.

c. Flow link between volume set and homogeneous fluid node

If (i_m, i_n) represents a homogeneous fluid node, $\alpha_{in'} = \alpha_{in}$, the following apply:

$$\begin{aligned}
\alpha &= \alpha_{i_m} && \text{if } W_m > 0,\ W_n > 0 \\
&= A_{n_j}/A_p && \text{if } W_m < 0,\ W_n < 0 \\
\alpha &= 0.5\,(\alpha_{im} + A_{nj}/A_p) && \text{if } W_m \cdot W_n < 0
\end{aligned} \qquad (6\text{-}21)$$

$$\begin{aligned}
a_m &= 0 && \text{if } W_m > 0 \\
&= \alpha_{jn} && \text{if } W_m < 0 \\
\alpha_n &= 1.0 && \text{if } W_n > 0 \\
&= \alpha_{jn} && \text{if } W_n < 0
\end{aligned}$$

In some cases it is known in advance or can be assumed that a volume will always "cover" a particular flow link. Then a single flow link can be specified, rather than a pair, and upstream and downstream quantities are calculated as in a regular flow link. In this case, the fraction of the pipe occupied by the flow link is always equal to one.

d. Flow Regimes in Horizontal Pipes

As the area occupied by each link in the pipe changes and the link flow rates change, the flow regime in the pipe can be expected to change. In the case of horizontal flow link pairs in which the upper link is nearly all vapor and the

lower link is nearly all liquid, a flow regime map due to Mandhane[11] is used (see Figure 6-3). "Liquid" and "vapor" fluxes are defined by:

$$j_\ell = W_m/\rho_m A_p \qquad (6\text{-}22a)$$

$$j_v = W_n/\rho_n A_p \qquad (6\text{-}22b)$$

The flow regime map is assumed to be applicable if the void fraction in link n is greater than 0.95 and the void fraction in link m is less than 0.4. The following models are then used to calculate the terms E and C in Eqs. (6-10) and (6-11).

e. Flow Regime 1 - Dispersed Flow

Assume droplets with diameter D_d determined by the droplet Weber number, We_d

$$We_d = \rho_n (U_n - U_m)^2 D_d/\sigma \qquad (6\text{-}23)$$

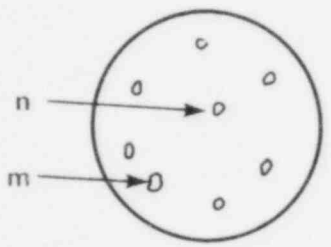

where

$$U_n = W_n/\rho_n A_n \quad , \quad U_m = W_m/\rho_m A_m$$

let $C_d = 0.4$ (typical for spheres in turbulent flow)

A_{om} = total projected area presented to the vapor stream by the droplets

$= 1.5 (1 - \alpha) (A_p) L_p/D_d$

ρ_c = continuous phase density = ρ_n

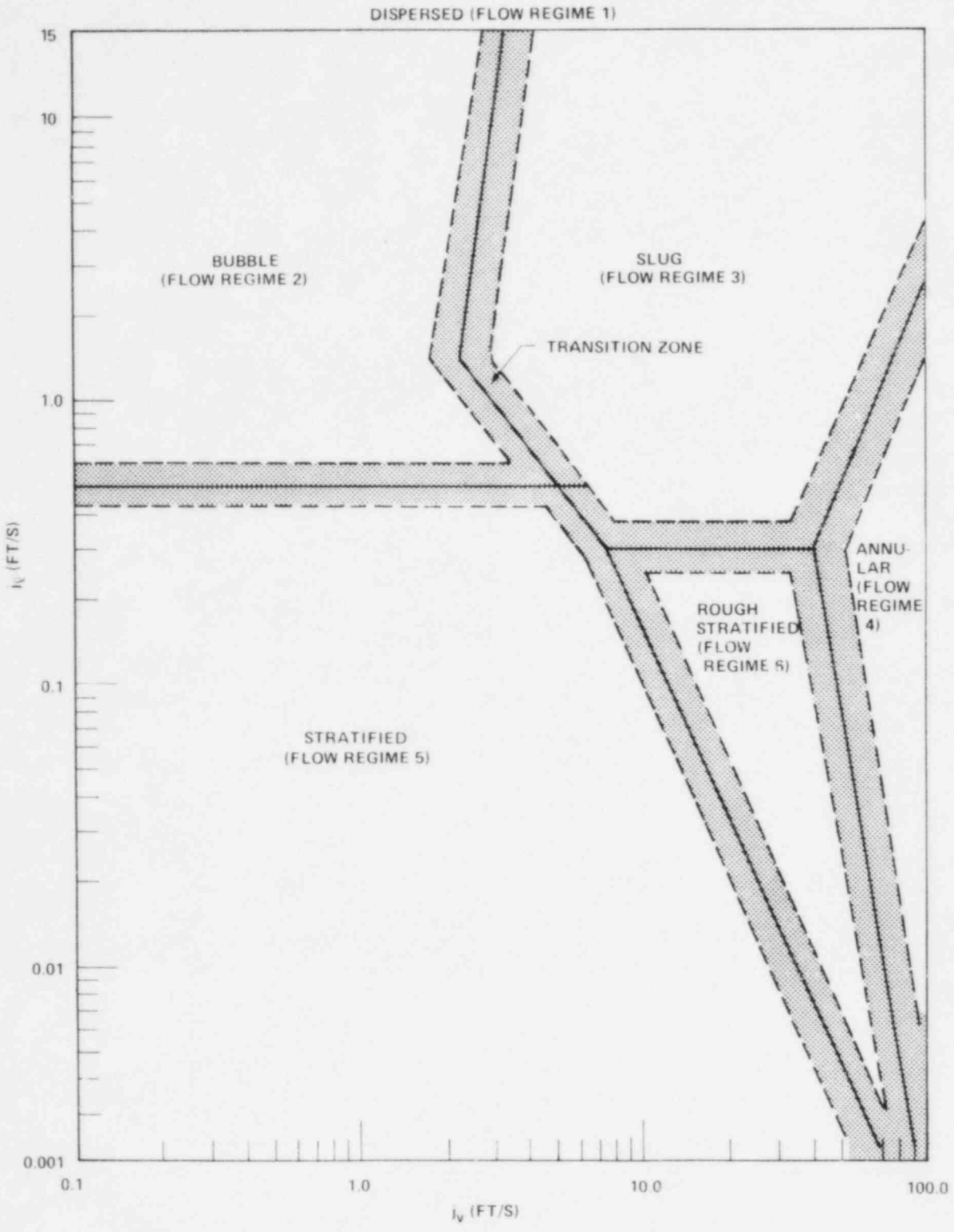

Figure 6-3. Mandhane Flow Regime Map for Horizontal Flow

It is assumed that the droplets make contact with the wall, covering a perimeter proportional to $\alpha^{1/2}$. That is:

$$P_{wm} = P_w (1 - \alpha^{1/2})$$

$$P_{wn} = P_w = \text{pipe perimeter } P_w \alpha^{1/2}$$

The wall friction factor, fw, is calculated using standard single-phase friction formulas; for example,

$$f_{wn} = 0.0055 \left[1 + \frac{20000\ \varepsilon}{D_n} + \frac{10^6}{Re_n}^{1/3}\right] \qquad (6\text{-}24)$$

where

ε = pipe roughness coefficient

$D_n = 4\ A_n/P_{wn}$

$Re_n = W_n\ D_n/(A_n\ \mu_n)$

Thus, for flow regime 1 the quantities $\bar{C}_m$, $\bar{C}_n$, $\bar{E}_m$ and $\bar{E}_n$ are:

[ ]a (6-25)

f. Flow Regime 2 - Bubbly Flow

Assume spherical bubbles of diameter D_b determined by:

$$D_b = 4.7\,[s/(\rho_m - \rho_n)]^{1/2} \qquad (6\text{-}26)$$

In a manner similar to the dispersed regime, the following quantities can be defined:

$$C_{db} = 0.4$$

$$A_{om} = 1.5\,\alpha\,A_p\,L_p/D_b$$

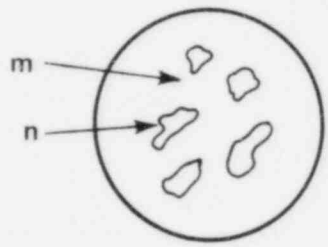

Assume that the bubbles make negligible contact with the wall; then $\bar{C}_m$, $\bar{C}_n$, $\bar{E}_m$ and $\bar{E}_n$ become:

[ ] a (6-27)

g. Flow Regime 4 - Annular Flow

Assume F_{mn} = 0.015 (smooth interface)

$$P_{mn} = 2\,(\pi\,\alpha\,A_p)^{1/2} = \alpha^{1/2}\,P_w$$

$$\bar{C}_m = (f_w\,P_w\,L_p/4)\,(1/2\,\rho_m\,A_m^3)$$

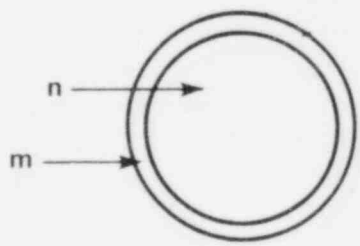

[ ]a

(6-28)

h. Flow Regimes 5 and 6 - Stratified Flow

assume: f_{mn} = 0.015 (smooth)
= 0.1 (rough)

The liquid/vapor, liquid/wall and vapor/wall interfacial areas (P_{mn}, P_{wm} and P_{wn}, respectively) are calculated from geometric principles:

$$P_{mn} = D_p \sin \theta$$

$$P_{wm} = p^{\theta}$$

$$P_{wn} = D_p (\pi - \theta)$$

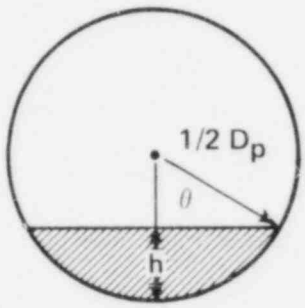

where θ (radians) is given by:

$$\theta = \cos^{-1} \frac{D_p - 2h}{D_p}$$

and h is the height of liquid in the pipe (height of liquid node m).

The interfacial area calculation is exact for the smooth surface but approximate for the rough interface.

[ ]a

(6-29)

[ ] a

1. Flow Regime 3 - Slug

Assume this flow regime is a combination of bubbles and annular flow:

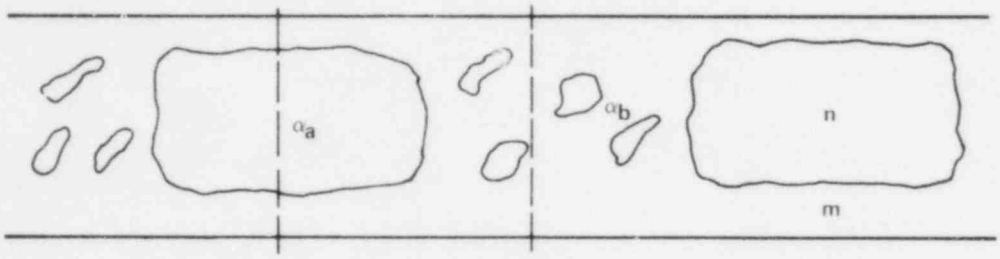

Assume the void fraction α_b in the bubbly regions is 0.1, and the void fraction α_a in the annular regions is 0.9. Then, using the models developed for the bubbly and annular regimes, with the modification that the continuous phase is assumed to be the vapor phase for slug flow.

[ ] a

(6-30)

where

$$F = (a_a - a)/(a_a - a_b)$$

and

$$a_a = \max (a, 0.9)$$

$$a_b = \min (a, 0.1)$$

6.1.3 Mass and Energy Flows Within a Volume Set

Heat and mass transfer across the interface of the two volumes of a volume set occur if the lower volume is subcooled or contains vapor, or the upper volume is superheated or contains liquid as shown in Figure 6-4. The flows between the volumes are given by:

Mass Flow Rate to Vapor Volume = $S_g + S_\ell + \Gamma$

Energy Flow Rate to Vapor Volume = $S_g h_g + S_\ell h_f + \Gamma h_f - q_{i\ell}$

Mass Flow Rate to Liquid Volume = S_f

Energy Flow Rate to Liquid Volume = $S_f h_f$

where

S_g = vapor mass flow rate from lower volume

S_ℓ = liquid mass flow rate from lower volume

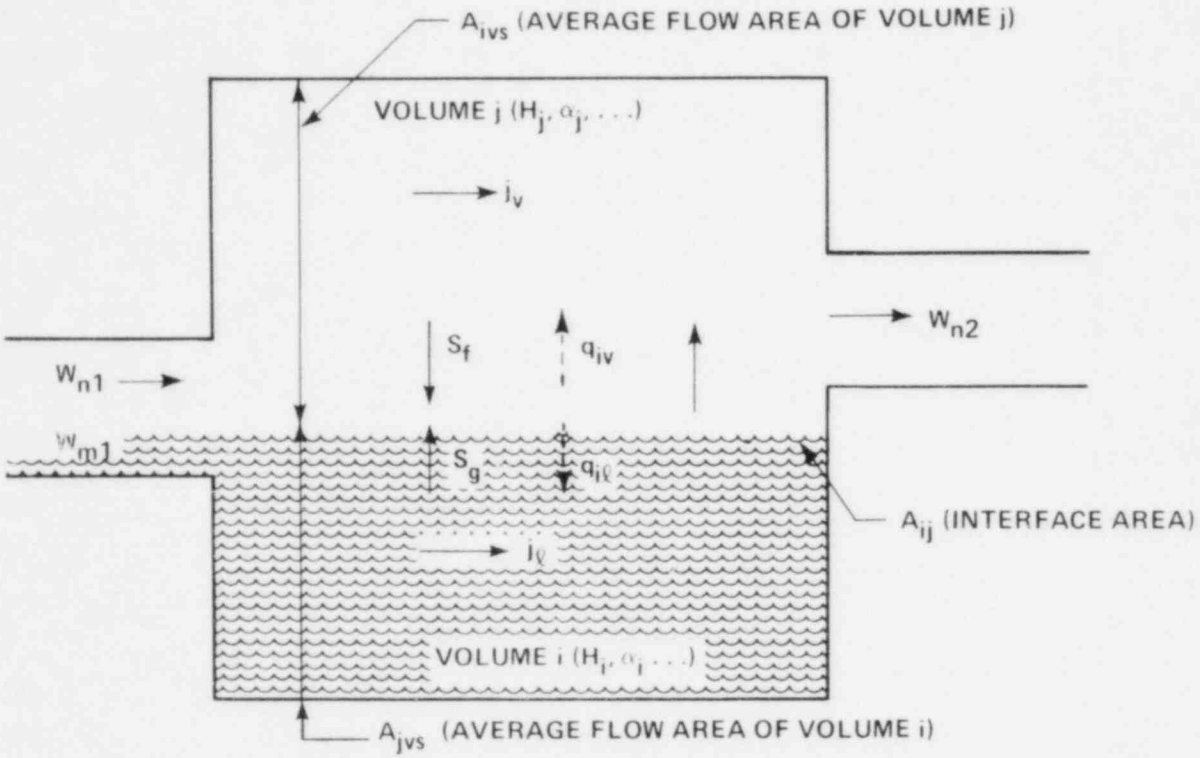

$$A_{vs} = A_{ivs} + A_{jvs}$$

Figure 6-4. Heat and Mass Transfer Within Volume Set

S_f = liquid mass flow rate from upper volume

Γ = net evaporation rate, given by

$\Gamma = (- q_{iv} - q_{i\ell})/h_{fg}$ (See Figure 6-4)

h = enthalpy (Btu/lbm)

$q_{iv} = h_g (T_S - T_J) A_{ij}$ = heat transfer rate to vapor from interface

$q_{i\ell} = h_f (T_S - T_i) A_{ij}$ = heat transfer rate to liquid from interface

a) S_g, S_ℓ, S_f

S_g, S_ℓ amd S_f can be determined by calculating the rate at which vapor and liquid rise through the lower phase and the rate at which liquid falls through the upper volume. It is assumed that the upper volume contains dispersed mixture at void fraction above 0.9 and the lower volume contains bubbly mixture at void fraction below 0.4.

The liquid flow rate from the upper volume, where the droplets fall at terminal velocity, is

$$S_f = (1- \alpha_j) U_{rd} \rho_f A_{ij} \qquad (6\text{-}31)$$

where

$$U_{rd} = [1.33 W_{ed} \sigma (\rho_f - \rho_g) g/(C_{dd} \rho_g^2)]^{0.25}$$

The droplet size is assumed to be controlled by the Weber number, W_{ed}.

At void fractions lower than 0.2, vapor flow rate S_g is calculated using the Yeh correlation[12], and no droplets are assumed to be entrained, giving

$$S_\ell = 0 \qquad (6\text{-}32)$$

and

$$S_g = \rho_g j_g A_{ij} \tag{6-33}$$

where A_{ij} is the interface area, and

$$j_g = U_{rb} [\alpha_i / .925)(\rho_f/\rho_g)^{0.239}]^K$$

$$U_{rb} = 1.53 [\sigma(\rho_f - \rho_g)\, g/\rho_f^2]^{0.25}$$

$$K = 1.49 \quad , \quad \text{if } j_g/U_{rb} \leq 1$$

$$= 2.13 \quad , \quad \text{if } j_g/U_{rb} \geq 1$$

At higher void fractions (>0.2), and depending on the mass flow rates entering and leaving the volume, the vapor flowing through the lower phase may entrain droplets.

The minimum vapor velocity for entraining liquid is taken to be equal to the free-fall velocity assuming a critical Weber number (7.5 - 10) and a suitable drag coefficient (~ 0.45).

$$U_{gm} = \left[\frac{4}{3} \frac{\sigma W_{ed} (\rho_f - \rho_g) g}{C_{dd} \rho_g^2} \right]^{1/4} = U_{rd} \tag{6-34}$$

If the vapor velocity is greater than U_{gm}, the droplets are entrained with void fraction α_d (0.9 - 0.99); α_B is defined such that

[ ]a

For

$$U_g < U_{gm} \; ; \quad S_g = \alpha_i \rho_g U_g A_{ij}, \; S_\ell = 0$$

For

$$U_g > U_{gm} \; ; \quad S_g = \alpha_i \rho_g U_g A_{ij} \; , \qquad (6\text{-}35)$$

$$S_\ell = \alpha_B \, (1 - \alpha_d) \, (U_g - U_{gm}) \, \rho_f \, A_{ij}$$

To calculate the vapor velocity, U_g, an estimate of the mass flow rate W_T is required.

For the upper plenum, for example, W_T is the net mass flow rate in the volume in the direction normal to the interface. Mass balance, then gives

$$W_T = [\alpha_i \, \rho_g \, U_g + (1 - \alpha_i) \, \rho_f \, U_f] \, A_{ij} \qquad (6\text{-}36)$$

Using a proper drift flux model, the above equation can be solved to obtain U_g.

i) With drift velocity V_{gj} recommended by Zuber[9], for churn turbulent bubbly flow as

$$V_{gj} = 1.41 \left[\frac{\alpha \, g \, (\rho_f - \rho_g)}{\rho_f^2} \right]^{1/4} \qquad (6\text{-}37)$$

we get

$$U_g = \left[\frac{W_T}{A_{ij}} + \rho_f \, V_{gj} \right] / \, [\alpha_i \, \rho_g + (1 - \alpha_i) \, \rho_f] \qquad (6\text{-}38)$$

ii) With U_r as the relative velocity in the bubbly regime, given by

$$U_r = \frac{V_{gj}}{(1 - \alpha_i)} = \frac{1.41}{(1 - \alpha_i)} \left[\frac{\sigma \, g \, (\rho_f - \rho_g)}{\rho_f^2} \right]^{1/4} \qquad (6\text{-}39)$$

we obtain

$$U_g = \left[\frac{W_T}{A_{ij}} + (1 - \alpha_i)\, \rho_f\, U_r \right] / \left[\alpha_i\, \rho_g + (1 - \alpha_i)\, \rho_f \right] \qquad (6\text{-}40)$$

The above equations can be used to obtain U_g with V_{gj} (or U_r) either given as above or specified by any other drift flux model.

b. Interfacial Heat Transfer

To calculate heat transfer rates, the flow regime within the volume set must be determined. This is accomplished with the flow regime map (Figure 6-3) using estimates for the vapor and liquid fluxes as follows:

$$j_v = \bar{W}_v / \rho_v A_{vs} \qquad (6\text{-}41a)$$

$$j_\ell = \bar{W}_\ell / \rho_\ell A_{vs} \qquad (6\text{-}41b)$$

where $\bar{W}_v$, $\bar{W}_p$ are appropriate average values of the link flowrates (for example $\bar{W}_v = 0.5\ (W_{n1} + W_{n2})$ in Figure 6-4) and A_{vs} = average volume set flow area (depends on component being modeled)

The only flow regime in which the heat transfer at the interface is reasonably well understood for subcooled liquid is the stratified regime. However, it can be assumed that the approach to equilibrium will be fairly rapid in the dispersed, bubble, and slug regimes. Thus large heat transfer surface area and large interfacial heat transfer coefficients are used in these regimes. For the stratified and annular regimes the following models are used.

For vapor to interface heat transfer, standard single-phase correlations are used:

$$h_{iv} = Nu_v \, k_v / D_{hv} \tag{6-42}$$

where

$$Nu_v = 4 \quad \text{if} \quad Re_g < 2000$$

$$Nu = .023 \, Re_v^{0.8} \, Pr_v^{0.4} \quad \text{if} \quad Re_v > 2000$$

$$Re_v = \bar{W}_v \, D_{hv} / A_{jvs} \mu_v$$

$$D_{hv} = 4 \, A_{jvs} / P_{wv} \quad \text{(See Figure 6-4)}$$

For liquid to interface heat transfer, a correlation developed by Bankoff and adapted by Sejev for horizontal stratified flow[13,14] is used.

$$h_{i\ell} = St_\ell \, C_{p\ell} \, W_\ell / A_{ivs} \tag{6-43}$$

where

$$St_\ell = 0.0045 \left[\frac{W_v}{W_\ell} \, \frac{A_{ivs}}{A_{jvs}} \, \frac{\mu_\ell}{\mu_v} \right]^{0.33}$$

6.1.4 Verification of Nonequilibrium Model

The predictive capability of the present nonequilibrium model has been checked against less mechanistic, more empirical two-phase pressure drop correlations. Specifically, the Harwell H.T.F.S. correlation[15] was chosen as a reference because it has been shown to be the most consistently accurate predictor over a wide range of flow conditions, encompassing all observed flow regimes.

For the verification, both the H.T.F.S. correlation and the two-volume non-equilibrium model were applied to two-phase flow in a system of horizontal pipes. The modeled system is shown in Figure 6-5. Several system pressures were included in the verification tests as well as many liquid and vapor flow rates to simulate all flow regimes. A sampling of the test series is presented in Table 6-1 and, graphically, in Figures 6-6 (a) and (b). The "50% lines" indicate where the pressure drop prediction by one method exceeded the prediction by one method exceeded the prediction by the other method by 50%.

With the sole exception of the annular regime, pressure drop predictions of the nonequilibrium model are well within $\pm$ 50% of the predictions of the H.T.F.S. correlation, quite good when compared to the scatter of experimental steam-water flow data, as presented in the Harwell Report H.T.F.S. predictions

The nonequilibrium model has the advantages of being essentially mechanistic and providing clear characterization of the flow pattern and related parameters (e.g., drop sizes, percent entrainment, stratified liquid depth, etc.).

6.2 METAL HEAT RELEASE MODEL

The metal heat release model calculates the transient temperature distribution inside a metal. Of particular interest is the amount of heat released (or absorbed) by the metal components inside a nuclear reactor during a loss-of-coolant accident. Generally, the heat transfer from these components is conduction-limited and cannot be accurately modeled with the simple lumped parameters approach used in NOTRUMP.

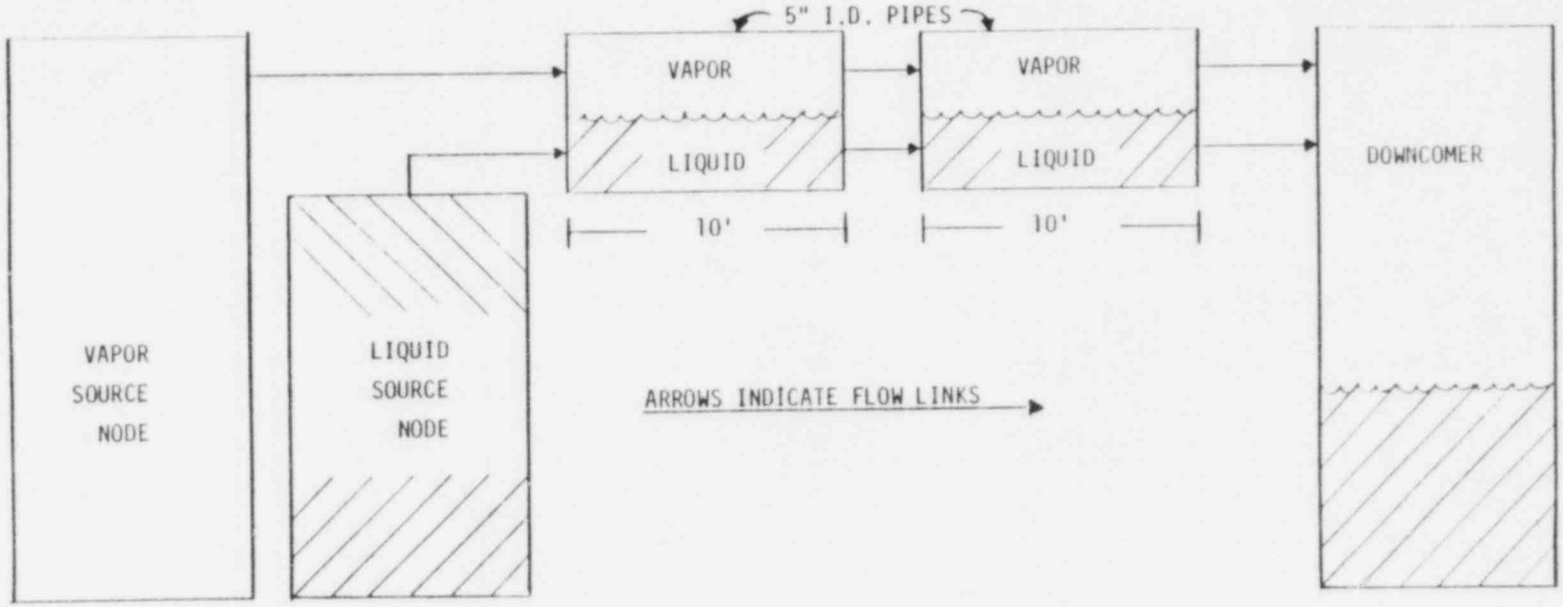

Figure 6-5. Piping System (per FLECHT-SET) for Comparison of Nonequilibrium Model and H.T.F.S. Correlation

TABLE 6-1

NONEQUILIBRIUM MODEL VERIFICATION
(10' LENGTH OF 5" I.D. PIPE, PER FLECHT)

Flow Regime	W_ℓ (lbm/s)	W_g (lbm/s)	System Pressure	HTFS ΔP	2-Vol ΔP	ΔP(2Vol) / ΔP(HTFS)
Dispersed	146.65	0.57225	215	0.587	0.738	1.26
"	161.00	0.23161	60	0.666	0.860	1.29
"	163.85	0.10222	14.7	0.776	0.874	1.13
Bubbly	19.874	0.023512	215	0.017	0.011	0.65
"	21.870	0.011531	60	0.020	0.022	1.10
"	13.449	0.003087	14.7	0.0098	0.0101	1.03
Slug	12.038	0.77861	215	0.069	0.054	0.78
"	13.265	0.38185	60	0.082	0.074	0.90
"	8.1574	0.10222	14.7	0.0364	0.0274	0.75
Annular	2.6860	5.7532	215	0.209	0.522	2.49
"	2.9598	2.8215	60	0.226	0.0461	2.03
"	1.8202	0.75529	14.7	0.09876	0.1327	1.51
Stratified	0.98814	0.00639122	215	0.0009	0.0005	0.56
"	1.0889	0.0311344	60	0.0012	0.0014	1.16
"	0.66960	0.0083906	14.7	0.0005	0.0003	0.50
Rough Str.	0.98814	1.2837	215	0.019	0.024	1.26
"	1.0889	0.49031	60	0.0163	0.0169	1.04
"	0.85979	0.13125	14.7	0.0079	0.0065	0.82

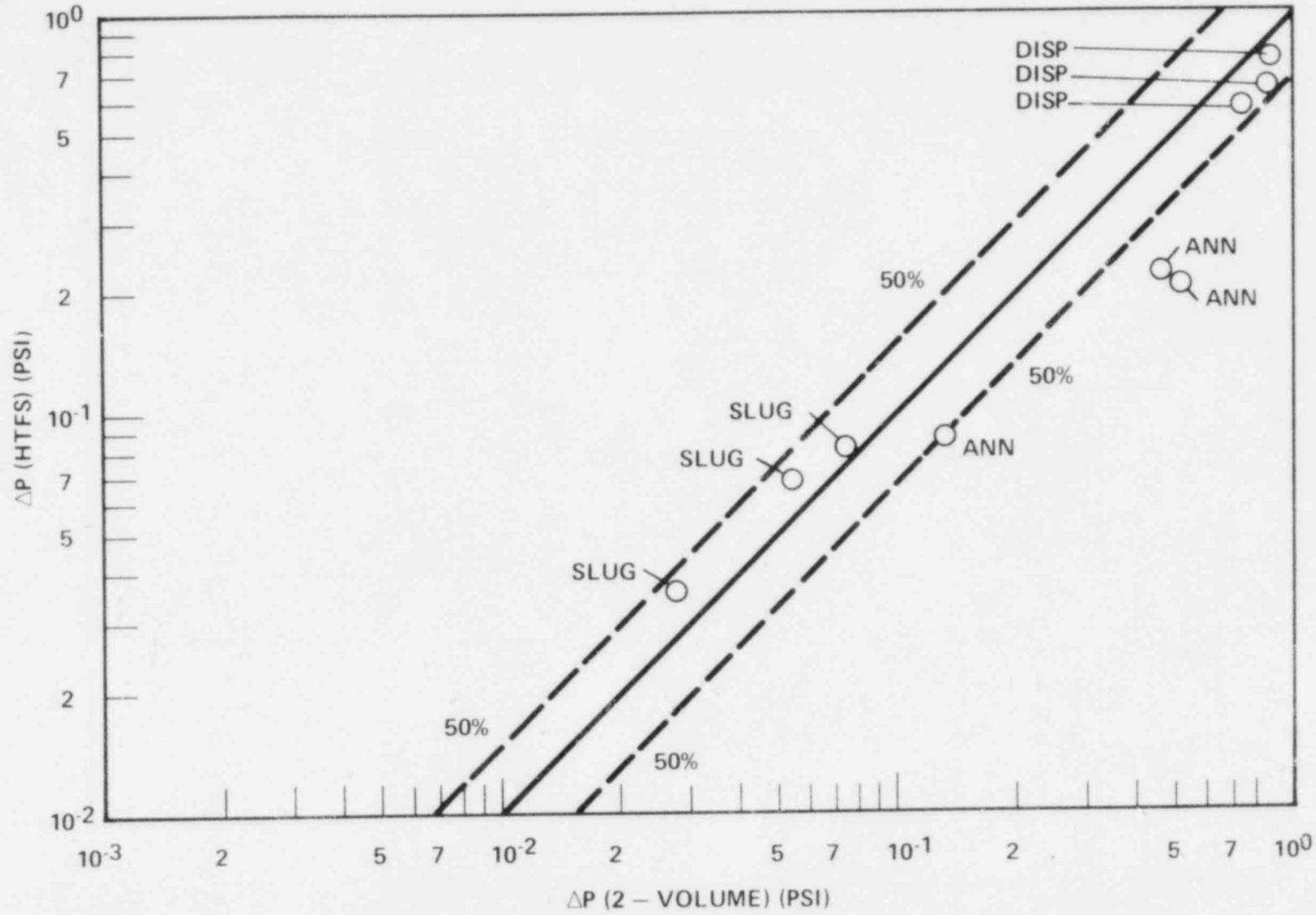

Figure 6-6a. Nonequilibrium Model and H.T.F.S. Correlation Comparison: Pressure Drop in Horizontal Pipe Flow; Dispersed, Annular and Slug Regime

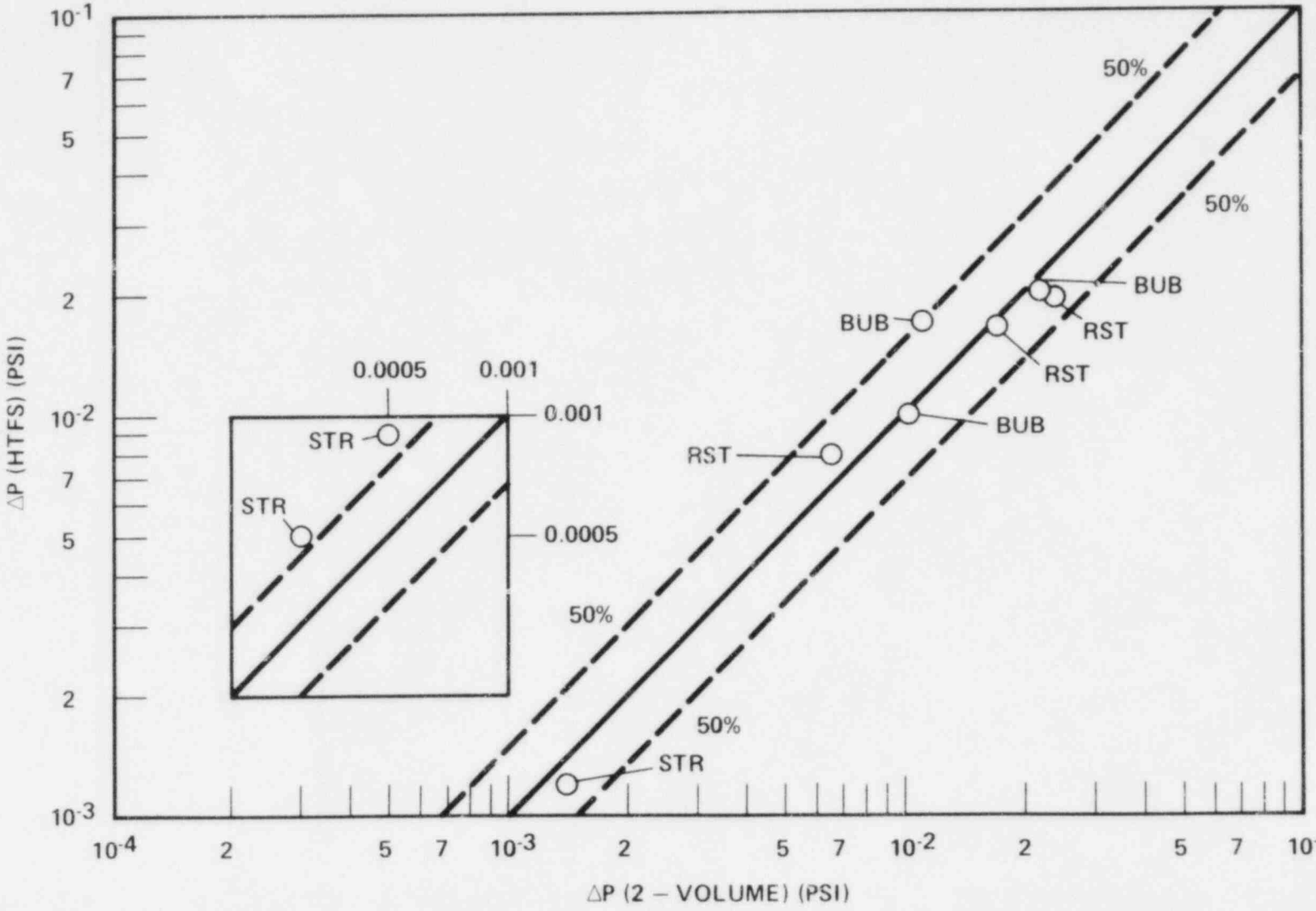

Figure 6-6b. Nonequilibrium Model and H.T.F.S. Correlation Comparison: Pressure Drop in Horizontal Pipe Flow; Bubbly, Stratified, and Rough Stratified Regimes

Heat flux at a metal surface is given by

$$q'' = - K\frac{\partial T}{\partial n}\Big|_w = h(Tw - Ta)$$

where

h = the heat transfer coefficient

T_w = the metal surface temperature

T_a = the surrounding coolant temperature

n = the direction normal to the surface

Transient one-dimensional heat conduction equations in a) rectangular, b) cylindrical (radial) and c) spherical (radial) coordinates is solved numerically using an implicit finite difference method.

For composite materials consisting of two or more layers, as in the case of a metal component with lining of a different material on its surface, the layers are assumed to be in perfect thermal contact at the interfaces.

The model assumes:

1. One-dimensional heat flow.

2. Constant thermal properties (for composite material, constant thermal properties within each layer).

3. No heat generation inside the metal.

Either of the following two boundary conditions can be considered on each of the two outside surfaces:

1. Temperature specified (T_w)

2. Heat transfer coefficient specified (h, T_a)

This model is used whenever large surface heat transfer coefficients require a detailed thermal conduction calculation within the metal. In other areas the simpler lumped parameters approach described in Section 3 is adequate.

SECTION 7
BASH VERIFICATION

In this chapter, the verification against experimental results of the BASH code's ability to predict reactor core and coolant loop responses to emergency cooling processes is described. Two sources of data for the verification were used. The first comes from the FLECHT-SET (Full Length Emergency Cooling Heat Transfer - System Effects Test) program, since this test series was designed specifically to closely match conditions expected in the reflood stage of a PWR loss-of-coolant accident. A comprehensive description of the FLECHT-SET system is contained in the Westinghouse report, WCAP-8410.[16] Additional information on test design philosophy, scaling basis and measurement techniques can be found in WCAP-7906.[17]

Additional verification was performed with data from the FLECHT-SEASET reflood test program.[18] These tests include gravity reflood tests with simple geometry.

7.1 FLECHT-SET SYSTEM DESCRIPTION

The FLECHT system description report opens with the statement, "The objective of the FLECHT-SET program is to provide experimental data on the influence of system effects on emergency core cooling behavior during the reflood phase of a LOCA. The data obtained could be used to verify and improve existing analytical techniques for evaluating ECCS performance or to serve as the basis for the development of new ones." To achieve the program objective, the FLECHT test facility was designed to preserve coupling of transient effects, as in a reactor. Within practical limitations, the facility realistically retains those system effects considered important during the reflood phase of a LOCA. As in most scaled experiments, limitations exist. However, for the task of providing data for code verification, the system response need only be similar, not necessarily identical, to that of a PWR.

The test facility simulates a four-loop PWR in which one loop is broken and three loops are intact. The scaled simulation includes the downcomer, piping, elevations, flow path lengths and overall loop flow resistances, while properly scaling volume flow areas and major heat sources. For the broken loop a single-scaled steam generator is used, and for the FLECHT intact loop a single "lumped" steam generator simulates the three corresponding PWR steam generators. Figure 7-1 presents a schematic of the facility, showing the major components of the system.

Brief descriptions of the main scaling bases and relationships of FLECHT to a PWR follow:

Phenomenon:	Scaling Approach:
Heat transfer and flow regimes	Preserve the power input per fluid volume in the core bundle and steam generator.
System initial conditions	Tests simulate many possible reflood situations. Initial conditions are prototypical of PWR.
Fluid conditions leaving the core	Preserve the power/fluid volume ratio. Flow regimes are representative of PWR conditions.
Loop pressure drop	Maintain the proper total hydraulic resistance.
System dynamic behavior	Maintain the same distribution of scaled volumes and the full system resistance as in a PWR. This simulates the damping effect on dynamic behavior.
Real time response in the experiment	Preserve the full-length distance between components so that transport times are preserved.
Downcomer and core fill-up rates	Preserve the scaled downcomer and core areas so that their ratio is the same as in a PWR.

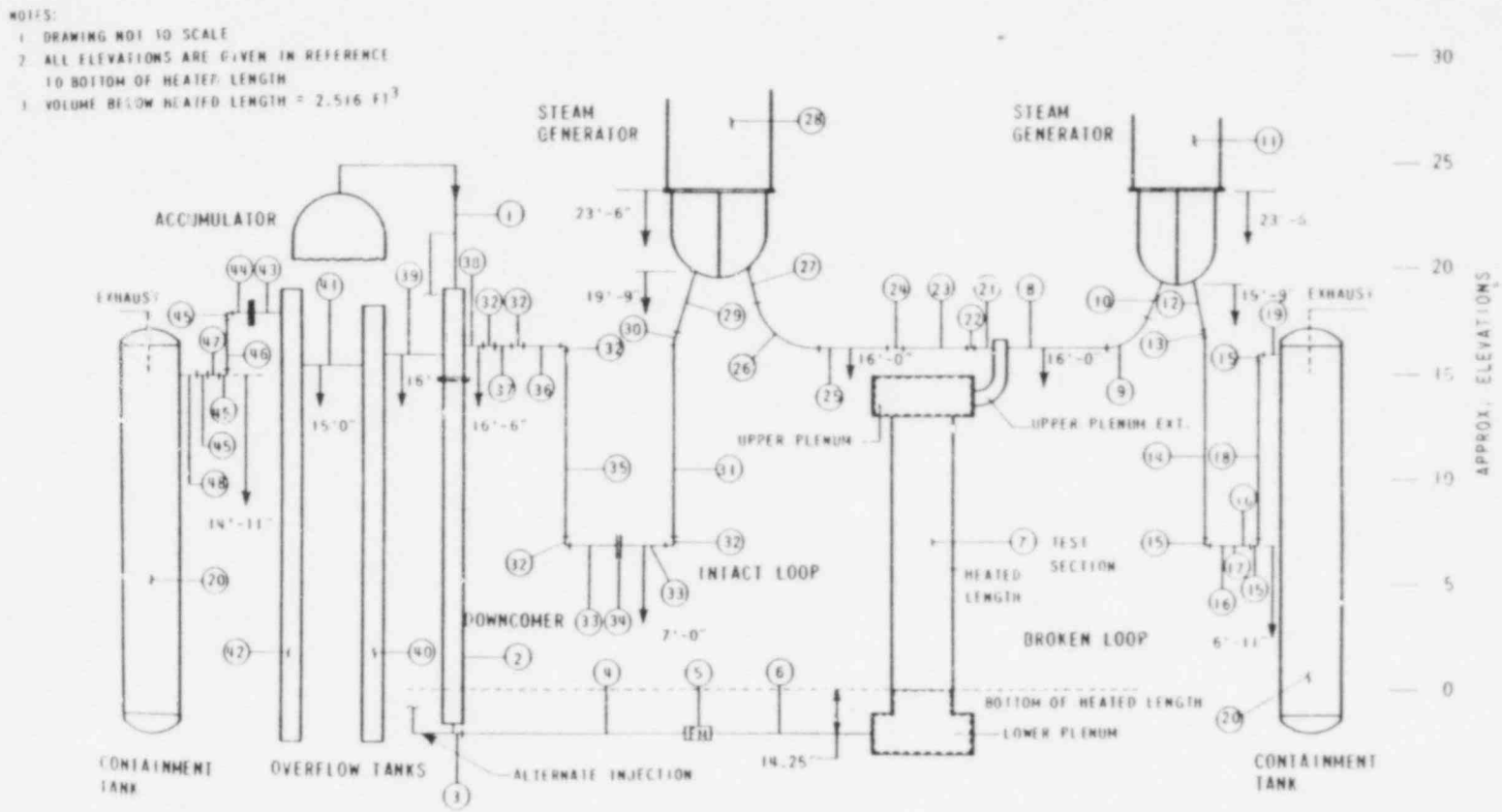

Figure 7-1. FLECHT-SET Phase B Facility Schematic

Core scaling ratio	FLECHT/PWR core cross-section fluid area = 1/370. The core fluid volume ratio is also 1/370, since the FLECHT core is full length.

The core of the FLECHT-SET facility is comprised of electrically heated simulated fuel rods in a 10 x 10 array. The rod bundle is full length (12-foot heated length) and has dimensions which are prototypical with respect to a 15 x 15 fuel assembly in a PWR (rod OD = 0.422 in., pitch = 0.563 in., thimble diam. = 0.545 in.). Rod power is varied both from rod to rod to simulate the power distribution across a fuel assembly and along the axis of each rod to model the axial core power profile. A longitudinal view of the test section and its upper and lower plenums is shown in Figure 7-2 and a cross-sectional view is shown in Figure 7-3.

7.2 FLECHT EXPERIMENT USED FOR BASH VERIFICATION

For verification of the BASH code, FLECHT SET phase B test 3105B was chosen for comparison. The data from this test are discussed in detail in Reference [19].

The following data were recorded as a function of time and location and used in the comparison of BASH predictions to experimental results:

1. Core Conditions

    a. Rod power input
    b. Cladding surface temperature
    c. Liquid and vapor temperatures
    d. Quench front elevation
    e. Core flooding rate
    f. Core mass inventory

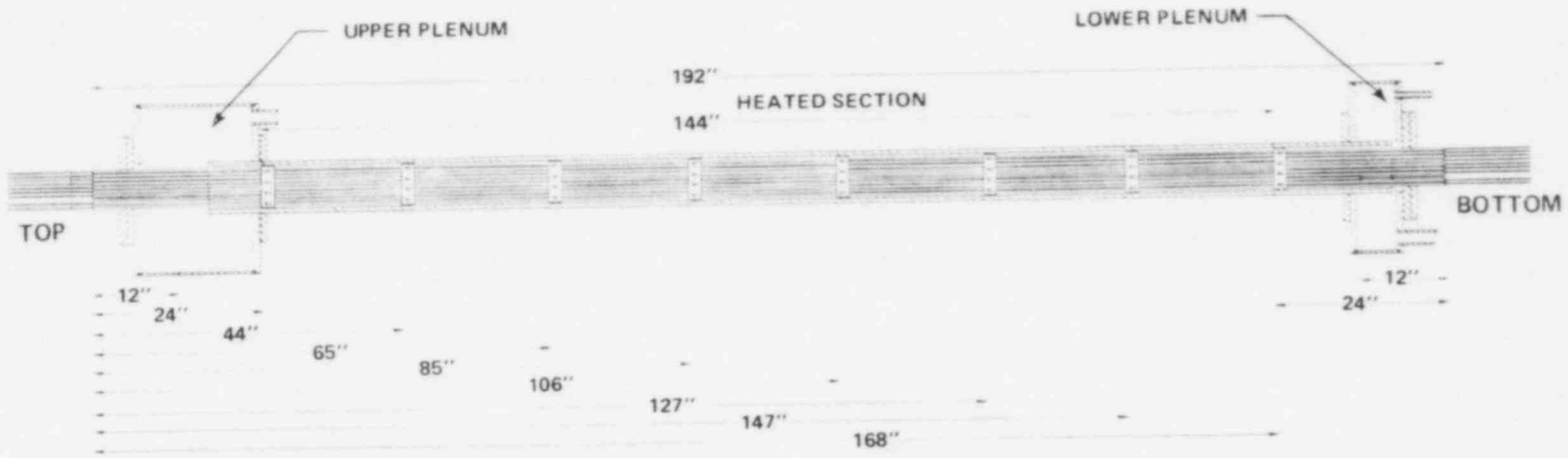

100 ROD BUNDLE

Figure 7-2. Test Vessel and Rod Bundle Details

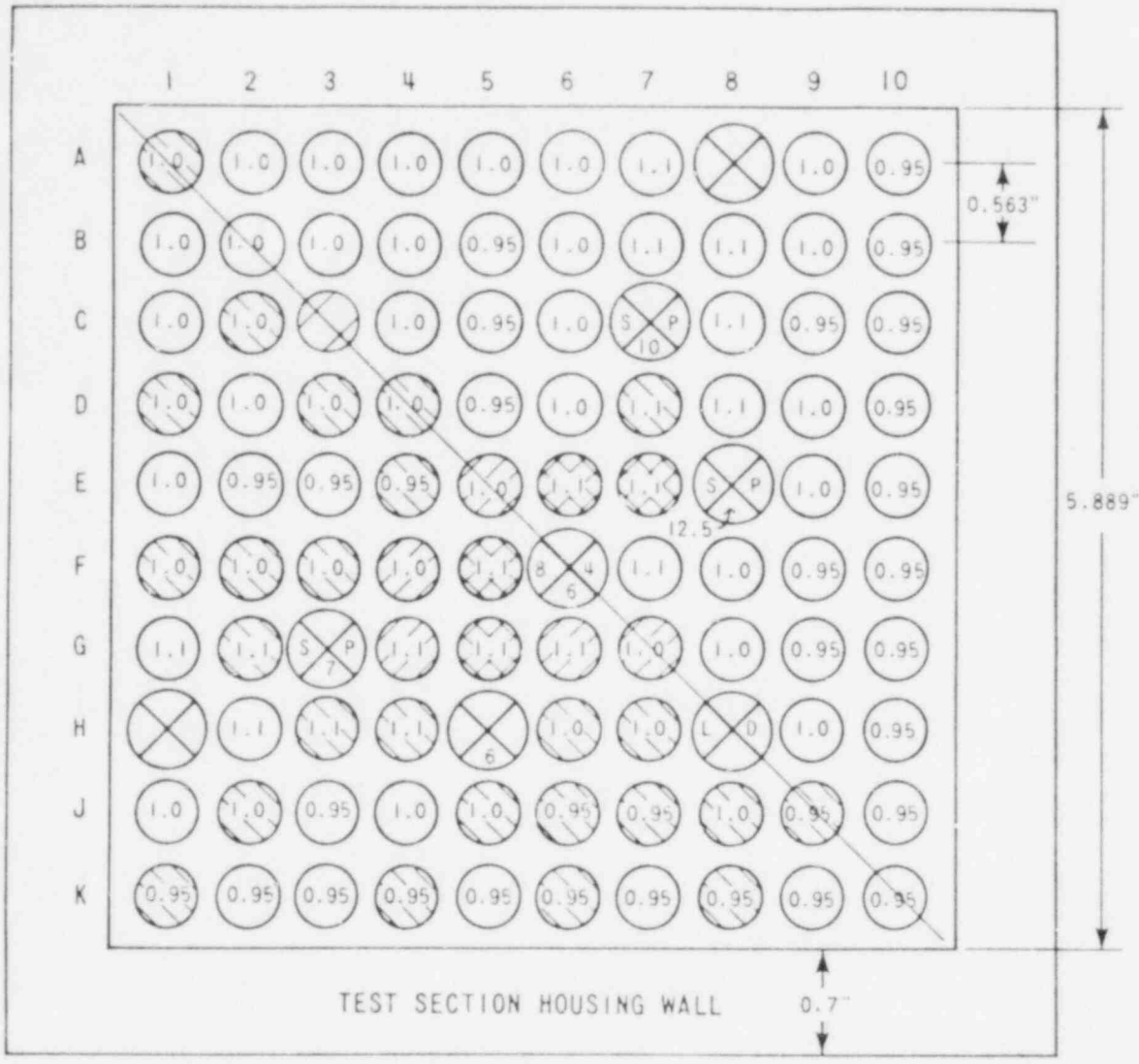

Figure 7-3. Cross Section of 10 x 10 Bundle Showing Instrument Locations and Radial Power Profiles

2. Loop Conditions in Selected Components and Location

a. Liquid and vapor inventories
b. Liquid and vapor flow rates
c. Liquid and vapor temperatures
d. Nodal pressures
e. Steam generator heat transfer
f. S. G. primary fluid evaporation rate

7.2.1 General Description of Run 3105B

This test was run for 154 seconds. Rod power input was reduced in time according to a preset program simulating decay heat release. The initial conditions of run 3105B were:

Containment pressure	= 59 psia
Initial cladding temperature	= 1100°F
Peak Power	= 0.84 kW/ft
Coolant injection temperature	= 152°F
Average housing temperature	= 306°F
Injection flow rate	= 12.3 lbm/sec for 14 sec, variable thereafter
S.G. secondary level (cold)	= 24.0 ft
S.G. secondary temperature	= 512°F

7.3 BASH MODELING OF FLECHT-SET

7.3.1 BART Noding

The BART core noding scheme used in modeling the FLECHT-SET tests is presented in Figure 7-4. The heater rods are divided into 21 nodes, with the actual heated length extending from node 3 to node 21 (defined as being from 0 to 12 feet). All nodes in the heated region were 7.2 inches in length, except for the highest two nodes, 20 and 21. This scheme achieved the refinement of detail desired with the minimum number of nodes. Figure 7-4 also shows the BART rod power profile discretization used.

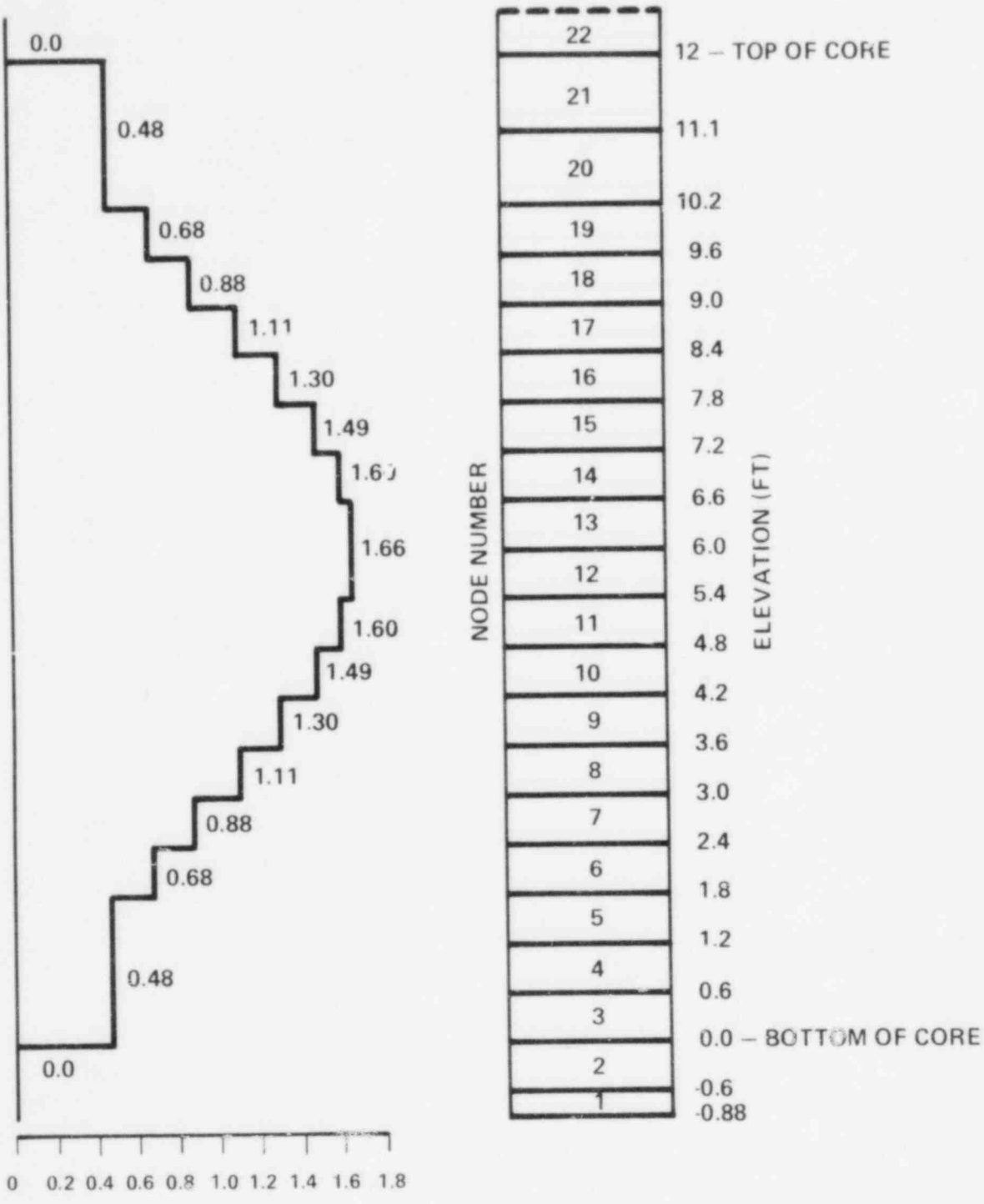

Figure 7-4. BART Core Noding for FLECHT-SET B

7.3.2 NOTRUMP Noding

The NOTRUMP noding scheme modeling the FLECHT-SET PHASE B tests is presented in Figure 7-5. The model includes control volume simulations of the core and its inlet and outlet plenums, the hot and cold legs of the broken and intact loops, the steam generators, the downcomer and safety injection line, and the blowdown line and containment tank.

The core node is a "dummy" node in that its transient conditions are provided by BART rather than being generated by NOTRUMP. All other nodes except the downcomer are assumed to contain a homogeneous mixture of liquid and/or vapor at thermal equilibrium. In the downcomer, the "two volume nonequilibrium" model is used to more accurately simulate the important thermal discontinuities and phase separation in the downcomer due to ECCS injection, intact loop recirculation and flow reversals in the core. The PWR primary coolant pumps were simulated in the FLECHT apparatus by orifices with flow resistances scaled to PWR pump resistances. In NOTRUMP, the FLECHT "pump" orifices are modeled as constant additive resistance coefficients in the appropriate flow links.

The NOTRUMP hydraulic simulations of the two FLECHT steam generators include an inlet and outlet plenum, a U-tube primary divided into a hot-side (ascending) node and a cold-side (descending) node and a secondary side (stagnant fluid, thermal boundary condition) node. Each steam generator's thermal model includes the secondary fluid boundary node, the primary fluid nodes, and two tube bundle metal nodes which correspond to the primary fluid nodes. These nodes are thermally connected by heat links with heat transfer coefficients defined to produce in BASH the same overall steam generator energy input to the primary fluid as was observed in the FLECHT tests.

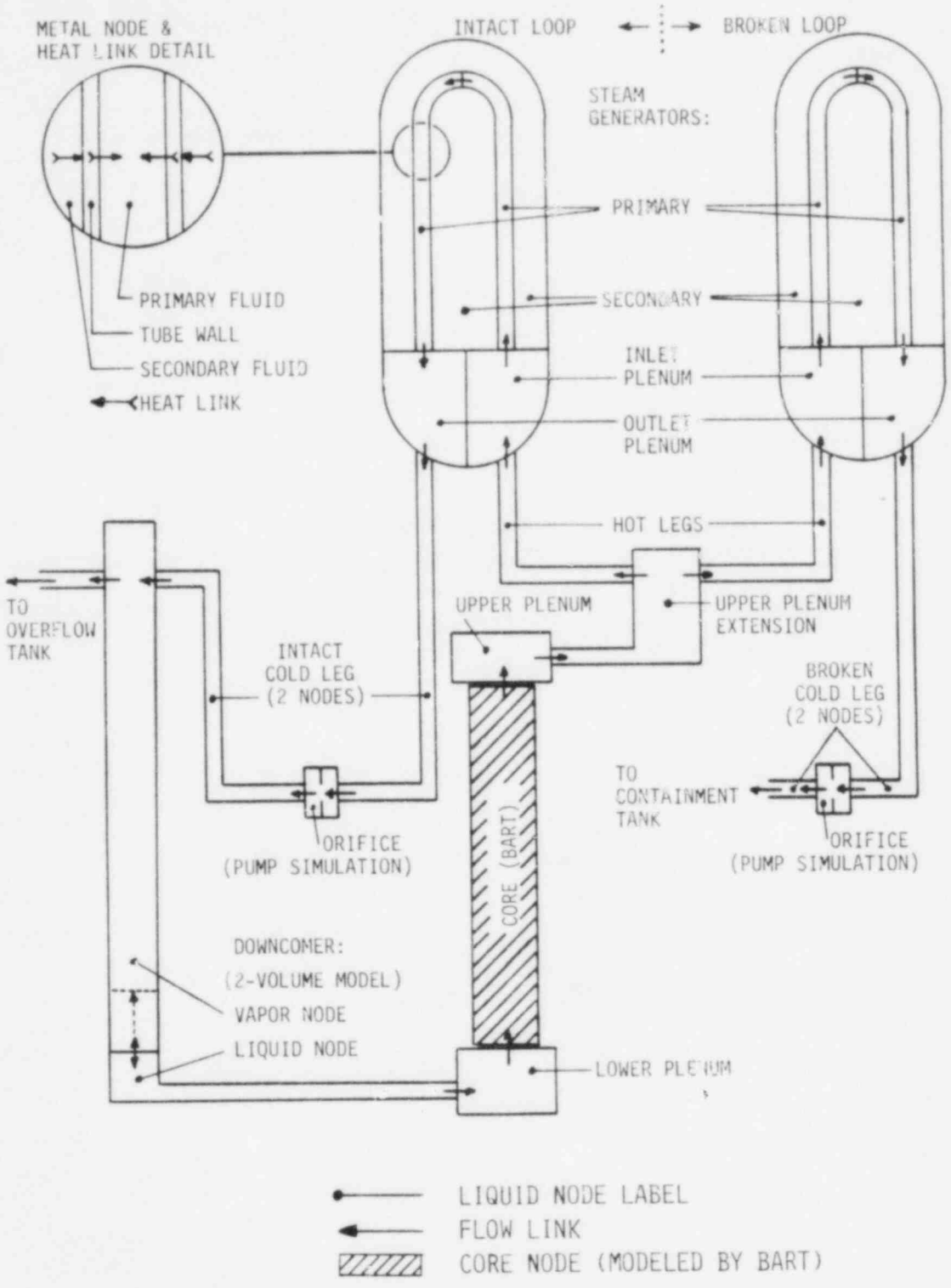

Figure 7-5. NOTRUMP Noding for FLECHT-SET B

7.4 BASH COMPARISON TO FLECHT-SET 3105B

Figures 7-6 and 7-7 present peak cladding temperature histories at the 6-foot and 8-foot core elevations, respectively, as measured in FLECHT and as predicted by BASH. The plots of FLECHT cladding temperature data show the mean temperature of all instrumented rods at given times as a dashed line and show the standard deviation of the recorded temperatures about the (sample) mean temperature as vertical bars.

Both the FLECHT and BASH cladding temperatures peak early in the transient. In the early phase of the transient (up to about 30 seconds), BASH conservatively predicts "average" rod temperatures and follows the trend of the FLECHT data well. After correctly beginning the gradual decline, however, BASH cladding temperatures tend to decline more slowly than observed in FLECHT at lower core elevations or actually rise once more later in the transient at higher elevations.

BASH predicts peak cladding temperatures well early in the transient. The later temperature rise, which is more pronounced the higher the elevation, is symptomatic of a key assumption in the present BASH model. The assumption is that a top-down quench front will not propagate into the core from above. This maintains vapor superheats at high levels in the upper regions of the bundle, a phenomenon not observed in the FLECHT experiments.

Through the complex interactions of upper elevation cladding temperatures, rod-to-fluid heat transfer, vapor generation, loop pressurization, core flooding rate, downcomer head, etc., the "no top-down quench" assumption manifests itself in all aspects of the transient. The effect is minor for most BASH transient variable predictions (the late-time, high elevation cladding temperature excursion is the most direct and pronounced effect) and the trend is always towards increased conservatism.

Figure 7-8 shows the envelope of quench front elevation versus time measured for all instrumented rods in FLECHT 3105B, along with the BART/BASH predicted quench front movement. Early in the transient the BASH results are precisely

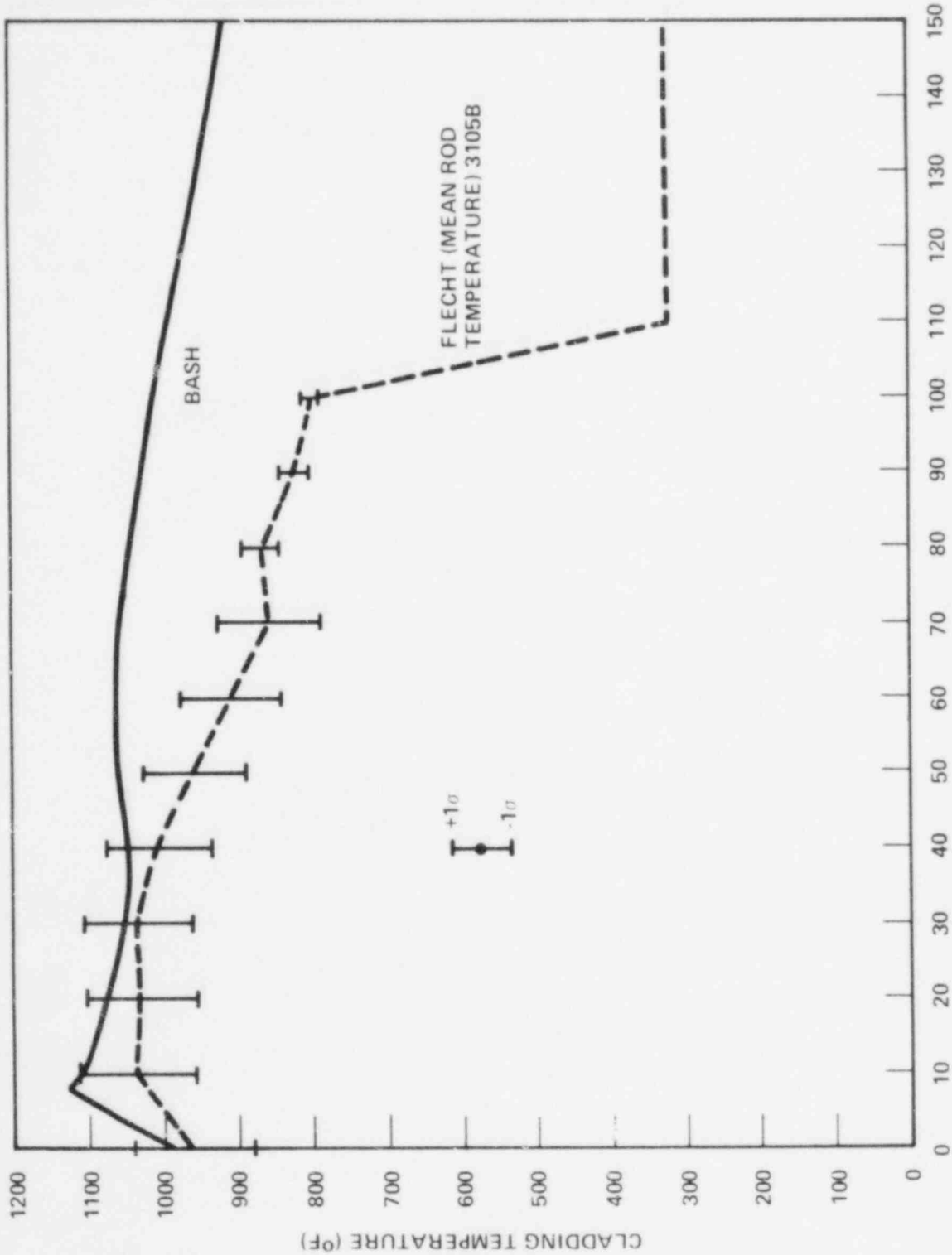

Figure 7-6. BASH/FLECHT 3105B Comparison: 6-Foot Elevation Cladding Temperatures

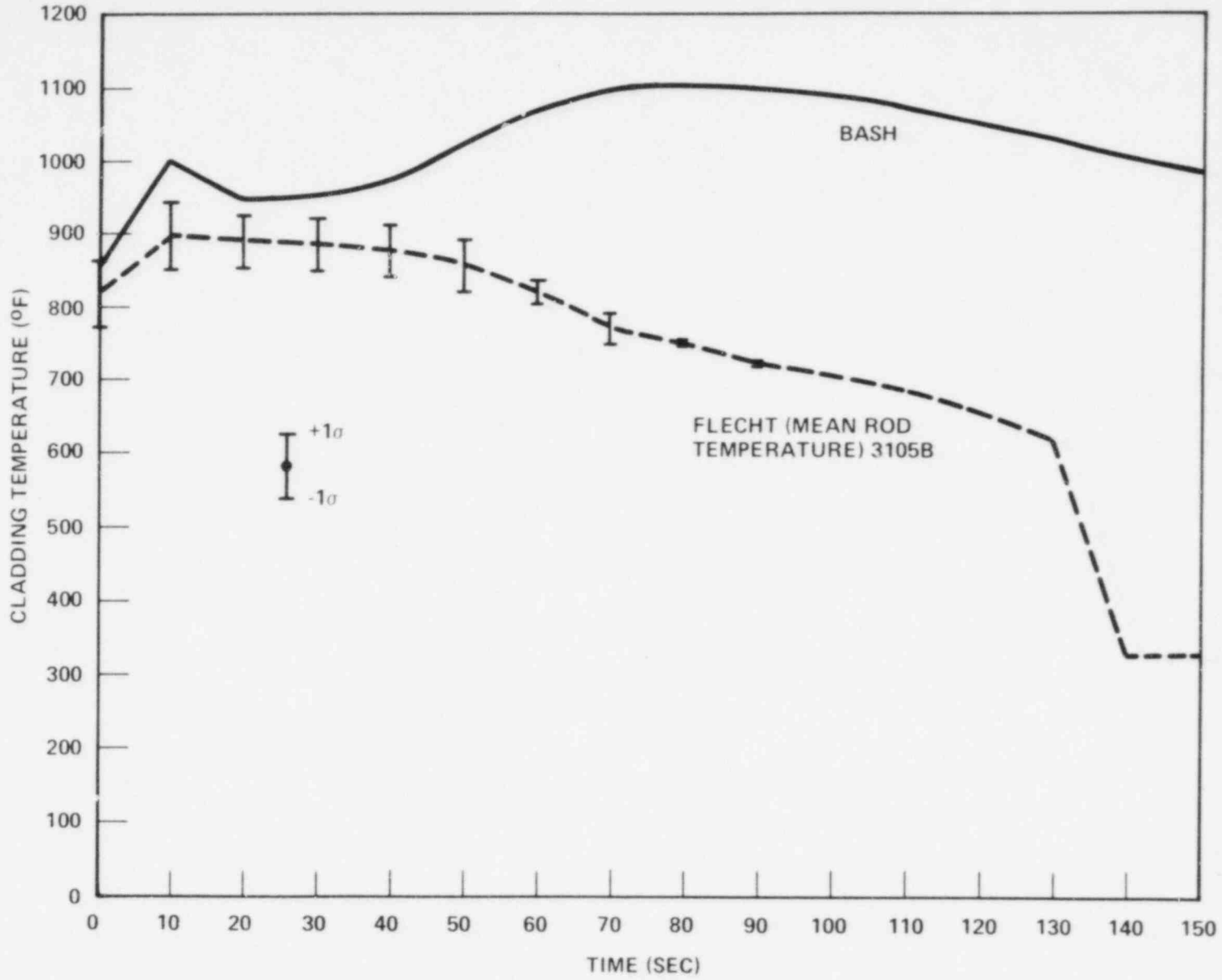

Figure 7-7. BASH/FLECHT 3105B Comparison: 8-Foot Elevation Cladding Temperatures

3832A:8

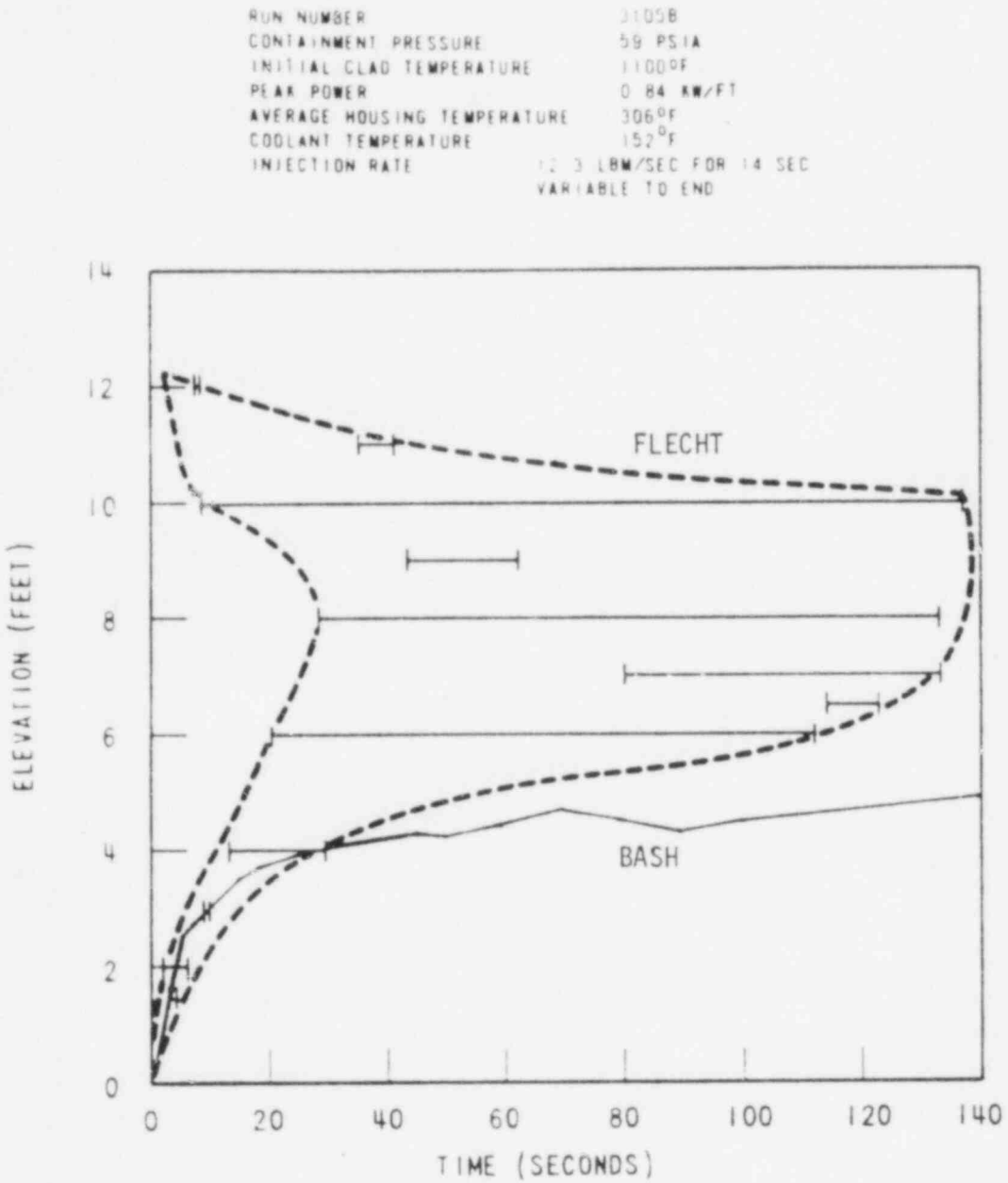

Figure 7-8. BASH/FLECHT 3105B Comparison: Quench Front Showing Maximum and Minimum Times for Each Elevation

within the experimental envelope. After approximately 30 seconds, the BASH quench front begins to lag behind the actual quench front rise. For the remainder of the transient, BASH predicts quench front movement slightly conservatively. That is, after about 30 seconds the BASH quench front remains slightly lower than the quench front elevation recorded for the latest-quenching rod.

By 30 seconds into the test, some rods have quenched completely from above and from below. Also, by 65 seconds, all rods have quenched from the top down to the 9-foot elevation (except for a single rod thermocouple record which indicates an odd unquenched "hot spot" on one rod at the 9.8-foot level). Here the absence of a top-down quench model in BART appears to slow the "lower" quench front movement.

The core flooding rate, as measured in FLECHT 3105B and as predicted by BASH are shown in Figure 7-9. Since both exhibit oscillations which make interpretation difficult, both curves are averaged over a slightly longer time scale for comparison in Figure 7-10. Both the actual and predicted core flooding rates show the same overall trends.

Figure 7-11 is a comparison of the actual and predicted integral mass entering the core. There is good agreement between test and prediction, an after the initial high injection flow phase (14 seconds) the BASH core flooding integral generally lags about a few pounds of water behind the cumulative mass injection calculated from FLECHT data.

With the ECCS injection rate programmed directly from test data, a conservative prediction of core flooding implies an overestimation of the downcomer liquid inventory. Figure 7-12, a comparison of FLECHT and BASH downcomer head, confirms that this is the so. Figure 7-13, the actual and predicted core mass inventory, also reflects this. BASH underpredicts the core mass by the same amount that it overpredicts the downcomer mass throughout the transient.

The amount of fluid which has left the top of the core is generally well predicted in BASH, as shown in the exit flow integral plot, Figure 7-14.

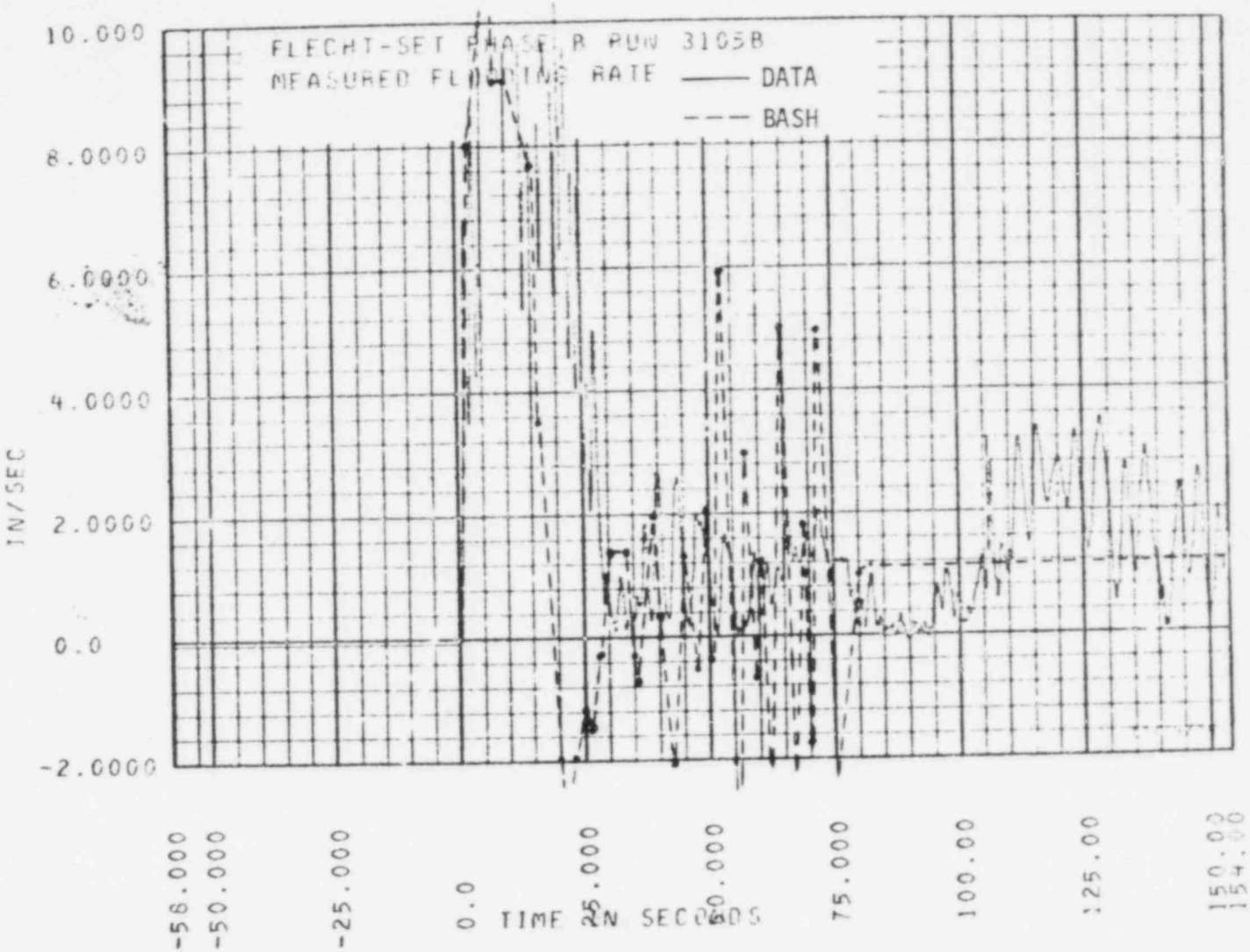

Figure 7-9. BASH/FLECHT 3105B Comparison: Core Flooding Rate (Raw Data)

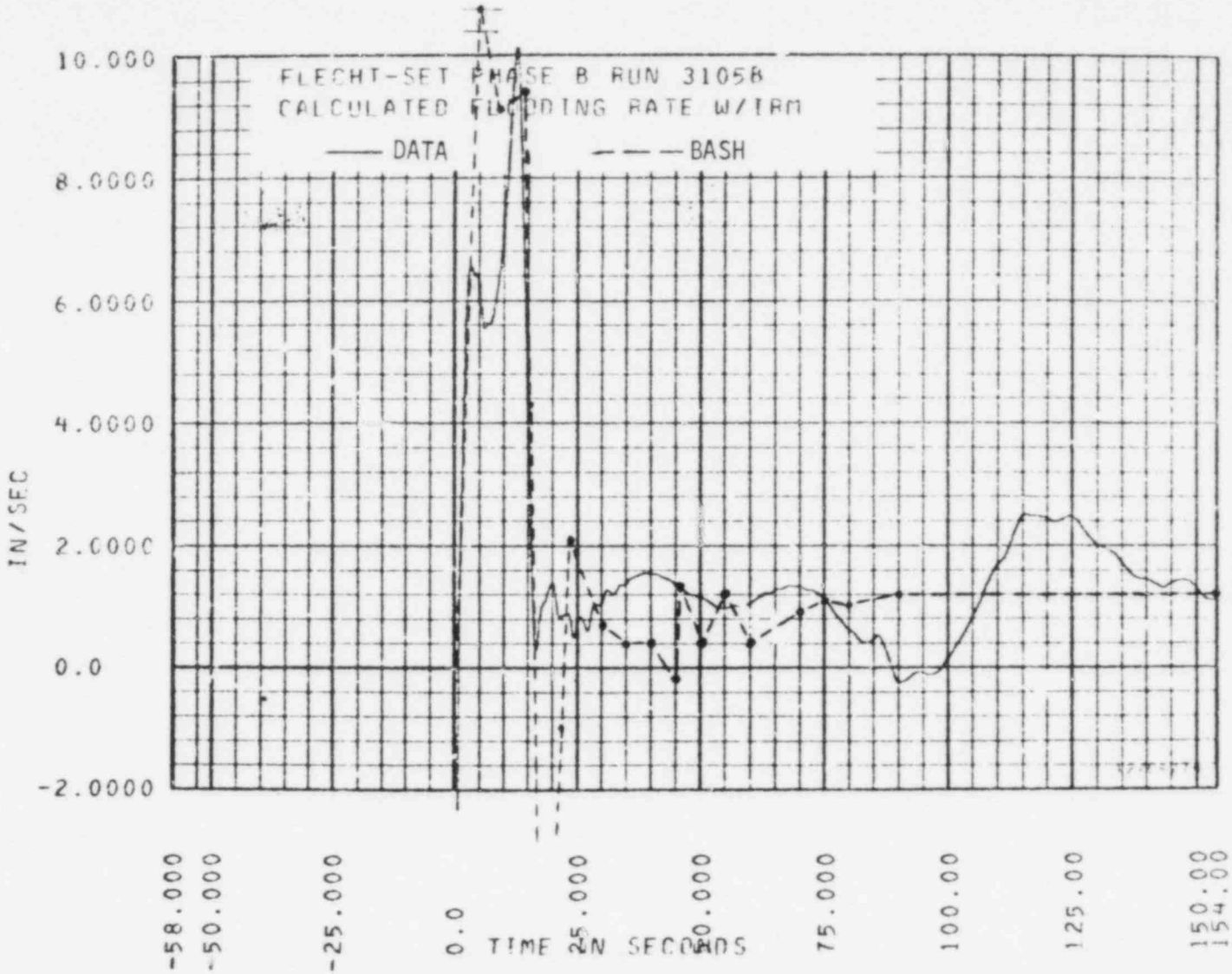

Figure 7-10. BASH/FLECHT 3105B Comparison: Core Flooding Rate (Smoothed)

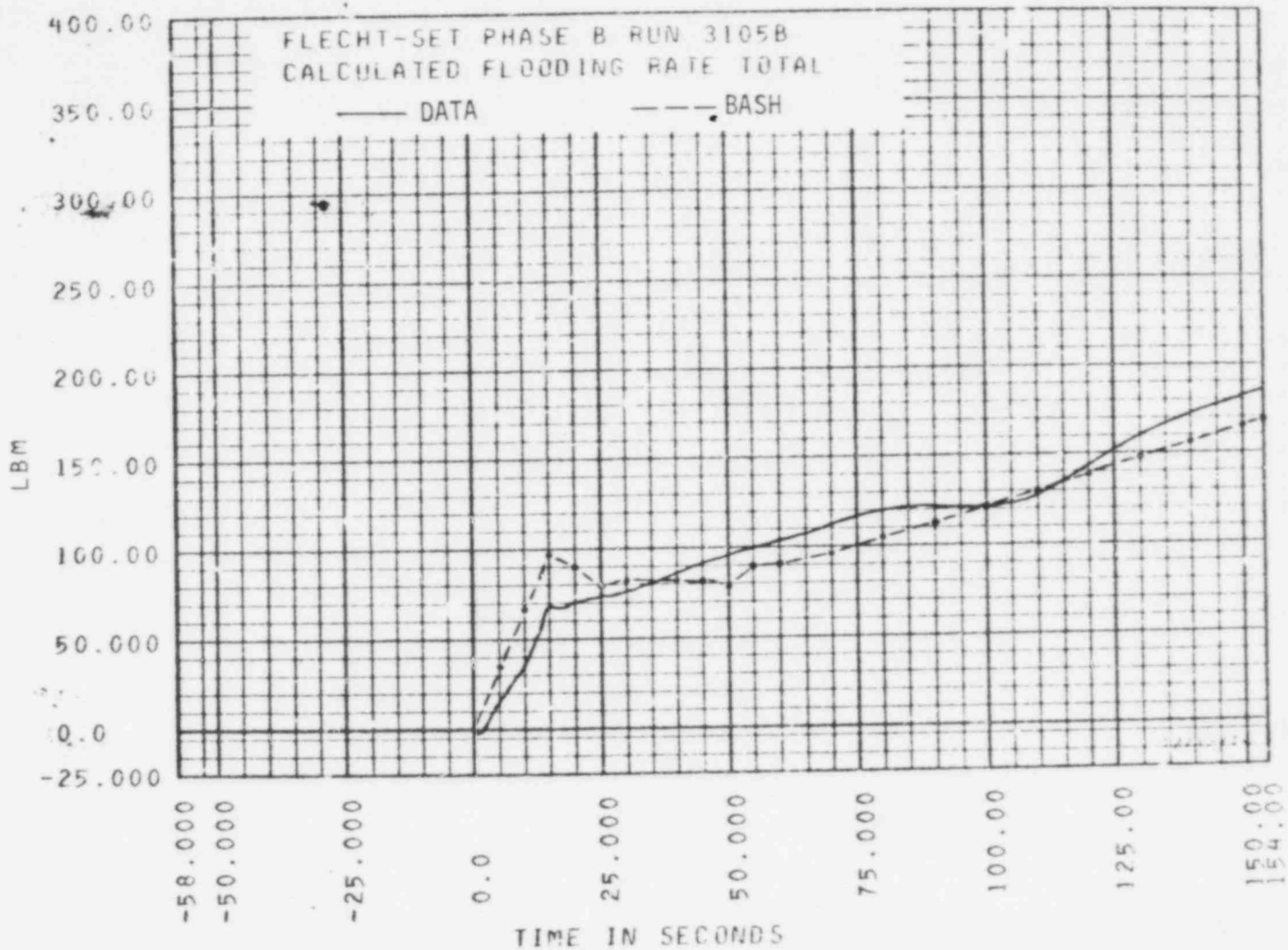

Figure 7-11. BASH/FLECHT 3105B Comparison: Integral of Mass Enteri the Core

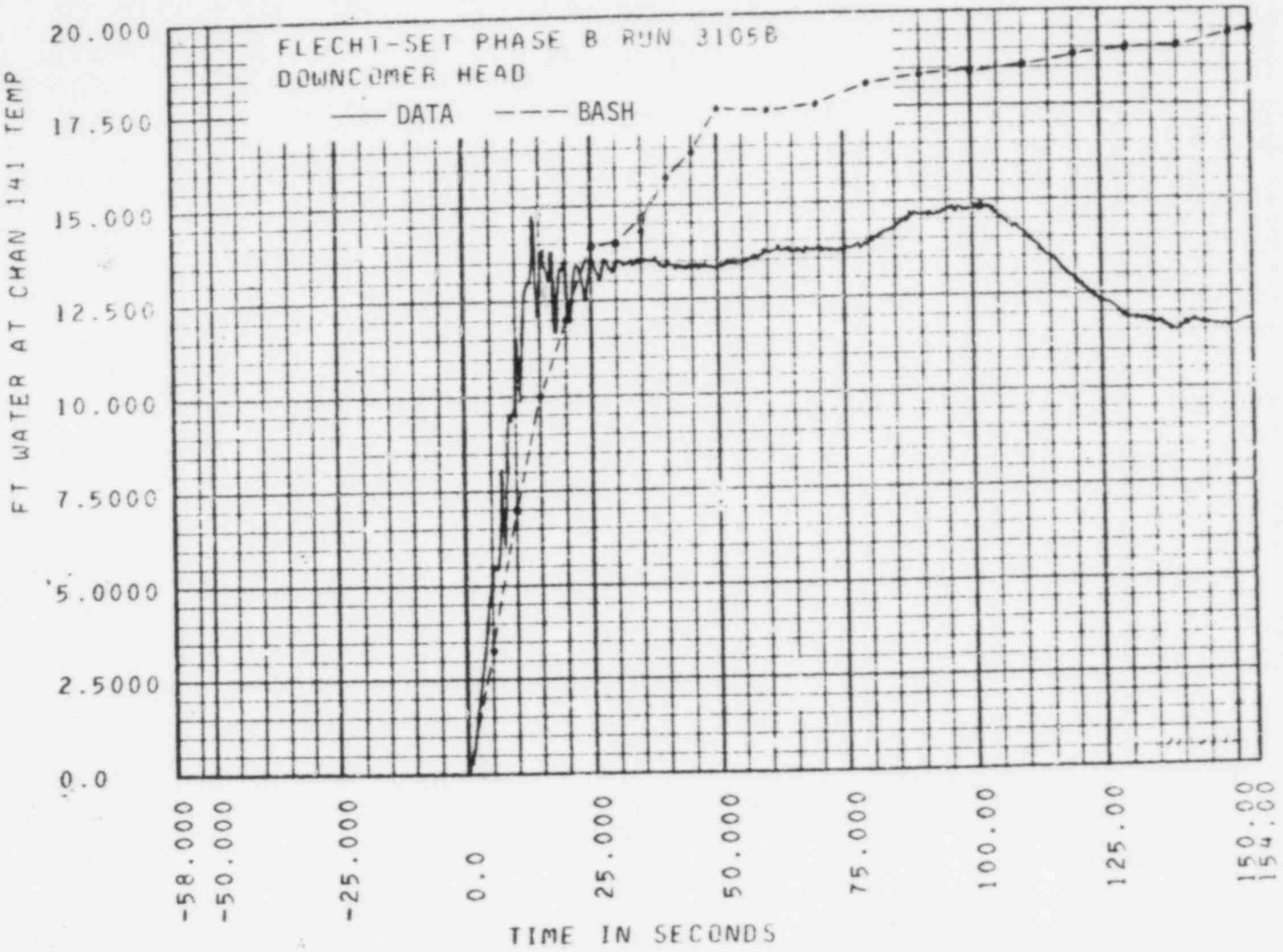

Figure 7-12. BASH/FLECHT 3105B Comparison: Downcomer Head

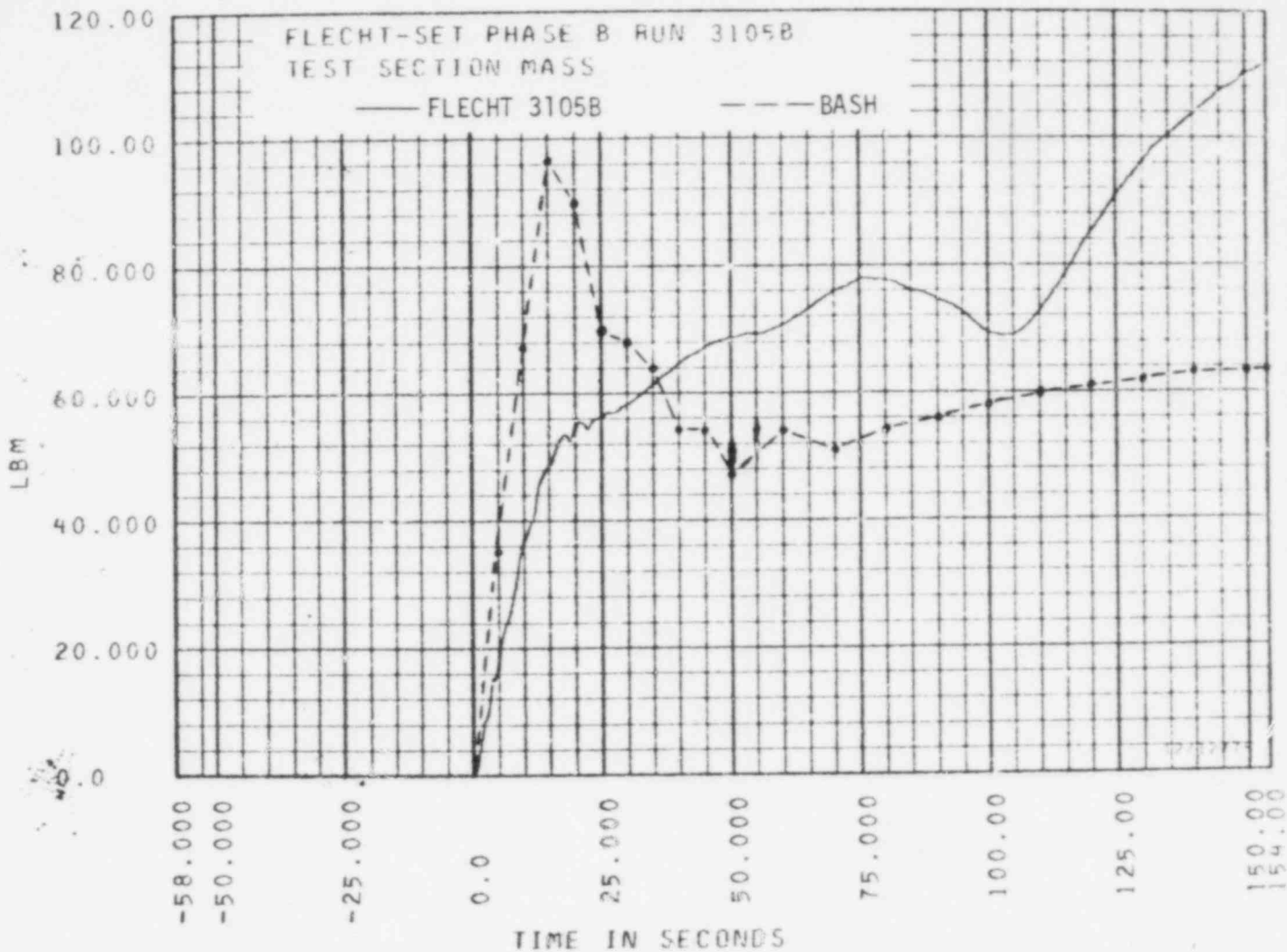

Figure 7-13. BASH/FLECHT 3105B Comparison: Test Section (Core) Mass

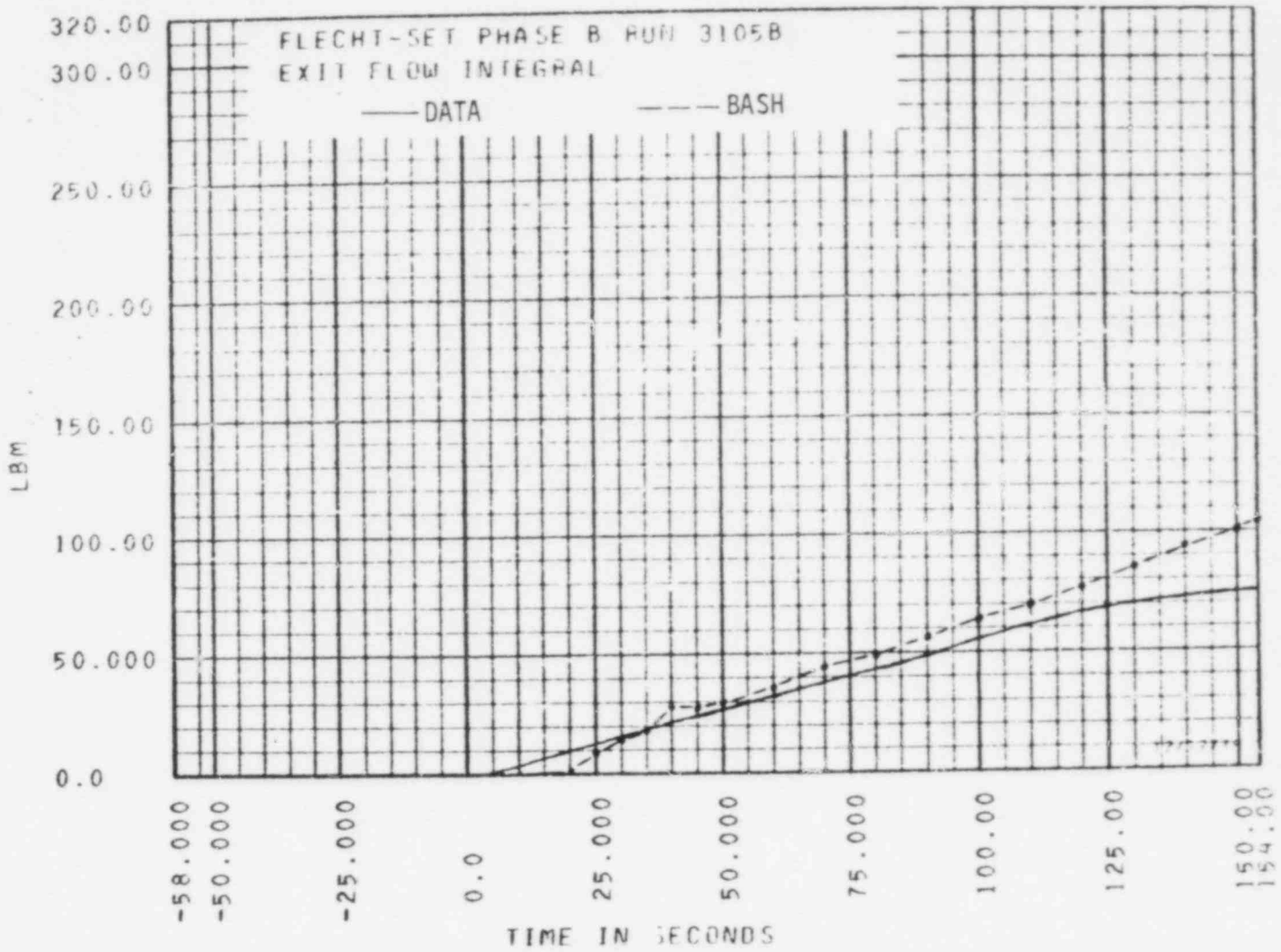

Figure 7-14. BASH/FLECHT 3105B Comparison: Exit Flow Mass Out Integral

Generally, BASH correctly predicts the FLECHT Phase B transient response. However, the cladding temperatures and quench times are overpredicted. The test section mass is also underpredicted late in time. It appears that these trends are due in large part to the tendency of gravity to drive the vapor superheat and void fraction down through top down quenching, grid rewetting, and flow regime changes. The dispersed flow model in BART tends to predict higher vapor superheats and void fractions (and therefore higher rod temperatures) due to the dispersed flow models based on low flooding rate data. However, it is clear that the results represent a conservative prediction of the rod heat transfer.

7.5 FLECHT-SEASET

BASH was used to simulate a FLECHT-SEASET Gravity Reflood Test to compare the results against the test data. The details of the test facility and procedure are provided in Reference [18]. In the test, hot leg resistance was simulated by an orifice plate installed in the line from the upper plenum to the steam separator. Pressure in the steam separator was maintained to a desired value by a control valve located in the exhaust line from the steam separator. Other components included downcomer, lower plenum, test vessel, carryover tank and a drain tank. Injection flow was introduced in the horizontal run of the downcomer pipe.

7.5.1 BASH Model

The BASH noding scheme for the Gravity Reflood Test is shown in Figure 7-15. The upper plenum, steam separator, drain tank and carryover tank were all modeled as NOTRUMP stratified nodes whereas the downcomer was modeled as a two-volume nonequilibrium fluid node.

The test bundle was represented in BART using 22 axial nodes. This included heater rods with an unheated length of 0.5 feet at the bottom and heated length extending from nodes 3 to 22.

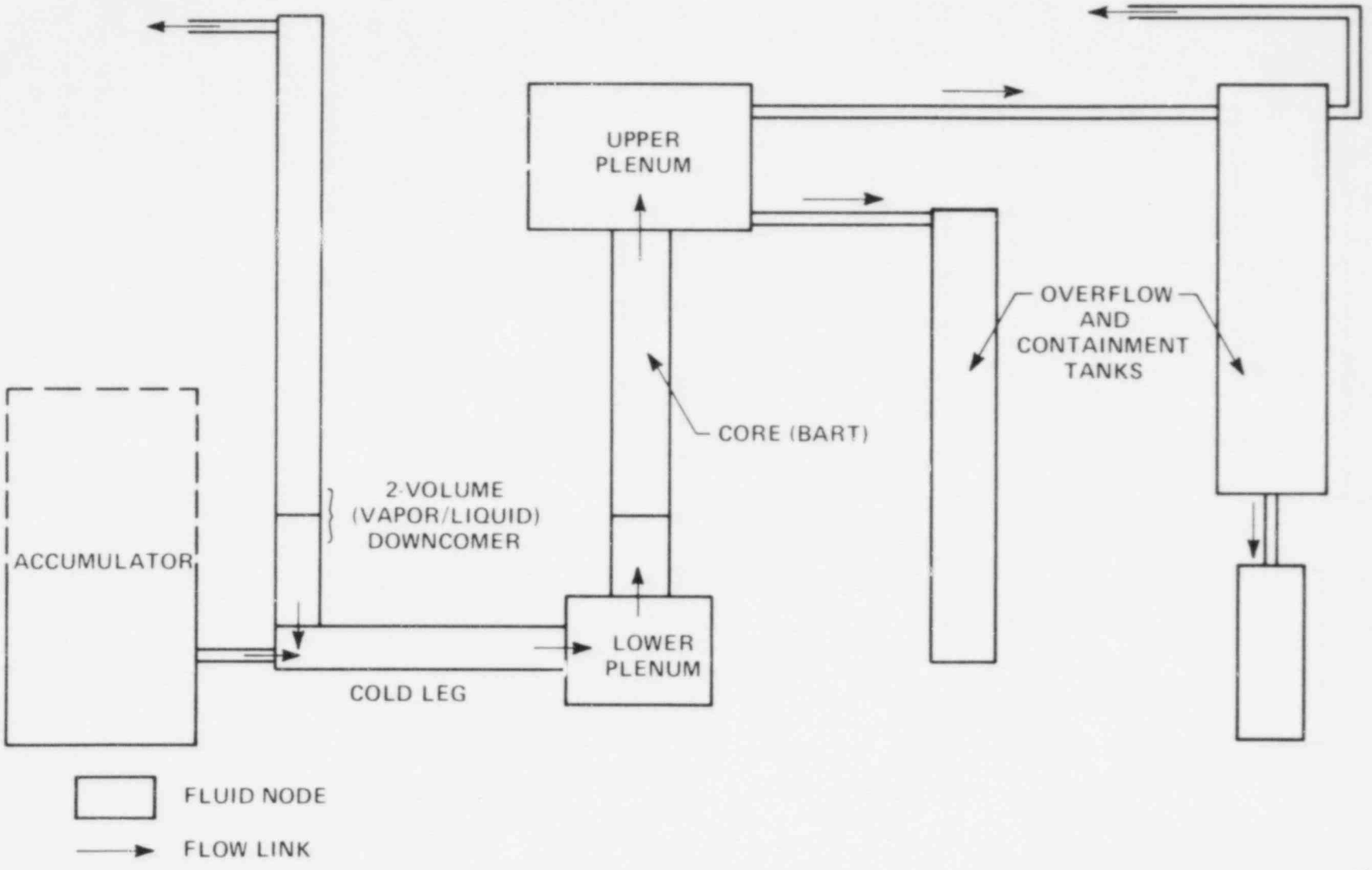

3832C-1

Figure 7-15. BASH Noding for FLECHT-SEASET Gravity Reflood Test

The orifice plate was represented by an equivalent resistance coefficient in the flow link from upper plenum to steam separator. To maintain a desired pressure in the steam separator, it was connected to a boundary node with specified pressure. A critical flow link was used to provide the necessary injection flow in the system.

7.5.2 Data Comparison

A comparison of BASH predictions against FLECHT-SEASET gravity reflood test data (Run No. 33436) is provided in Figures 7-16 through 7-21. The injection flow rate in the test was 13 lbm/sec for the first 15 seconds and 1.72 lbm/sec after 15 seconds. The nominal test pressure was 40 psia.

The flooding rate calculated by BASH is in good agreement with the test data, particularly at later times, as shown in Figure 7-16. The test data for Figure 7-16 were obtained from mass balance calculations. BASH yields a higher flooding rate than occurred in the test early in time, leading to more mass accumulation in the vessel, as shown in Figure 7-17. Consequently, the downcomer fills at a slower rate in BASH than was observed in the test. However, the delayed entrainment results in an overprediction of rod temperature, as seen in Figures 7-19 to 7-21.

Figure 7-18 presents a comparison of the movement of the quench front during the test, as measured and as computed by BASH. Late in the test BASH tends to predict a lower quench front elevation. This is due to the accumulated effect of higher predicted cladding temperatures in BASH.

Figures 7-19, 7-20, and 7-21 show heater rod surface temperatures at the 4-foot, 6-1/2 foot, and 9-foot core elevations, respectively. BASH predicts rod temperatures well at the two lower elevations, while remaining conservative in its calculated peak cladding temperature. At successively higher elevations, the conservatism of the BASH rod temperature and the delay of the quench time becomes more pronounced, as seen in the figures. This is due to the fact that the BASH calculation does not contain the effect of grids, which, as shown in Reference [8], have a strong heat transfer effect at upper elevations.

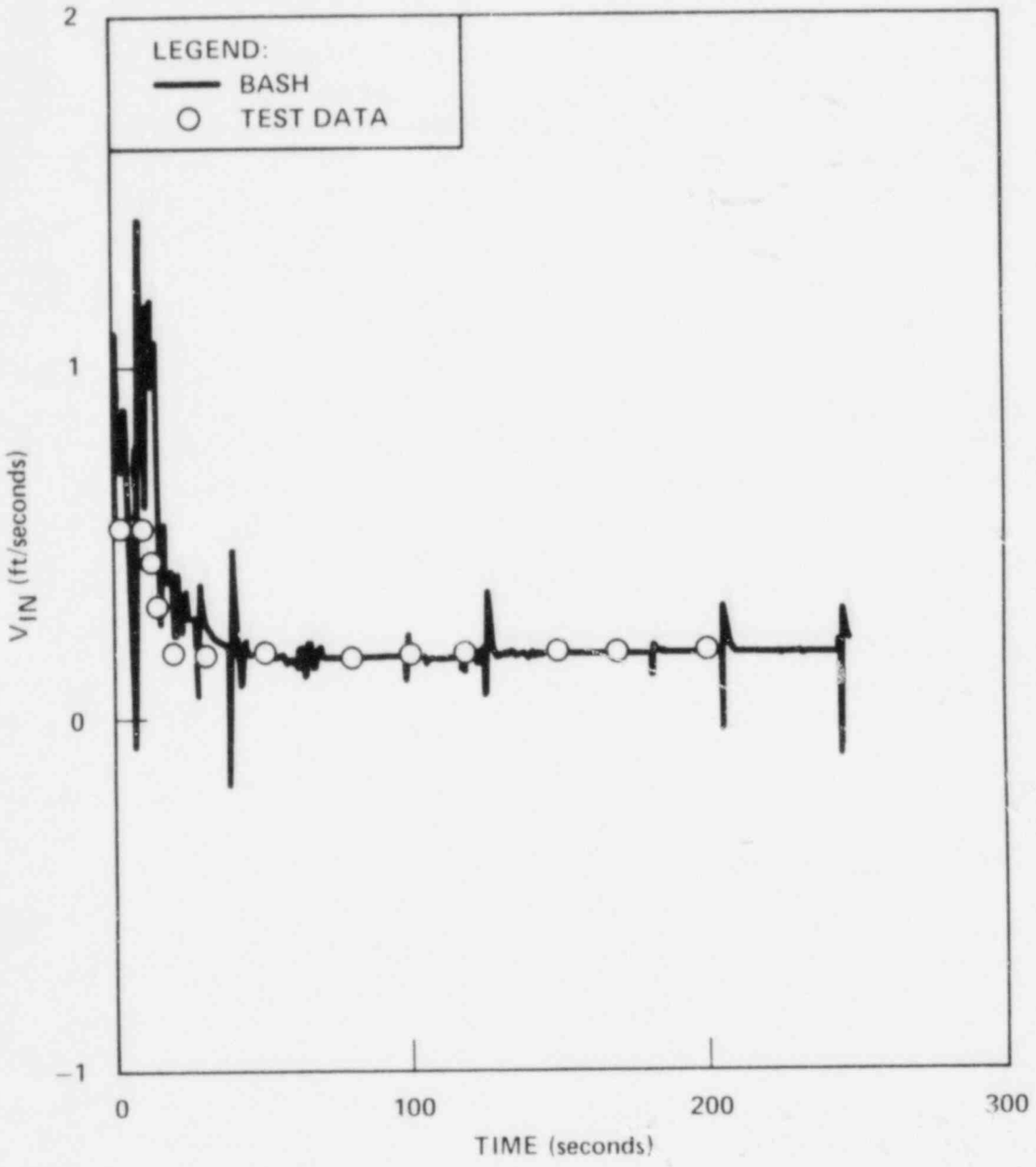

Figure 7-16. Comparison of Flooding Rates from BASH and Test Data (Calculated From Mass Balances)

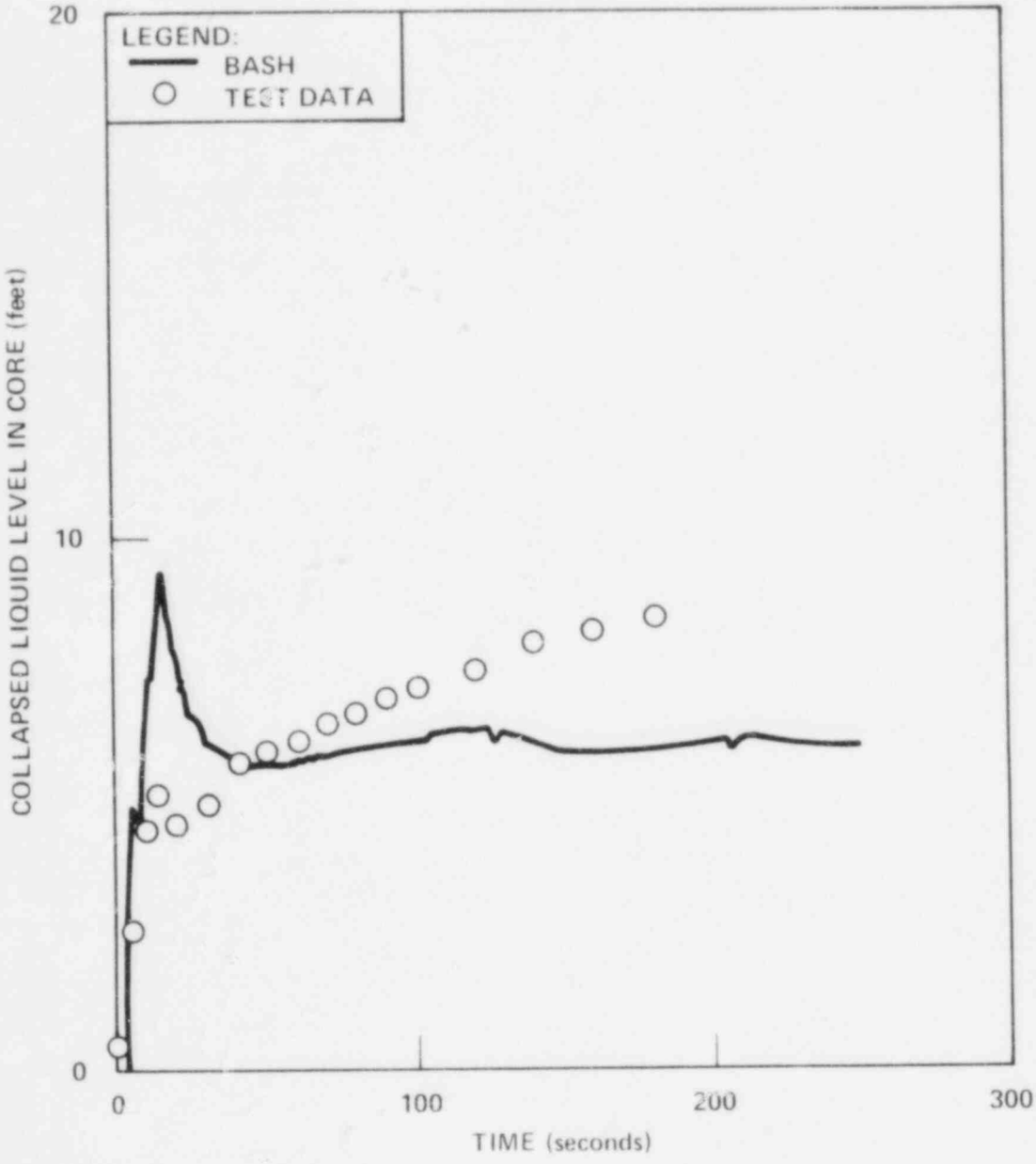

Figure 7-17. Collapsed Liquid Level in Core (Indicates Mass Stored in Test Vessel)

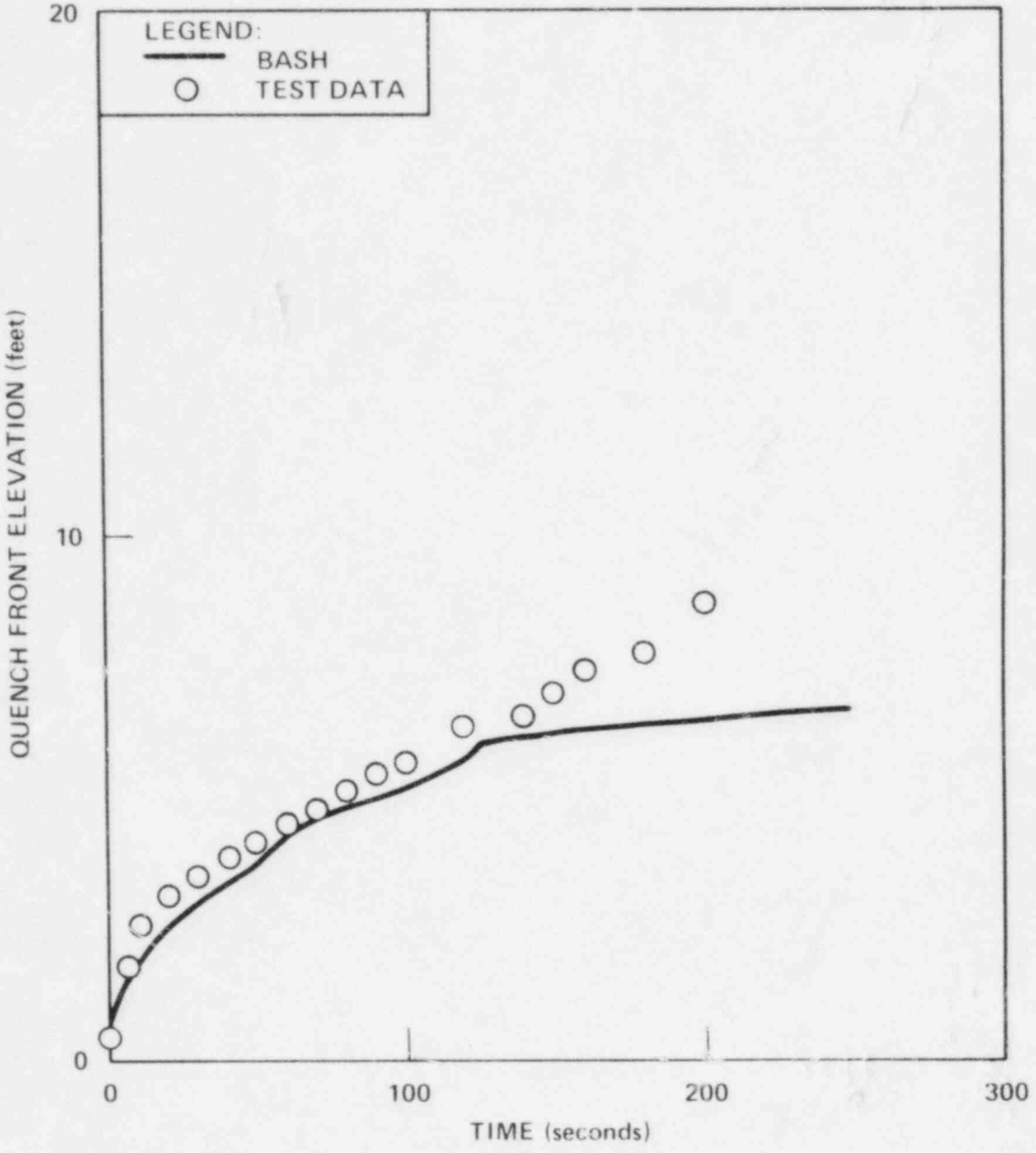

Figure 7-18. Quench Front Elevation

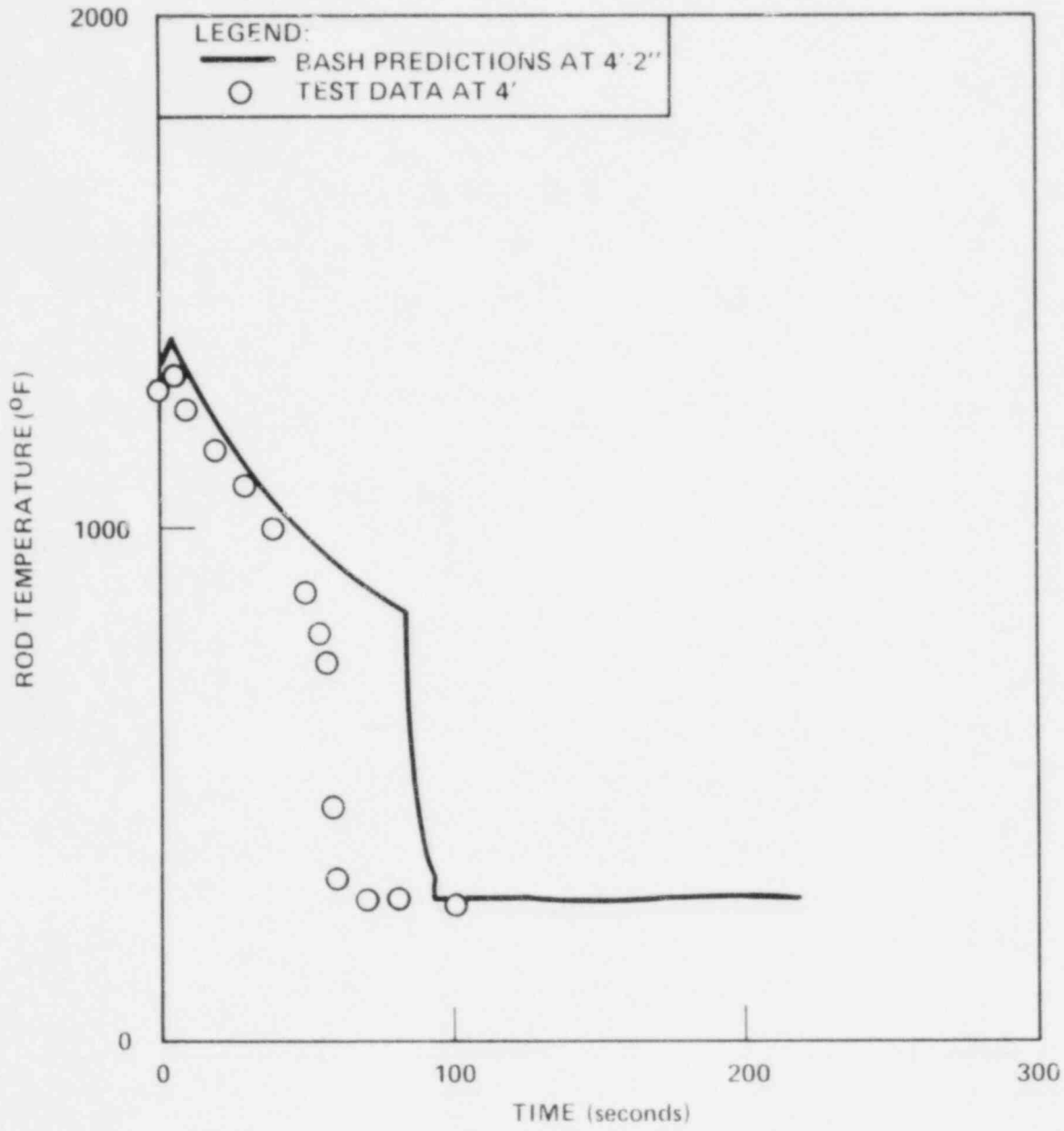

Figure 7-19. Rod Temperature at Approximately 4 Feet

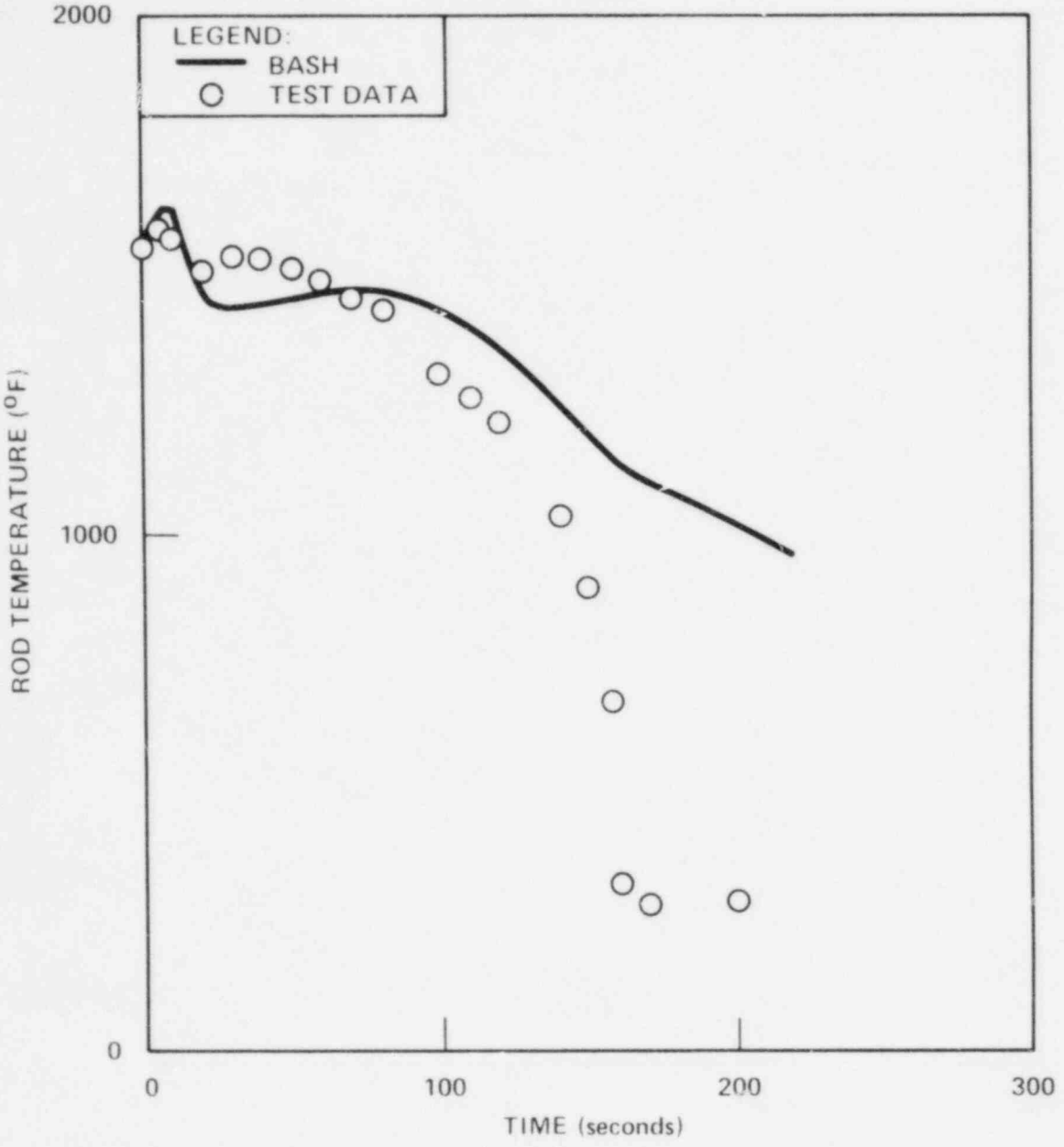

Figure 7-20. Rod Temperatures at Six Feet Six Inches

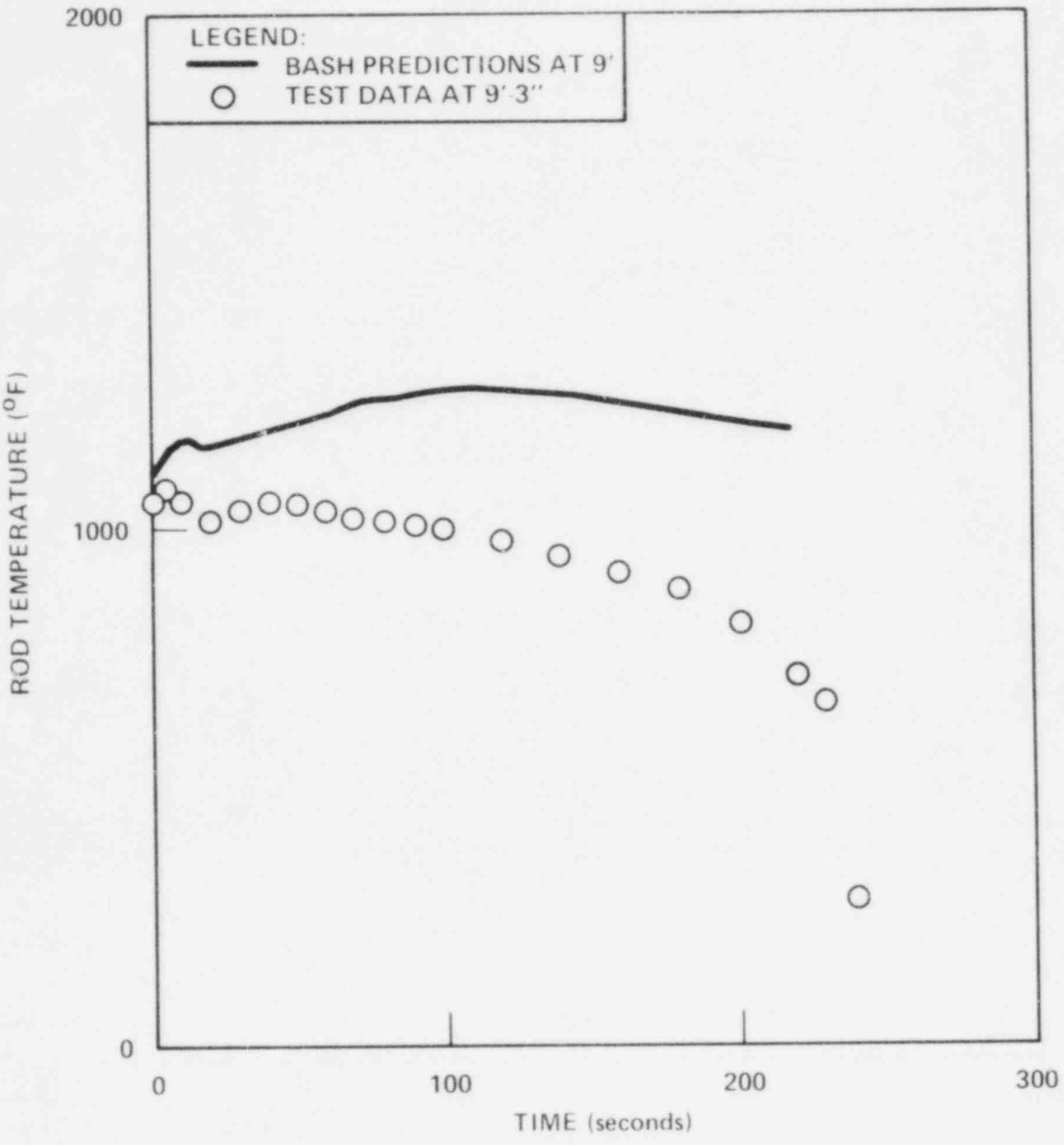

Figure 7-21. Rod Temperatures at Approximately 9 Feet

CONCLUSIONS

BASH has been compared with data from two tests with widely different geometries. It has been shown that BASH properly predicts the system behavior, and in particular, the inlet flooding rate. The present heat transfer model predicts conservatively high rod temperatures due to the absence of grid effects and a "top-down" quench model. This in turn leads to a slower quench front movement and slightly lower flooding rates late in time.

SECTION 8
PROPOSED ECCS EVALUATION MODEL USING BART/BASH

8.1 DESCRIPTIONS OF THE CODES IN THE MODEL

The BASH program can be used alone to analyze the reflood portion of a loss-of-coolant accident. As an integrated reactor core and reactor coolant system model, it provides a comprehensive prediction of the performance of the emergency core cooling system during reflood. In this section, BASH is considered as a part of a larger ECCS evaluation model, capable of performing an analysis of all phases of a loss-of-coolant accident from break initiation through to cladding temperature turnaround.

An integrated ECCS analysis model exists. The present model would be the foundation for the proposed ECCS model, which would incorporate BASH and, for particular purposes, BART to replace much of the present empiricism with more analytic modeling techniques.

This section presents descriptions of both the present and the proposed comprehensive ECCS evaluation models. Brief descriptions of the individual codes which make up the present and proposed models are provided, followed by a discussion of the structure and assumptions of the overall ECCS models.

8.1.1 SATAN

The SATAN program is an analytical model for the blowdown portion of a loss-of-coolant accicent which is part of the present Westinghouse ECCS evaluation model and which is planned for inclusion in a slightly modified role in the ECCS model now under development. A brief summary of SATAN's key function and features is given here. A more comprehensive description of the code is contained in the Westinghouse report, WCAP-8302.[20]

8.1.1.1 SATAN VI: Current Version - SATAN is a finite element code which models thermal/hydraulic phenomena in a reactor core and the reactor coolant system during after a large break of a primary coolant pipe. It was developed

specifically as part of the evaluation model that meets Appendix K requirements. The code provides blowdown thermal/hydraulic parameters which define the heat transfer boundary conditions in the LOCTA code (outlined in paragraph 8.1.5), which is used to calculate the fuel cladding temperature transient during a LOCA. SATAN also provides mass and energy discharge rates from the RCS to containment to the COCO code (paragraph 8.1.4), which is used for containment backpressure and integrity calculations.

Some specific features of the SATAN code include the use of a drift flux model and the use of a two-phase friction multiplier. In the core, a hot channel and an average channel flow calculation, effects of crossflow between channels, cladding swelling and rupture effects and metal-water reaction effects are considered. In the rest of the primary loop, accumulator bypass effects and a two-phase pump model are included.

SATAN begins calculation of the transient at the time the break opens. Calculations continue until two conditions are met; downflow in the downcomer exceeds total ECCS flow, and breakflow goes to zero. When both of the conditions are met, SATAN will terminate and the refill phase calculations will begin, using WREFLOOD. WREFLOOD operates from the end of bypass until water refloods the bottom of the core, at which time BASH takes over. For some accidents (e.g. hot leg break), refill is not a distinct phase of the transient, but is concurrent with blowdown. In these cases, when SATAN terminates at the third condition (namely, bottom of core recovery), the reflood phase calculations will begin using BASH, entirely bypassing WREFLOOD.

8.1.1.2 SATAN MODIFICATIONS: Metal Heat Release - The original SATAN metal heat release model assumed: (1) lumped heat capacity (i.e. infinite thermal conductivity) for the components of the reactor; and (2) a constant, user input heat transfer coefficient. This coefficient was chosen to match the integrated heat release throughout the SATAN-calculated transient with the heat release predicted by a separate, more detailed analysis. This method released most of the metal's stored energy late in the transient, leading to unrealistially large steam generation rates near the end of blowdown. The new

model proposed for SATAN utilizes the metal heat release model described earlier in paragraph 6.2 to calculate the transient temperature distribution in each metal componment and to provide the following improvements to the original SATAN approach:

1. Calculation of the metal-water interfacial heat transfer coefficient using the standard correlations for forced convection, nucleate boiling, transition and film boiling heat transfer regimes employed in the LOCTA code.[5]

2. Modeling of the stainless steel surface layer on metal components by the composite material capability of the metal heat release model discussed in paragraph 6.2.

3. Programming logic to allow a number of geometries in each SATAN metal element.

4. More detailed modeling of the steam generator primary-to-secondary heat transfer. The old approach made independent calculations of the tube stored heat release and the primary-to-secondary heat transfer. The proposed method uses the two-sided boundary condition capability of the new metal heat release model to rigorously treat primary-to-secondary heat transfer, including the tube heat capacity.

8.1.2 BASH

The BASH code (the combination of BART and NORTRUMP) is described extensively in this report. Sections 2 and 5 present BART, the mechanistic core thermal/hydraulic model, while Sections 3 and 6 discuss NOTRUMP, the detailed reactor coolant system model.

BASH is planned as an integral part of the proposed ECCS evaluation model, replacing WREFLOOD to provide a more realistic thermal/hydraulic simulation of the reactor core and RCS during the reflood phase of a LOCA. Figures 8-1 and 8-2 illustrate how BASH will be substituted for WREFLOOD in calculating transient values of core inlet flow, enthalpy, and pressure for the detailed fuel

rod model, LOCTA. Instantaneous values of accumulator flow, safety injection flow, containment ambient temperature and pressure, and the time of completion of RV lower plenum refill will be provided to BASH by WREFLOOD/COCO, which, in the proposed ECCS model, has been relegated solely to providing these required boundary conditions.

8.1.3 WREFLOOD

The WREFLOOD code provides mass and energy discharge rates from the reactor coolant system to the containment during a core reflood transient. A brief overview is presented here. A complete description of the code is available in WCAP-8170.[3]

The basic goemetric configuration in WREFLOOD divides the primary coolant system into three sections; the reactor vessel, the broken loop, and a second loop which combines all unbroken loops. The reactor vessel region is further divided into a downcomer, lower plenum, and core. Using the injection characteristics of the ECCS as input, the code calculates the downcomer and core water levels as the reflood transient continues. Other basic input to WREFLOOD includes geometric data and initial and boundary conditions in the core, steam generators, and containment.

WREFLOOD permits hydraulic modeling of the two parallel flow paths available for discharging steam and entrained water from the core to the break; i.e. the path through the broken loop and the path through the intact loops. Each of these flow paths may be subdivided into as many as 29 nodes connected in series. The code calculates the flow split between the two paths and the total flow discharged from the core based on the resistances of the flow paths and the calculated local fluid conditions throughout the primary system. Another condition satisfied in WREFLOOD is that the pressure drop in the flow path from the core through the intact loops to the top of the downcomer must equal the hydrostatic pressure of the column of water connecting the downcomer and core.

In the current ECCS evaluation model, the portions of the LOCA transient addressed by WREFLOOD are the core refill and reflood phases, which occur after the primary coolant system has depressurized due to water loss through the break (the blowdown phase). WREFLOOD calculates the variations in basic thermal/hydraulic parameters such as core flooding rate, core and downcomer water levels, and fluid thermodynamic properties and mass flow rates throughout the primary system.

In the proposed ECCS model, however, after the end of the refill stage of the LOCA (i.e., when the RV lower plenum has been refilled and core flooding begins) WREFLOOD is relieved of all of the above responsibilities by BASH. The WREFLOOD code, less detailed in its thermal/hydraulic models than BASH, is used in the proposed model only to provide values for accumulator flow, SI flow, and containment pressure and temperature boundary conditions during the reflood.

To do this WREFLOOD runs a simplified RCS simulation prior to BASH. For containment calculations WREFLOOD, the RCS code, supplies COCO, the containment model, with the break mass and energy discharge rates. COCO calculates and returns updated values of containment temperature and pressure. The basic inputs to WREFLOOD are provided through input data for the overall ECCS model and through SATAN output at the end of blowdown. WREFLOOD will run its simulation of RCS response concurrent with, but independent of BASH during the reflood phase, returning containment boundary conditions at each timestep. WREFLOOD, in this respect, can be utilized as a verification of the BASH transient calculation.

8.1.4 COCO

The COCO code is a mathematical model of the containment. Selection of various options in the code allows the creation of models of particular containment buildings. COCO is described in detail in WCAP-8327.[21]

The containment analysis is based on time-dependent conservation equations for mass and energy, equations of state, and other auxiliary functions and tables. Transient conditions are determined for both the containment steam-air mixture and the sump water. The energy equation is applied to the containment shell to obtain temperature gradients, energy storage, and heat conduction in the structure. Heat removal from the containment atmosphere by venting, sprays, energy storage in equipment, ventilation fan coolers, and sump water recirculation is considered.

For analytical rigor, the containment air-steam-water mixture is separated into two distinct systems, the air-steam phase and the water phase in the containment sump. This division permits a more accurate representation of the different physical phenomena occuring in the two systems. At the RCS break point, the discharge flow flashes into steam with entrained water during the two-phase portion of the LOCA. The water falls into the sumps while the steam remains aloft, joining the steam-air mixture.

The steam-air mixture and the sump water each are assumed to have uniform properties. Specifically, thermal equilibrium between air and steam is assumed, along with complete thermal mixing of the sump water. This does not, however, imply thermal equilibrium between the steam-air and the water phases. Relationships to determine the interphase heat transfer behavior are included.

Air inside the containment is treated as an ideal gas. Thermodynamic properties of water and steam are derived from available compressed water and steam tables.

Heat transfer through, and heat storage in the walls of the containment structure, are treated using a multi-layer flat wall model. Heat transfer in any direction other than perpendicular to the wall surface is neglected. Also, the thermal conductivity, density, and specific heat of each layer are assumed to be independent of temperature.

Mass and energy flow rates through the RCS rupture are provided to COCO by separate analysis of the reactor vessel blowdown and core thermal transient. Reflood mass and energy releases may be supplied either by input or by a concurrent analysis of the reflood rate and containment pressure.

In both the present and proposed ECCS models, COCO is run simultaneously with WREFLOOD, which provides the necessary mass and energy inputs to the containment on a continuous basis. In the proposed model, though, WREFLOOD is only a subsidiary code, running parallel to the main transient analysis code, BASH. During reflood, the WREFLOOD/COCO system is used only to provide containment boundary conditions required by BASH.

8.1.5 LOCTA/BART

The LOCTA code is a computer program that evaluates fuel, cladding and coolant temperatures during a LOCA. A more complete description than is presented here can be found in WCAP-8301.[5]

In LOCTA, the highest power fuel assembly is analyzed and is considered to be composed of a high-power rod surrounded by average rods. The fuel rods are analyzed with finite-difference conduction equations in both the radial and axial directions. Descriptions of the fuel rods are flexible in that a rod can be divided into an arbitrary number of radial and axial nodes.

Internal heat generation is calculated, including fission product decay heat (ANS infinite +20 percent). Also considered in the code are heat generation due to the exothermic Zircaloy-water reaction and the effects of cladding swelling and burst.

During blowdown, before the core is uncovered, heat transfer regimes analyzed by LOCTA include single-phase convection, nucleate boiling, transition boiling and stable film boiling. After the core is uncovered, laminar or turbulent heat transfer film coefficients are used in computing heat transfer from rods to steam. Heat transfer coefficients are computed for each axial node on the basis of local coolant flows, qualities, and temperatures. During lower plenum refill the rod-to-rod radiation heat transfer is also considered.

In the reflood phase, the core is cooled by a two-phase mixture. In the current version of LOCTA, employed in the present ECCS model, heat transfer coefficients based on FLECHT test data are used, except when the core flooding rate is less than one inch per second and the average rod has burst. In that case, the heat transfer coefficients are based on a steam cooling assumption.

In both the present and proposed ECCS models LOCTA calculates thermal and mechanical fuel rod conditions for selected rods in the hottest assembly in the core (Figures 8-1 and 8-2). The selected rods are the hottest rod, the average rod, and a nominal rod adjacent to the hottest rod.

During blowdown, the two versions of the ECCS model use the same version of LOCTA, with SATAN providing the required mass flow and pressure information to the fuel rod code. However, during refill and reflood, the proposed ECCS model uses a modified version of LOCTA to yield a significant improvement in fuel rod behavior prediction.

In the proposed BART/LOCTA detailed fuel rod model, for the calculation of local heat transfer coefficients, the empirical FLECHT correlation is replaced by the BART code. BART employs rigorous mechanistic models to generate heat transfer coefficients appropriate to the actual flow and heat transfer regimes experienced by the LOCTA fuel rods. This is considered a more flexible, realistic approach than relying on a static empirical correlation.

Finally, in the proposed detailed fuel rod model, BART does not generate rod temperature profiles internally (as in the BASH version of BART), but uses fuel rod temperatures provided by LOCTA at each timestep, conserving computation time and ensuring consistency between BART coefficients and LOCTA rod properties in the hot assembly and hot rod analysis. In addition, the blockage distribution calculated as a result of cladding swelling and rupture is supplied to BART for flow redistribution calculations.

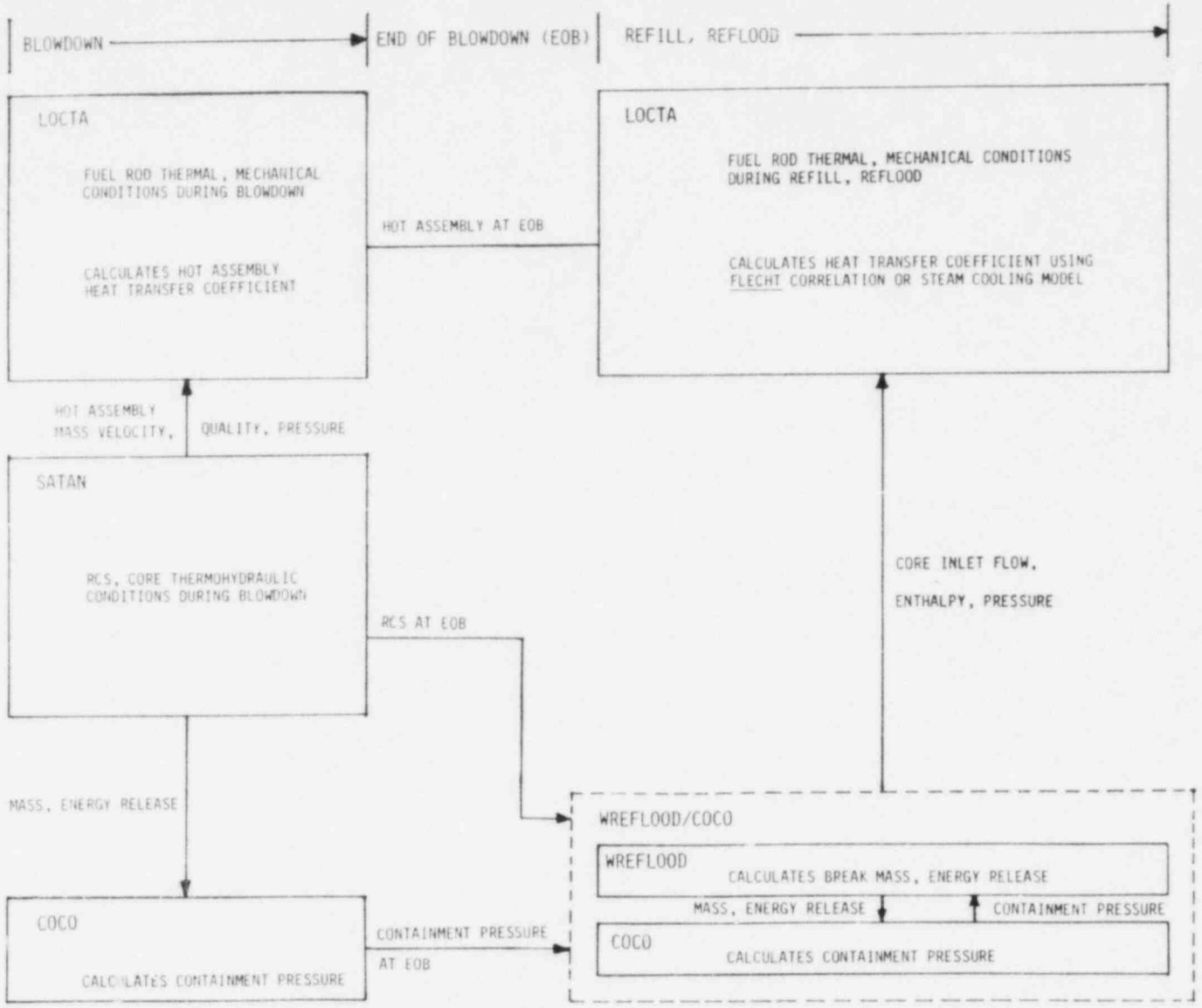

Figure 8-1. Current ECCS Evaluation Model

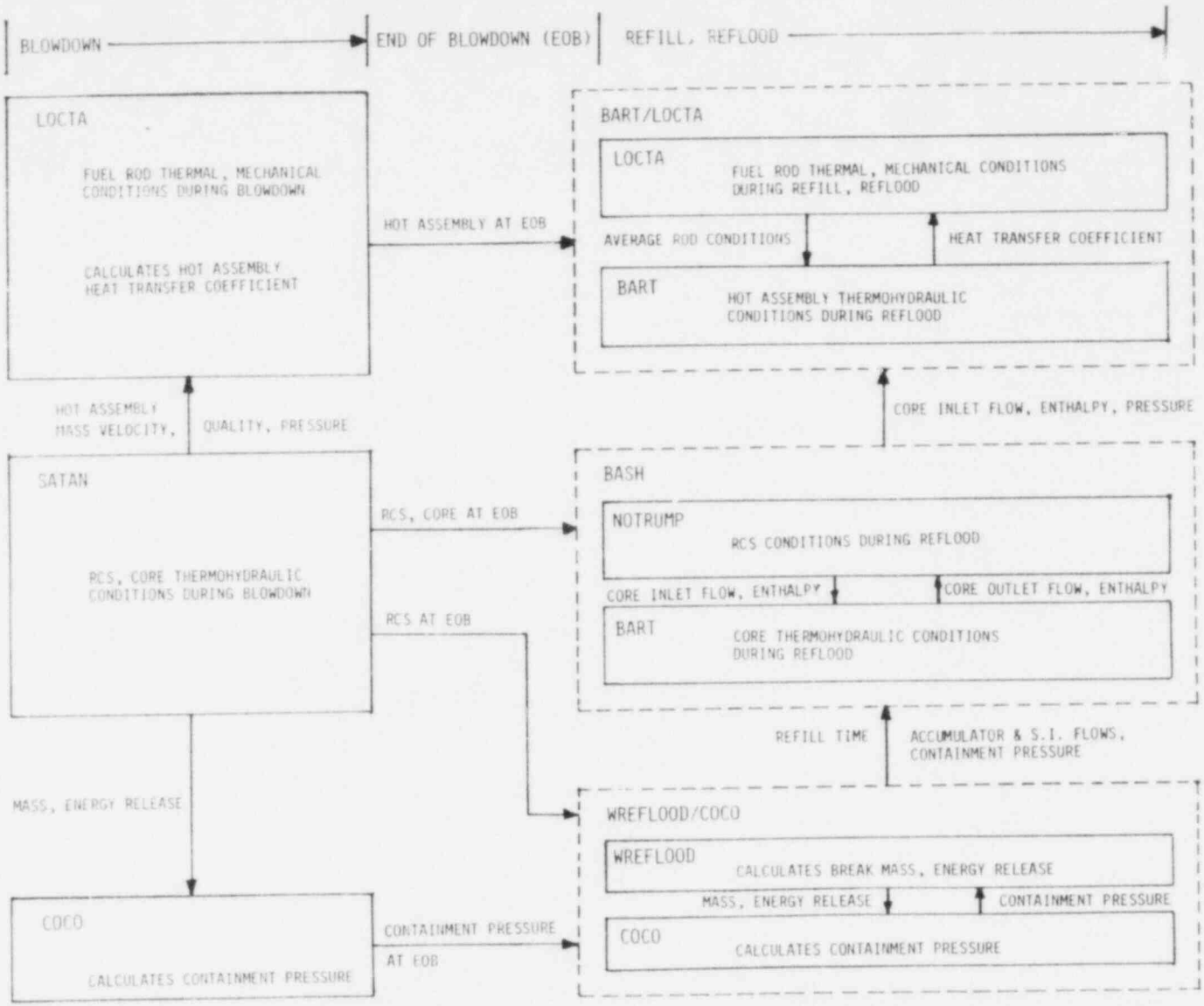

Figure 8-2. Proposed ECCS Evaluation Model

8.2 PROPOSED ECCS EVAULATION MODEL CODE INTEGRATION

The previous paragraphs have described the models available for calculating a more realistic reflood transient. The following paragraphs deal with the methods used to obtain a conservative prediction of a PWR reflood transient.

8.2.1 Comprehensive Calculational Scheme

Figures 8-1 and 8-2 illustrate, respectively, the current and proposed calculational steps and information flow among the computer codes which make up the ECCS evaluation model. Both models are used to predict the peak cladding temperature during a large LOCA. The main differences between the two versions are: (1) the use of BASH to calculate the flooding rate for input into hot channel computations (superseding WREFLOOD); and (2) the use of BART to calculate hot channel fluid conditions and heat transfer coefficients for the LOCTA hot rod calculations (replacing the FLECHT correlations).

8.2.2 Reflood Assumptions in the Proposed Model

Several conservative assumptions are made in the proposed model to ensure that the calculations yield pessimistic predictions of core reflood rate and associated phenomena. In other areas a mechanistic approach is employed. A detailed discussion of the important reflood models and assumptions follows.

8.2.2.1 Entrainment Rate - The entrainment rate controls the mass accumulation in the core and therefore the flooding rate. The current model employs a correlation derived from FLECHT data[3], which is based on low flooding rate tests. This results in predictions of early entrainment, regardless of the initial flooding rate, as can be seen in typical WREFLOOD calculations.

In BASH, the entrainment rate will be calculated by BART. In this model, entrainment may be delayed due to the high initial flooding rates, which suppress boiling. Tests have shown that this interaction between the core and the system leads to a period of oscillatory flooding which tends to enhance heat transfer and bundle quenching.[18]

After entrainment begins, the mass in the core is controlled by the movement of the saturation line, since most of the mass is stored below it. To ensure a conservative estimate of the elevation of the saturation line, it is assumed that no mixing of the subcooled water occurs within the core. Consequently, cold water remains near the bottom of the core, and boiling occurs at low eleva- tions.

8.2.2.2 Deentrainment in the Upper Plenum - The upper plenum contains ample surface and flow area for deentrainment of liquid leaving the core. This liquid is then unavailable for vapor generation in the steam generators and may fall back into the core. Some uncertainty exists, however, with respect to the distribution of liquid on the upper core plate and the degree of deentrainment in the complex geometry of the upper plenum.

A conservative assumption of "no deentrainment" is made to account for the uncertainty. The upper plenum and all fluid nodes in the loops are assumed to be homogeneous. This reduces the mass storage capability of the upper plenum region and completely discounts the additional core cooling capability of deentrained liquid falling back into the core.

8.2.2.3 Steam Generator Heat Transfer - There are data[19] which indicate that the two-phase mixture entering the steam generators during reflood is not completely evaporated and superheated to secondary side temperature, due to nonequilibrium between vapor and liquid (similar to core heat transfer effects) and to thermal stratification of emergency feedwater. In BASH, the two-phase mixture is assumed to remain in thermal equilibrium. Also, primary and secondary heat transfer coefficients are chosen so that the primary fluid exit temperature is nearly equal to the secondary side temperature. This, of course, maximizes the pressure drop through the pump and reduces the flooding rate.

8.2.2.4 Pumps - In BASH the pumps are assumed to be locked. The loss coeffi- cients used are identical to those used in current design analysis.

8.2.2.5 Metal Heat Release - All structural metal in the RCS is considered in calculating heat release to the fluid leaving the core. In the reactor vessel downcomer and plenums the heat transfer may be considered conduction-limited due to the presence of liquid. In these components, the detailed metal heat release model described in paragraph 6.2 is used. In other components, where the fluid is expected to be hotter, the simpler lumped parameter metal node (paragraph 3.2) is used.

8.2.2.6 ECCS Mixing - Data from steam/water mixing tests[22] indicate that the injected ECCS water mixes completely with steam flowing through the cold legs, so that equilibrium conditions are achieved only a short distance downstream of the injection point. The cold leg is therefore modeled with an equilibrium fluid node. An additional resistance is applied in the current model during accumulator injection to account for increased resistance arising from pressure oscillations. This extra resistance will also be applied in BASH.

8.2.2.7 Downcomer - The downcomer will be modeled with the "two volume" configuration described in paragraph 6.1. This will permit the calculation of liquid level changes in the downcomer and spillage from the broken cold leg.

8.2.2.8 Core Heat Transfer - Hot assembly heat transfer is calculated using the BART code. The models in BART are designed to give a realistic representation of the core heat transfer for a given transient flooding rate. The assumptions outlined above ensure that the calculated inlet flooding rate will be conservatively low. There are, however, additional conservatisms within the BART core heat transfer model which should be pointed out:

a. Top down quench and thimble quench: There is no provision for calculating the top down quenching of fuel rods, nor the quenching of thimbles, both of which would enhance the core heat transfer through vapor desuperheating and increased core liquid accumulation.

b. Flow blockage: As mentioned previously, the amount of flow blockage in the hot assembly is calculated according to the requirements of NUREG-0630. This blockage is considered conservatively high for the amount of cladding strain and the degree of noncoplanarity expected of the ruptures in an actual PWR.[10]

c. Dispersed flow heat transfer: There is increasing evidence that a gravity reflood situation tends to improve the heat transfer in the core by driving the thermohydraulic conditions toward equilibrium.[18] This is in contrast to a forced flooding situation such as in the FLECHT experiments, which have been shown to exhibit significant nonequilibrium (i.e., vapor superheating). It is clear that an equilibrium condition would result in improved core heat transfer, since this condition represents more effective use of the cooling capacity of the liquid before it exits the core. The detailed heat transfer and fluid flow mechanisms which lead to the near equilibrium conditions in gravity reflood are not clear at this stage. In view of this, the proposed ECCS evaluation model will employ the BART nonequilibrium dispersed flow model for the hot channel analysis, thereby ensuring additional conservative margin in the calculations, as demonstrated in the preceding paragraphs.

SECTION 9
CONCLUSION

The BASH computer code has been developed to improve several aspects of the prediction of core and RCS behavior in the reflood phase of a LOCA. The proposed models incorporated in BART and NOTRUMP as portions of BASH build upon models already submitted; the BART interim model[18] and the NOTRUMP model.[4] At this point, review of BASH should concentrate on overall system behavior prediction capability.

Modeling assumptions have been included with the explicit intent of ensuring conservatism in the model and compliance with 10CFR50, Appendix K requirements. The proposed BASH model is <u>not</u> presently a best-estimate model.

SECTION 10
REFERENCES

1. "Westinghouse ECCS Evaluation Model," 1981 Version, WCAP-9220-P-A-REV-1, February 1982. (Westinghouse Proprietary)

2. Collier, G., et al., "BART-A1: A Computer Code for the Best-Estimate Analysis of Reflood Transient," WCAP-9561, January 1980. (Westinghouse Proprietary)

3. Collier, G., et al., "Calculational Model for Core Reflooding After a Loss-of-Coolant Accident (WREFLOOD Code)," WCAP-8170, June 1974. (Westinghouse Proprietary)

4. Meyer, P. E. and Frick, G. K., "NOTRUMP: A Nodal Transient, Steam Generator and General Network Code," WCAP-9236, February 1978. (Westinghouse Proprietary)

5. Bordelon, F. M. et al., "LOCTA-IV Program: Loss-of-Coolant Transient Analysis," WCAP-8301, June 1974 (Westinghouse Proprietary).

6. Lilly, G. P., et al., "PWR FLECHT Cosine Low Flooding Rate Test Series Evaluation Report," WCAP-8838, March 1977.

7. Lilly, G. P., et al., "PWR FLECHT Skewed Profile Low Flooding Rate Test Series Evaluation Report," WCAP-9183, November 1977.

8. Chiou, J. S., et al., "Models for PWR Reflood Calculations Using the BART Code," WCAP-10062.

9. Zuber, N., and Staub, F. W., "An Analytical Investigation of the Transient Response of the Volumetric Concentration in a Boiling Forced-Flow System," Nuclear Science and Engineering, 30, pp. 268-278 (1967).

10. Powers, D. A. and Meyer, R. O., Cladding Swelling and Rupture Models for LOCA Analysis, NUREG-0630, April 1980.

11. Mandhane, J. M., Gregory, G. A., and K. Aziz, "A Flow Pattern Map for Gas-Liquid Flow in Horizontal Pipes," Int. Journal Multi-Phase Flow, 1, 537-553 (1974).

12. Cunningham, J. P., and Yeh, H. C., "Experiments and Void Correlation for PWR Small Break LOCA Conditions," Trans. Am. Nucl. Soc. Vol. 17, p. 369-370 (1973).

13. Segev, A., et al., "Countercurrent Steam Condensation and its Application to ECC Penetration," paper presented at the 19th National Heat Transfer Conference, July, 1980 pp. 101-108, Orlando, Florida.

14. Lim, I. S., et al., "Cocurrent Steam/Water Flow in a Horizontal Channel," NUREG/CR-2289, August 1981.

15. Claxton, K. T., et al., "H.T.F.S. Correlations for Two-Phase Pressure Drop and Void Fraction in Tubes," Harwell H.T.F.S. Design Report No. 28, pp. 9-14 (1972).

16. Cleary, W. F., et al., "FLECHT-SET Phase B System Design Descriptions," WCAP-8410, AEC-W-EPRI Cooperative Research and Development Report, October 1974.

17. Cadek, F. F., et al., "PWR FLECHT System Effects Test Program Plan," WCAP-7906, April 1972.

18. Loftus, M. J., et al., "PWR FLECHT SEASET Unblocked Bundle, Forced and Gravity Reflood Task Data Report," WCAP-9699, June 1980.

19. Waring, J. P. and Hochreiter, L. E., "PWR FLECHT-SET Phase B Evaluation Report," WCAP-8583, August 1975.

20. Boredelon, F. M., et al., "SATAN VI Program: Comprehensive Space-Time Dependent Analysis of Loss of Coolant," WCAP-8302, June 1974. (Westinghouse Proprietary)

21. Boredelon, F. M., E. T. Murphy, "Containment Pressure Analysis Code (COCO)," WCAP-8327, July 1974. (Westinghouse Proprietary)

22. Lilly, G. P. and L. E. Hochreiter, "Mixing of Emergency Core Cooling Water with Steam: 1/3-Scale Test and Summary," WCAP-8423, June 1975.